An experimental study of the solubility and speciation of uranium(IV) in reduced fluoride-bearing solutions

By: Kira Fuller

January 2024

A thesis submitted to McGill University in partial fulfillment of the requirements of the degree of Master of Science

Department of Earth Science

McGill University

Montreal, Quebec

Canada

Abstract

The solubility of UO_2 solid and the speciation of U(IV) in fluoride-bearing aqueous fluids were investigated experimentally at a temperature of 200 °C and vapour-saturated water pressure. Oxygen fugacity was controlled by the hematite-magnetite buffer to ensure that it was below that of the UO_3/UO_2 equilibrium boundary and that dissolved uranium was dominantly as U(IV). The experiments were performed at a fluoride activity ranging from $1.6x10^{-7}$ to 0.17 m and pH values from 2.1 to 7.5.

The concentration of dissolved uranium increased with decreasing pH and increasing fluoride activity from about $1.28x10^{-5}$ to $2.32x10^{-3}$ m, suggesting that H^+ and F^- are important ligands in the species that control UO_2 solubility and that the stability of dissolved U(IV) species is high enough to ensure the efficient transport of uranium in reduced hydrothermal fluids. The dissolved U(IV) species were determined to be a mixture of $UO_{2\ (aq)}$, HUO_2^+, UO_2F^- and $HUO_2F_{(aq)}$ and the $\Delta_f G^{T,P,0}$ values for these species were calculated to be -1006.5 ± 1.1, -1039.6 ± 2.8, -1299.7 ± 0.4 and -1360.8 ± 0.7 kJ/mol , respectively; the logarithms of the equilibrium constants (log K) for the corresponding formation reactions were calculated to be -4.7 ± 0.1, -1.0 ± 0.3, -2.64 ± 0.04 and 4.10 ± 0.07, respectively.

The relative importance of the aqueous uranium species identified above varies with aF^- and aH^+. In solutions with low aF^- and low aH^+, the dominant species is $UO_{2(aq)}$, and HUO_2^+ is the next most important species. The species UO_2F^- predominates in solutions with high aF^- and low aH^+, and $HUO_2F_{(aq)}$ predominates in solutions with moderate to high aF^- and high aH^+.

The results of this study show that U(IV) is highly mobile in fluorine-enriched, low to intermediate pH aqueous fluids at 200 °C and a fO_2 near that of the hematite-magnetite buffer

and that this is due to the formation of fluoride and hydroxy-fluoride complexes (UO_2F^-, $HUO_2F_{(aq)}$) These conditions coincide with those of many hydrothermal uranium deposits, particularly breccia- and vein-hosted deposits associated with fluoride-rich magmas, including the giant IOCG-type Olympic Dam deposit, South Australia (e.g., Cuney, 2009, Skirrow et al., 2009). This study, therefore, provides strong evidence that the deposit-types mentioned here could have formed following the transport of uranium as U(IV) species, instead of the oxidised uranium species that are commonly invoked for uranium transport in models explaining their genesis.

Résumé

La solubilité et la spéciation de l'U(IV) dans des fluides aqueux fluorés ont été déterminées expérimentalement à une température de 200 °C et une pression de 15,5 bars. Le système était contraint par le tampon hématite-magnétite pour garantir que la fugacité de l'oxygène était inférieure à celle de la limite d'équilibre UO_3/UO_2. Les expériences ont été réalisées à des activités de fluorure allant de $1,6x10^{-7}$ à 0,17 m et des valeurs de pH allant de 2,1 à 7,5. Les concentrations d'uranium dissout trouvées dans les conditions indiquées varient d'environ $1,28x10^{-5}$ à $2,32x10^{-3}$ m. On a observé que la concentration d'uranium dissout augmentait avec une diminution du pH et une augmentation de l'activité du fluorure.

Les espèces U(IV) dissout dans les conditions expérimentales (200 °C, 15,5 bars) ont été constituées d'mélange de $UO_{2(aq)}$, HUO_2^+, UO_2F^- et $HUO_2F_{(aq)}$ et les valeurs $\Delta_fG^{T,P,0}$ pour ces espèces ont été calculés comme étant respectivement -1 006,5 ± 1,1, -1 039,6 ± 2,8, -1 299,7 ± 0,4 et -1 360,8 ± 0,7 kJ/mol et les valeurs du log K pour leurs réactions de formation, basées sur la dissolution de l'uraninite dans les conditions expérimentales, sont de -4,7 ± 0,1, -1,0 ± 0,3, -2,64 ± 0,04 et 4,10 ± 0,07, respectivement.

Les espèces dissoutes observées varient en dominance selon aF^- et aH^+. L'espèce $UO_{2\,(aq)}$ prédomine dans les solutions à faibles aF^- et aH^+, tandis que HUO_2^+ faible aF^- et faible aH^+; la plus abondante. L'espèce UO_2F^- prédomine dans les solutions à aF^- élevé et faible aH^+, alors que l'espèce $HUO_2F_{(aq)}$ prédomine dans les solutions à aF^- modéré à élevé et aH^+ élevé. La présence de multiples espèces de fluorure d'uranium réduit dans les solutions indique qu'il est possible qu'une partie de l'uranium relocalisé dans un gisement hydrothermal soit transportée dans des conditions réduites.

Acknowledgments

I would like to thank Professor Williams-Jones for his continual guidance throughout my thesis. Without his help I would not have been able accomplish nearly as much as I did. I would also like to thank Kirsten Rempel who helped to make this thesis cleaner than I could have ever managed on my own and provided guidance in many laboratory aspects.

I would also like to thank all the people in the Zoo who have been there to both bounce ideas off as well as provide endless amounts of entertainment with constant bickering. Hanging out with you guys made all the difference and always brightened my day. I will miss all of you and I hope that I will get to see you at future conventions.

Finally, I would like to thank my parents for always being there to provide emotional support without whom I could never have dreamed of accomplishing what I have. Their support throughout this process means the world to me.

Table of Contents

List of Figures

List of Tables

Chapter 1 Introduction

Uranium occurs naturally in the U(III), U(IV), U(V), and U(VI) oxidation states, but tetra- and hexavalent uranium are the most common and geologically relevant (Dahlkamp, 1993, Murphy and Shock, 1999, Skirrow et al., 2009). Uranium is generally thought to be present in aqueous fluids as U(VI) complexes, and deposited as U(IV) minerals, such as uraninite during the formation of hydrothermal uranium deposits, (Langmuir, 1978, Barnes, 1979, Cunningham et al., 1998, Bastrakov et al., 2010, Eriksen et al., 2012). However, a recent experimental study by Timofeev et al. (2018) showed that at elevated temperatures, U(IV) can be transported as chloride complexes in concentrations of parts per million, suggesting that reduced uranium may be much more soluble in ore-forming hydrothermal solutions than previously thought.

In addition to chloride, other ligands such as fluoride and hydroxide are predicted to be relevant for uranium speciation at hydrothermal conditions based on hard-soft-acid-base theory (HSAB; Pearson, 1963, Williams-Jones and Migdisov, 2014). Uranium is commonly associated with fluorite in hydrothermal mineral deposits such as Olympic Dam, Australia and Xiangshan, China (Roberts and Hudson, 1983, Hu et al., 2008). There is a particularly strong association between uranium and fluorine-bearing minerals in deposits that hosts fluorine-rich felsic intrusions and in caldera complexes (Rogers et al., 1978, Burt and Sheridan, 1981, Cuney, 2014). Experiments show that the partitioning of uranium into hydrothermal fluids from granitic magmas is greatly enhanced in the presence of fluorine (Keppler and Wyllie, 1990, Peiffert et al., 1996). These observations suggest that uranium fluoride species may be important in the transport of uranium in hydrothermal ore-forming systems.

Numerous experimental studies assessing uranium fluoride speciation have been performed at ambient conditions (e.g., Savage and Browne 1960, Grenthe and Varfeldt 1969, Norén 1969, Kakihana and Ishiguro 1974, Choppin and Unrein 1976, Sawant et al. 1990), but little experimental data exists for these species at elevated temperatures. The only study at conditions above ambient was performed by Kovalenko et al. (2012) at 500 °C and 1 kbar, but as discussed below, their neutral-species model is not applicable to most hydrothermal uranium deposits, which form at about 100-360 °C (Robinson and Ohmoto, 1973, Oreskes and Einaudi, 1992, Cunningham et al., 1998, Hu et al., 2008). Furthermore, if fluoride is important in the transport of uranium in these deposits, the transport likely takes place at relatively low temperatures, as fluorite has prograde solubility below 100 °C and retrograde solubility above 100 °C in low-to-moderate salinity solutions (6-7 wt. %; Richardson and Holland, 1979). By lowering the activity of F^- in the fluid, the retrograde solubility of fluorite will destabilize most uranium fluoride species and promote uranium precipitation. Considering these observations, reliable modeling of uranium deposits in fluorine-rich systems requires experimental data for uranium fluoride speciation at temperatures the which these deposits have been shown to form.

In order to assess the possibility of uranium transport in acidic fluids with fluoride as a ligand, the research described in this thesis was undertaken to experimentally evaluate the solubility of UO_2 in fluoride-bearing hydrothermal fluids. This chapter provides a review of the common types of hydrothermal uranium ore deposits and their association with fluorine, the physicochemical parameters controlling uranium speciation, and the existing experimental data for the solubility and speciation of uranium in aqueous fluids.

1.1 Hydrothermal uranium deposits

For several classes of hydrothermal uranium deposits, particularly those linked to felsic magmatic rocks, the uranium ore is associated with fluorite (Burt and Sheridan, 1981, Cuney, 2014). Given the high uranium and fluoride contents of felsic rocks, rhyolites and granites are a likely source of both elements. Important examples include the granitic breccias of the Olympic Dam iron oxide-copper-gold (IOCG) district, Australia, the volcanic complex-hosted vein deposits of the Xiangshan ore field, China, and the Marysvale volcanic field, Utah. Similar deposits are found in Canada, notably those of the Great Bear Magmatic zone. The characteristics of these deposits are discussed below and summarized in Table 1-1.

The uranium deposits of the Xiangshan ore field, located in the Gan-Hang Metallogenic Belt, South China, are mainly hosted in the felsic volcanic-intrusive complex of the Xiangshan caldera (Fig. 1-1; Jiang et al., 2006, Hu et al., 2008). In these deposits, the ore occurs in fault-hosted veins and lenses with grades of 0.1-0.3 % U, and comprises a mixture of pitchblende, uranothorite and brannerite. Additional hydrothermal vein minerals include fluorite, quartz, calcite, chlorite, apatite, magnetite, pyrite, molybdenite and other sulphides, and the main alteration assemblage is quartz-illite-calcite-hematite (Hu et al., 2008, Wei et al., 2021). Magnetite was precipitated during early hydrothermal activity, but the main iron mineral to form during the ore stage was hematite, pointing to an oxygen fugacity (fO_2) near that of the magnetite-hematite buffer and the possibility that dissolved U(IV) species may be stable.

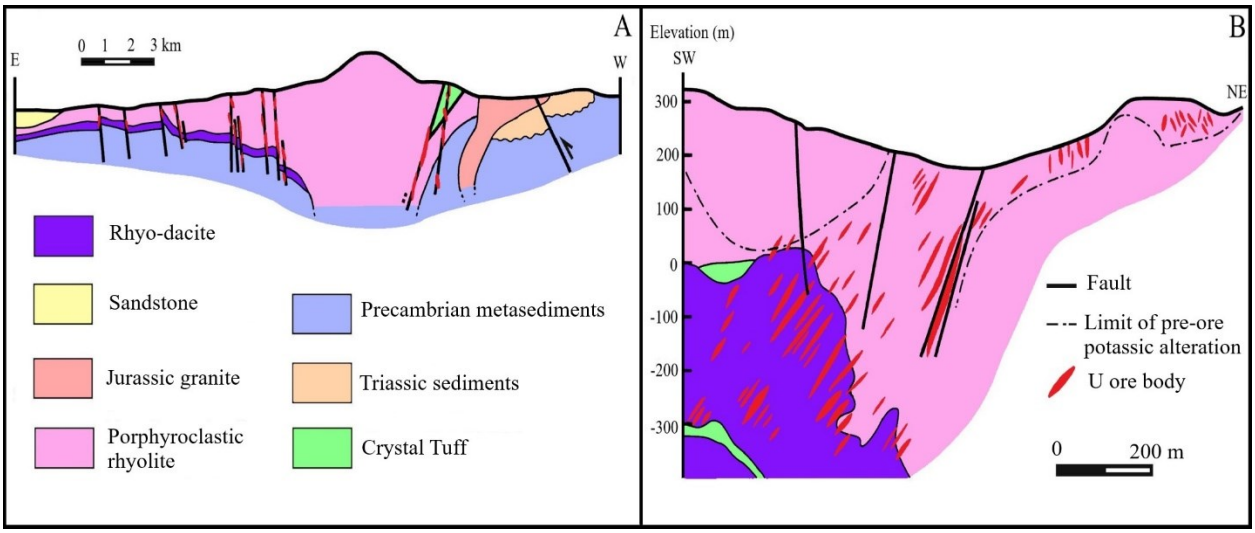

Figure 1-1 Cross-sections through a) the Xiangshan Caldera, and b) the Zoujiashan deposit, modified from Bonnetti et al. (2020).

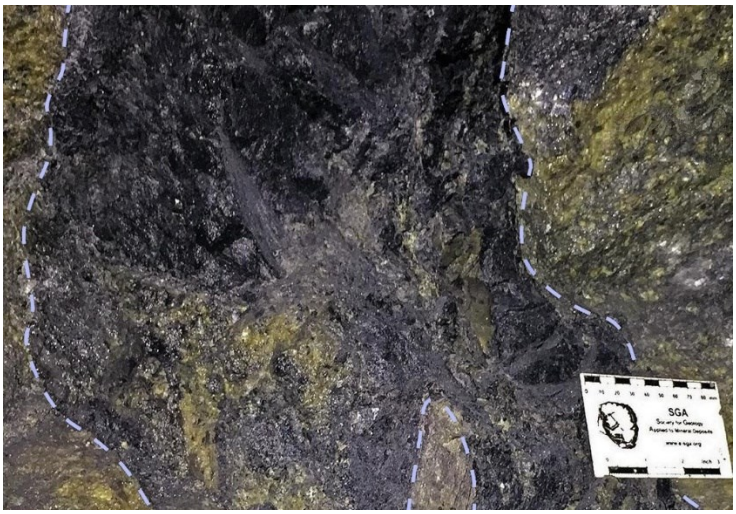

Figure 1-2 A photograph of a uranium-fluorite vein in altered porphyroclastic rhyolite host rocks at the Zoujiashan deposit, Xiangshan ore field, modified from Bonnetti et al. (2020).

As illustrated in Figure 1-2, the fluorite in the Xiangshan deposits is closely associated with uranium ore (Table 1-1). Analysis of the fluorine content of ore-related chlorite in the granitic porphyry-hosted Baquan deposit (0.039–0.172 wt. % F), as well as fluid inclusions from the Xiangshan ore field (0.04 – 2.66 mol/l F), suggests that the main-stage ore fluid contained a

high concentration of fluoride (Hu et al., 2008; Wei et al., 2021). Fluid inclusion studies also show that the mineralizing fluids for deposits in the district had a temperature range of 115 to 275 °C, and the salinity of fluid inclusions ranges from 1.3–8.9 wt. % NaCl equiv. (Hu et al., 2008), in keeping with the temperature-salinity conditions for fluoride speciation (Richardson and Holland, 1979). The pH range for the Xiangshan deposit is estimated to have been 4.8 to 5.5 (Hu et al., 2008, Wei et al., 2021). Mixing of a low-salinity, CO_2-bearing mantle-derived fluid with cooler meteoric waters has been proposed as the precipitation mechanism for fluorite and the uranium ore (Jiang et al., 2006).

The uranium deposits of the Marysvale volcanic field in Utah, USA, are hosted primarily in a quartz monazite porphyry associated with the Monroe Peak caldera complex (Kerr et al., 1957, Cunningham et al., 1998; Table 1-1). The main uranium ore minerals in these deposits are coffinite ($U(SiO_4)_{1-x}(OH)_{4x}$) and pitchblende (UO_2) and occur in vertically-zoned quartz-fluorite-jordisite veins (Cunningham et al., 1998). The main alteration assemblage at depth is sericite-pyrite, which grades to hematite-kaolinite at shallow levels. Late uranium minerals include autunite($Ca(UO_2)_2(PO_4)_2 \cdot 10\text{-}12H_2O$), torbernite($Cu(UO_2)_2(PO_4)_2 \cdot 12H_2O$), schroeckingerite ($NaCa_3(UO_2)(CO_3)_3(SO_4)F \cdot 10H_2O$), uranophane ($Ca(UO_2)_2(SiO_3OH)_2 \cdot 5H_2O$), β-uranotile (polymorph of uranophane) and umohoite ($(UO_2)MoO_4 \cdot 2H_2O$) (Kerr et al., 1957, Cunningham et al., 1998). As indicated by oxygen isotopes, the vertical zonation of the deposits is linked to a dominantly magmatic fluid at depth, which grades into dominantly meteoric fluids at shallow levels (Cunningham et al., 1998). Fluid inclusion homogenization temperatures reported in Cunningham et al. (1998) show that the ore fluids were of low salinity (up to 2.6 wt. % NaCl equiv.) with a homogenisation temperature range from 170 to 260 °C. Mineral assemblage constraints indicate that the fluid had a near neutral pH and was reducing (below the hematite-

magnetite buffer) at depth, but was more acidic and oxidized nearer the surface (Cunningham et al., 1998).

The Olympic Dam Cu-U-Au deposit in the Gawler Craton, South Australia, is the world's largest U-bearing iron oxide-copper-gold (IOCG) deposit, hosting 650 Mt of ore containing 425 ppm U (Hitzman and Valenta, 2005). Smaller uranium-bearing IOCG deposits in the area include Prominent Hill and Oak Dam (Hitzman and Valenta, 2005, Davidson et al., 2007). The uranium at Olympic Dam, thought to be sourced from local granites, occurs as uraninite with some coffinite and brannerite, and is hosted largely in a hematite-rich breccia as matrix fill and massive sulphide clasts (Roberts and Hudson, 1983). The sulphides are vertically and laterally zoned, grading upward and outward from pyrite to chalcopyrite-pyrite, chalcopyrite-bornite, and bornite-chalcocite (Fig. 1-3). Other minerals commonly associated with the uranium ore include fluorite, barite, and rutile, whereas the main alteration assemblage comprises hematite, sericite, chlorite, silica, and carbonate (Roberts and Hudson, 1983, Oreskes and Einaudi, 1992; McPhie et al., 2011). Hematite is the dominant iron mineral, but magnetite associated with pyrite and siderite, which is thought to pre-date the hematite, is commonly present in trace amounts and locally abundant (Oreskes and Einaudi, 1992). The presence of both hematite and magnetite indicates that the fO_2 of the hydrothermal system was near that of the hematite-magnetite buffer, suggesting the presence of U(IV) complexes. Studies of fluid inclusions from Olympic Dam indicate that the hydrothermal fluids had a temperature range of about 100-360 °C and a salinity of 7.3 to 24 wt. % NaCl equivalent (Oreskes and Einaudi, 1992), providing appropriate conditions for the hydrothermal transport of uranium as fluoride complexes.

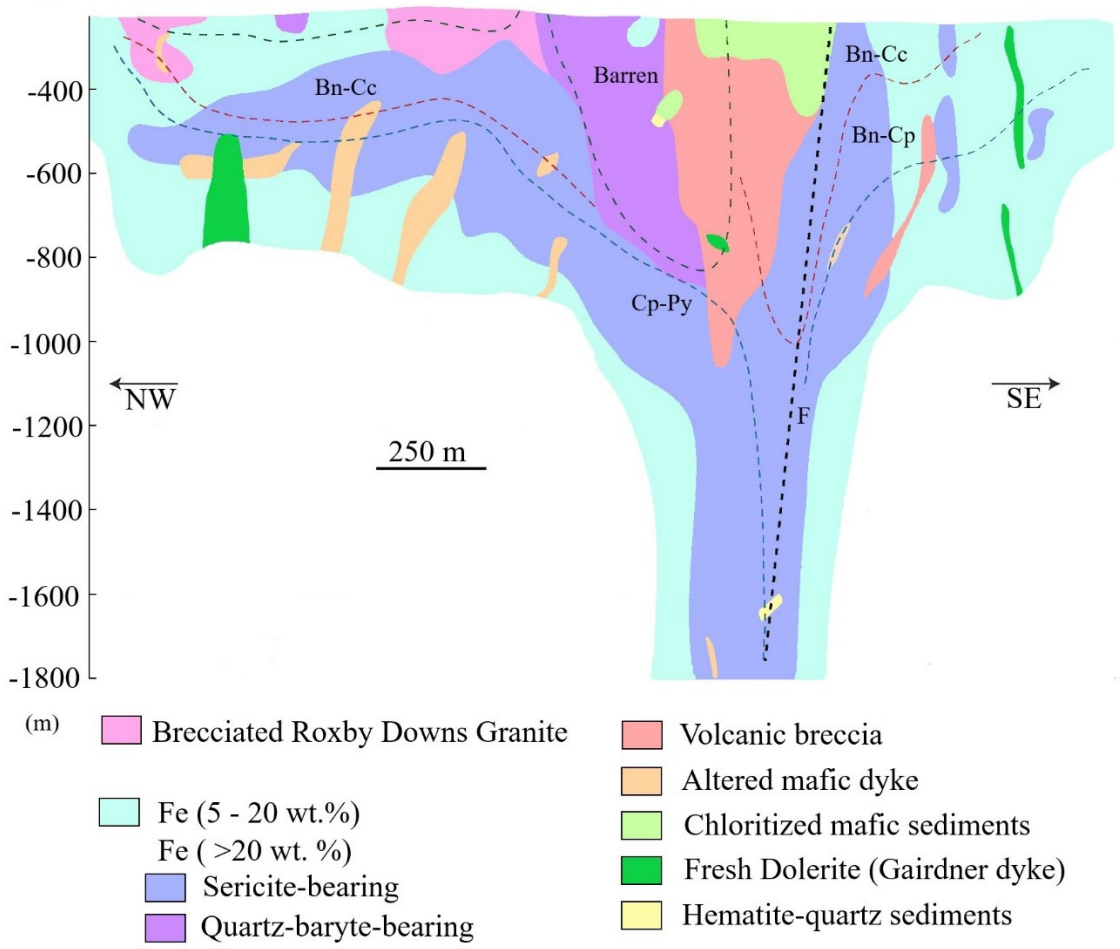

Figure 1-3 A cross-section through the Olympic Dam deposit illustrating the zonation of Fe and Cu minerals, with an overlay of inferred Cu sulphide zone boundaries, modified after Dmitrijeva et al. (2019) (Bn is bornite, Cc is chalcocite, Py is pyrite and Cp is chalcopyrite).

The uranium-bearing, albitite-hosted Southern Breccia prospect, located in the polymetallic IOCG district of the Great Bear Magmatic Zone, Northwest Territories, Canada, is classed as an iron oxide alkali-altered (IOAA) deposit (Montreuil et al., 2015). It is composed of vein networks and breccia zones hosted in metasediments and felsic volcanics, with uranium grades of up to 1 wt. % present as uraninite and pitchblende (Goad et al., 2000, Montreuil et al., 2015). The uraninite was precipitated early in the paragenesis within albitized host rocks together with minor brannerite, coffinite, spatially related to K-feldspar-magnetite-ilmenite alteration

(Montreuil et al., 2015). Later deposition of pitchblende in hematite-chlorite veins was accompanied by widespread hematitization of earlier K-feldspar, suggesting that the oxygen fugacity of the mineralizing system increased from below to above that of the hematite-magnetite buffer (Montreuil et al., 2015; Montreuil et al., 2016). Thorium concentrations of up to 13 wt. % in uraninite point to an ore fluid with a temperature >450 °C, and boron isotope signatures are suggestive of a magmatic origin (Frimmel et al., 2014; Potter et al., 2019; Kelly et al., 2020).

Table 1-1 Examples of hydrothermal uranium deposits in which the uranium ore is associated with fluorite. HM refers to the hematite-magnetite fO_2 buffer.

Deposit name and location	**Host rock & ore morphology**	**Uranium minerals, grade & tonnage**	**Other minerals**	**T& P**	**pH & fO_2**	**References**
Marysvale volcanic field, Utah, USA	Quartz-fluorite epithermal veins in quartz monzonite, granite, rhyolite	Pitchblende, coffinite 640 t, U_3O_8 at ~0.3% U	Alteration: sericite and pyrite at depth (115 m), hematite mid-level, kaolinite, and hematite near surface. Vein minerals: fluorite, quartz, pyrite, marcasite, magnetite (at depth), chlorite, jordisite, molybdenite, ilsemannite and late carbonate.	170-260 °C, median at ~200; 14 bars	At depth, pH = 6-7, fO_2 below HM	Kerr et al., 1957, Cunningham et al., 1998
Xiangshan, Gan-Hang Metallogenic Belt, South China	Epi- to mesothermal veins and lenticular orebodies in granites, quartz monzonite	Brannerite, pitchblende, uranothorite; 0.02- 0.05 Mt at 0.1-0.3% U	Alteration: quartz, hematite, calcite, illite, hydromica, albite; Vein minerals: fluorite, quartz, calcite, chlorite, apatite, pyrite, molybdenite	115-275 °C; 250-800 bars	pH = 4.8-5.5, fO_2 near HM	Jiang et al., 2006, Hu et al., 2008, Wei et al., 2021
Olympic Dam, South Australia	Crosscutting veinlets, patches, and breccia matrix within granitic breccia	Brannerite, coffinite, uraninite; 650 Mt, 425 ppm	Alteration: sericite, hematite, chlorite, silica, carbonate. Hydrothermal assemblage: pyrite, chalcopyrite, bornite, chalcocite, siderite, fluorite, quartz, barite, and early magnetite followed by hematite.	100-360 °C; 150-165 bars	fO_2 near HM	Roberts and Hudson, 1983, Oreskes and Einaudi, 1992, McPhie et al., 2011
Southern Breccia, Great Bear Magmatic zone, NWT, Canada	Matrix fill and veins in albitite breccia, hosted in rhyolite and metasiltstone	Uraninite, pitchblende coffinite, brannerite; up to 1%	Early: pyrite, chalcopyrite, molybdenite, fluorapatite with K-spar-magnetite-ilmenite alteration. Late: hematite, chlorite, Cu sulphides with K-spar-hematite-rutile alteration.	>450 °C	fO_2 below to above HM	Goad et al., 2000, Montreuil et al., 2015, Potter et al., 2019

1.2 Factors influencing uranium solubility

In the current understanding of hydrothermal uranium ore formation, uranium is dissolved in the fluid and transported as U(VI), then deposited as U(IV) ore minerals as a result of decreased oxygen fugacity (Cunningham et al., 1998, Hu et al., 2008). This interpretation is built on the commonly-held belief that U(IV) is insoluble in reduced hydrothermal fluids. However, under conditions such as those observed in experiments performed by Timofeev et al. (2018), it is possible for U(IV) to dissolve in appreciable concentrations in reduced aqueous liquids. Therefore, although most researchers consider that U is transported predominantly as U(VI), U(IV) may also play a role. This is most likely if ligands with which U(IV) species bind are more stable than U(VI) species are present at high concentrations, but this possibility has been given limited consideration. The impact of oxygen fugacity on U transport in ore fluids is expanded upon later in this section and applied in section 1.2.3.

The solubility and chemical speciation of uranium are controlled by several factors including temperature, pH, and oxygen fugacity, as well as ligand type and concentration (Kakihana and Ishiguro, 1974, Langmuir, 1978, Sawant et al., 1990, Fayek and Kyser, 1999). According to the HSAB theory of Pearson (1963), both U(IV) and U(VI) are hard acids and are therefore most likely to form strong complexes with hard bases such as fluoride, hydroxide, and carbonate (Table 1-2). Whether a particular complex forms, however, also depends on the concentration of the base (ligand) in solution (Barnes, 1979, Wood and Samson, 1998, Murphy and Shock, 1999). This is particularly well-illustrated by chloride, which is a borderline base that forms its strongest complexes with intermediate acids. Because this is the dominant base in most hydrothermal solutions and forms relatively stable uranium chloride complexes (Day et al., 1955, Sobkowski, 1961, Timofeev et al., 2018), it has been predicted to play a more important role in

uranium transport in hydrothermal fluids than some hard bases owing to the relatively low concentrations of the latter (Robinson and Ohmoto, 1973, Barnes 1979, Roedder, 1984).

The ligand number of aqueous metallic species tends to increase with increasing ligand concentration, or in the case of hydroxide species, with pH. The stoichiometry of the predominant hydroxide species in solution progresses from lower to higher numbers of OH^- groups with increasing alkalinity (OH^- availability). This speciation behaviour is illustrated using solubility constants (K_{sp}) at ambient conditions taken from Opel et al. (2007) in Figure 1-4, which shows a progressive change in the primary uranium complex from U^{4+} to $U(OH)_4$. The stability of the uranium hydroxide species at 25 and 200 °C, as modeled by Shock et al. (1997), is also shown in fH_2-pH space in Figure 1-5.

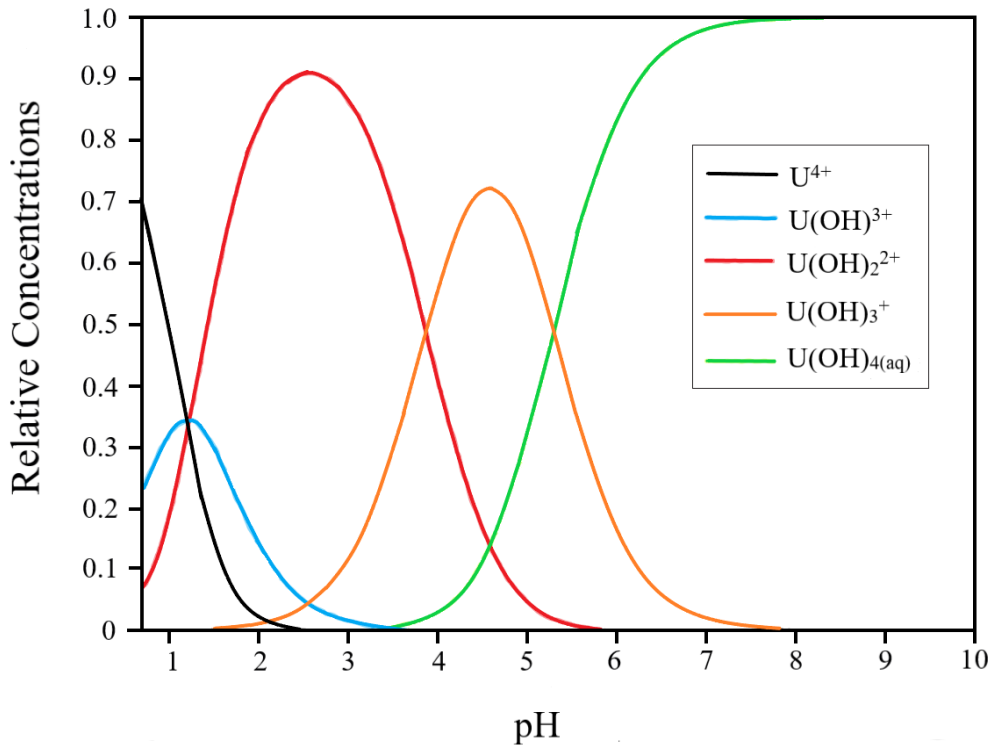

Figure 1-4 A speciation diagram displaying the dominant uranium(IV) hydroxide species as a function of pH at ambient conditions after Opel et al. (2007), based on their calculated solubility product; formation constants for UOH^{3+} to $U(OH)_3^+$ were taken from Neck and Kim (2001).

A more complex, mixed ligand example can be viewed in phase diagrams calculated by Bastrakov et al. (2010) at 25-50 °C, based on data collected at ambient P-T conditions (Fig. 1-6). The concentrations of fluoride, carbonate, phosphate, sulphate, and hydroxide species shown in these diagrams are not only controlled by ligand concentration but also by temperature, pH and fO_2. The temperature increases the abundance of certain species over others (Fig. 1-4 vs Fig. 1-7a). The pH of the ore fluid affects the stability of individual ligands, resulting in ligand changes as fluid properties change from acidic to alkaline (Shock et al., 1997, Wood and Samson, 1998, Bastrakov et al., 2010). Specifically, uranium fluoride and sulphate species are predicted to form under more acidic conditions, whereas U(IV) phosphate, carbonate and hydroxide species appear at higher pH. Furthermore, the pH at which a given species is predominant decreases with increasing temperature, as illustrated by the shift to lower pH of the predominance fields of pH-dependent species such as $U(OH)_3^+$ and $UO_2(OH)_3^-$ in Figure 1-6. The prevalence of these individual uranium species is largely impacted by the concentration of the individual ligands in the solution, as seen when comparing Figure 1-6 to Figure 1-8.

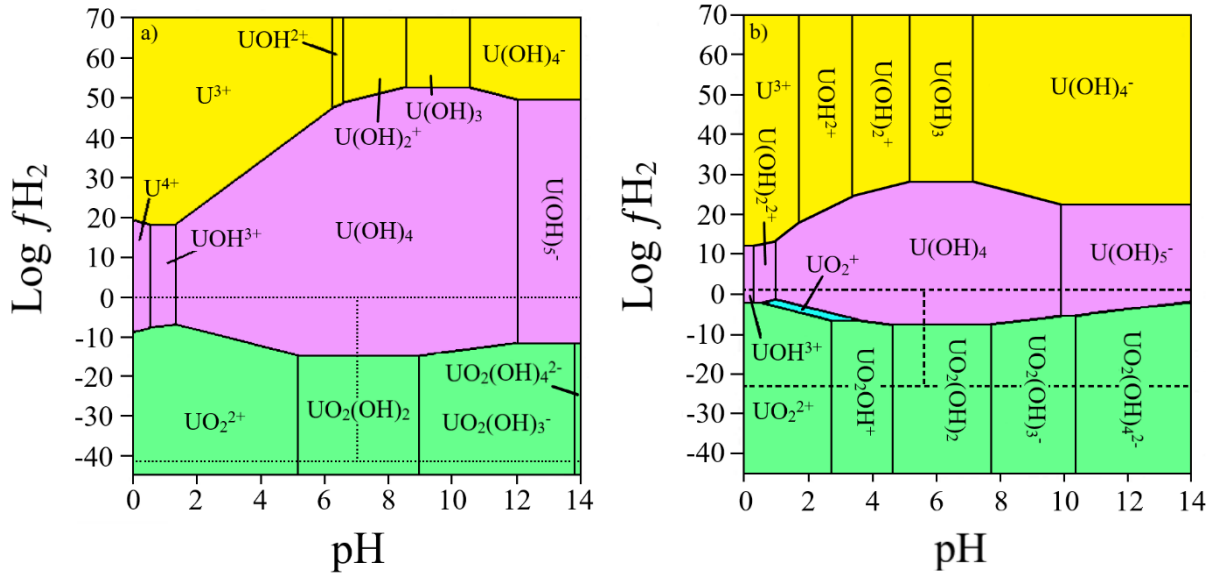

Figure 1-5 LogfH_2-pH diagrams at saturated pressure at a) 25°C and b) 200 °C calculated from Shock et al. (1997). LogfO_2 is related to logfH_2 through the expression $H_2 + 0.5O_2 = H_2O$ The colours in Figures 1-5 and 1-6 correspond to the charge on the uranium (pink is U^{4+}, blue is U^{5+}, and green is U^{6+}), whereas fluoride complexes are identified in light orange.

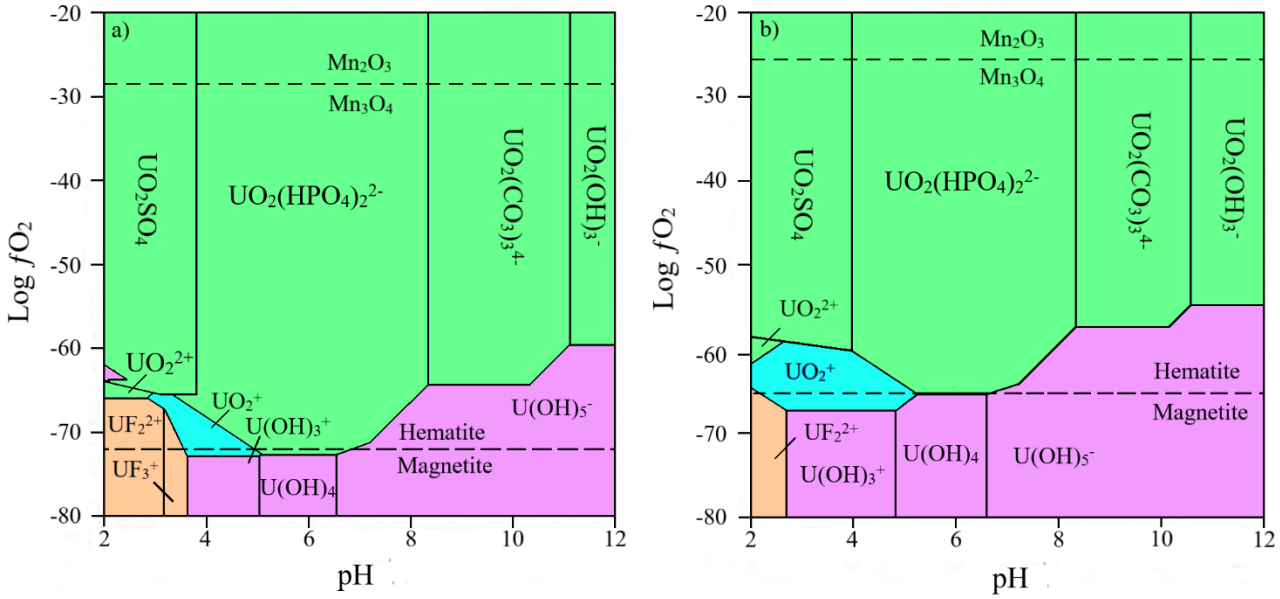

Figure 1-6 LogfO_2-pH diagrams calculated by Bastrakov et al. (2010), representing fluids with 0.15 m Cl^-, 0.003 m C, 0.016 m S, $4x10^{-6}$ m P, $4x10^{-6}$ m F^- and $8x10^{-5}$ m SiO_2 at a) 25 °C, and b) 50 °C.

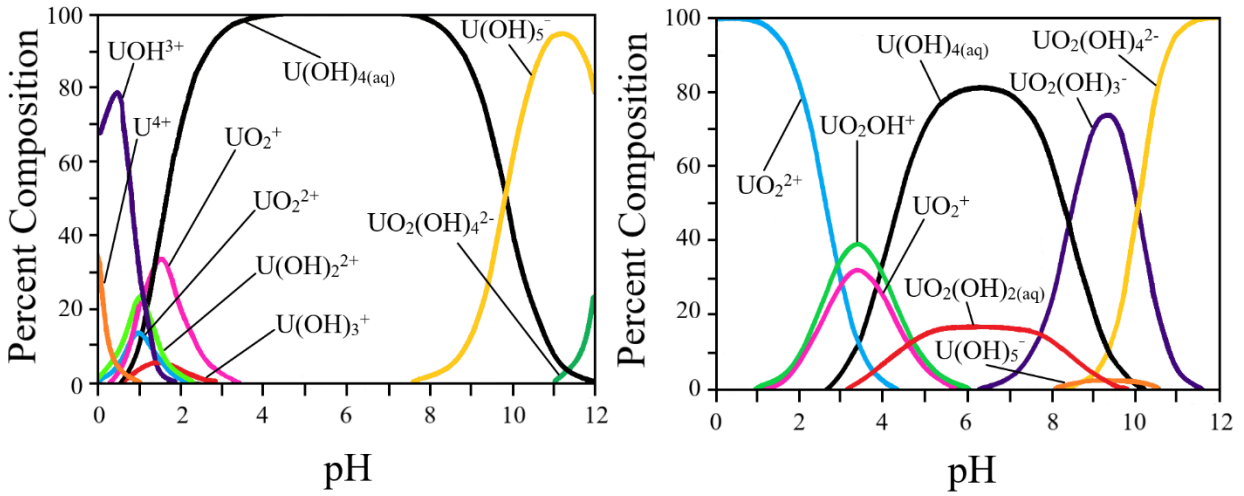

Figure 1-7 Plots of the predicted predominance of uranium species at 200 °C with respect to pH, modified from Shock et al. (1997), at a) logfH_2 = -2, and b) logfH_2 = -7.

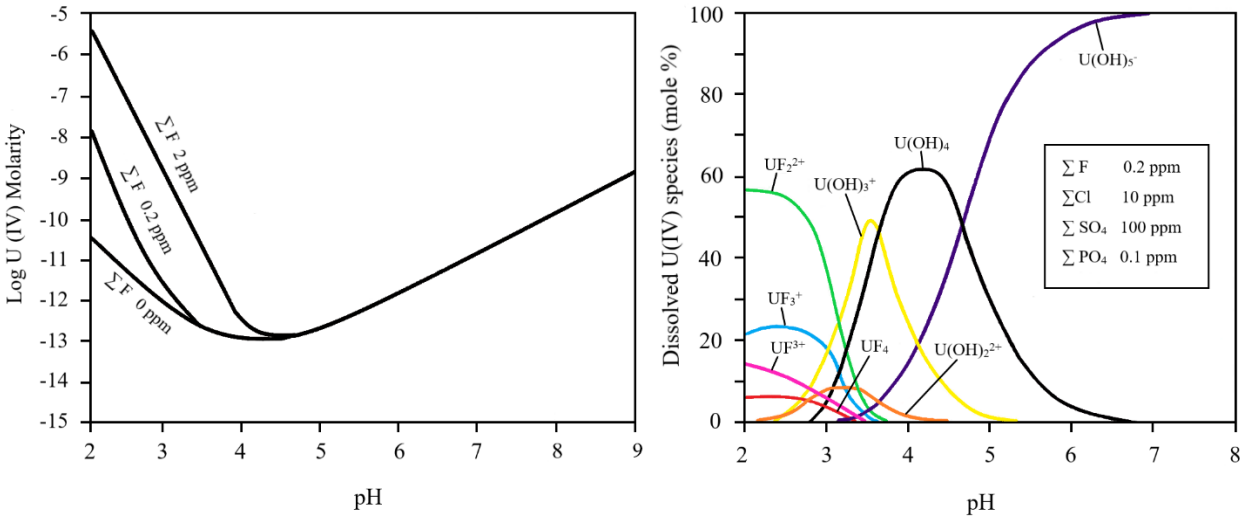

Figure 1-8 a) The influence of fluoride concentration on uranium solubility at 25 °C b) A speciation diagram showing the relative concentration of U(IV) species as a function of pH for ground water at 25°C, modified from Langmuir et al. (1978).

The oxygen fugacity of ore fluids, critical in maintaining the valence state of dissolved uranium, also acts to stabilize individual U(IV) species. As shown in Figure 1-6, U(IV) and (V) species are more stable near or below the hematite-magnetite buffer, whereas the U(VI) species

predominate under more oxidizing conditions. In Figure 1-5, the U(III) species appear at more reduced conditions than those involving U(IV). The fO_2 of the system increases with increasing temperature, as shown by the higher fO_2 of the hematite-magnetite and Mn_2O_3-Mn_3O_4 buffer boundaries (Fig. 1-6a vs. 1-6b), and this increase is accompanied by a shift in the stability fields of the more reduced U(IV) and (V) species to higher fO_2 values. The modeled distributions of uranium (VI) and (IV) species in oxidized and reduced fluids are shown at 200 °C in Figure 1-7. The buffering of oxygen fugacity can be used to set the valence state of uranium in solution; the experiments performed in this study used the hematite-magnetite buffer in order to maintain the uranium in the 4+ state (Fig. 1-9).

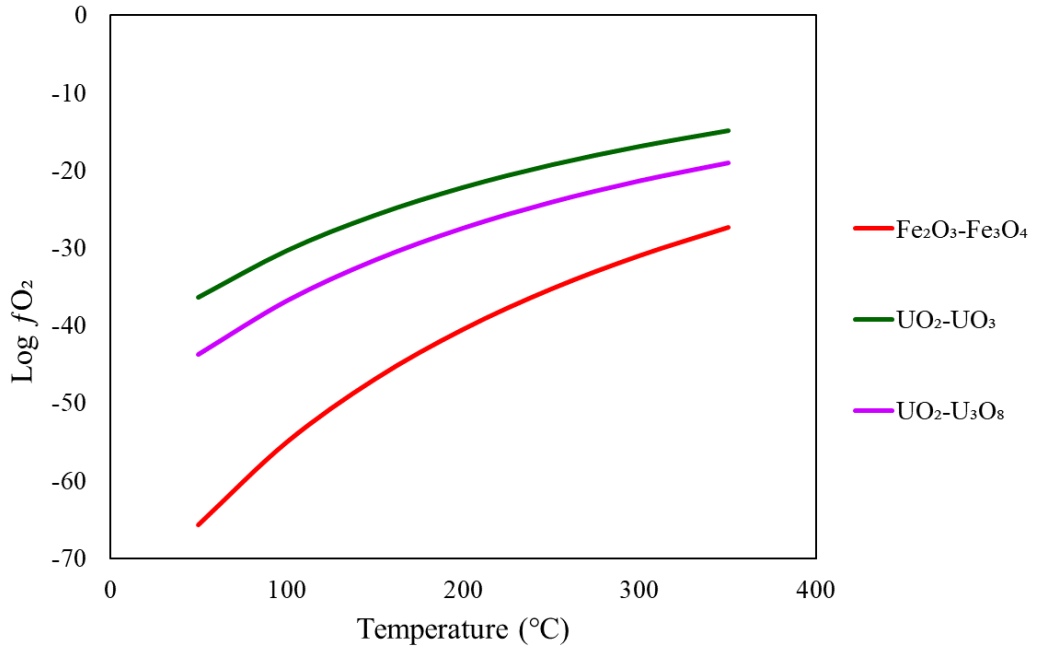

Figure 1-9 A logfO_2-T (°C) diagram displaying the changes in fugacity of uranium solids and the hematite-magnetite buffer, calculated using HCh (Shvarov and Bastrakov, 1999).

Like most metals, uranium possesses prograde solubility with respect to temperature and pressure, or fluid density (Parks and Pohl, 1988, Murphy and Shock, 1999, Guillaumont et al.,

2003, Timofeev et al., 2018). Most dissolved salts also display this behaviour, though fluorite is a notable exception in low-salinity (<6-7 wt. % NaCl) fluids, reaching a solubility maximum near 100 °C, and then precipitating with increasing temperature, becoming insoluble at 260 °C (Richardson and Holland, 1979). Both solubility and speciation are affected by the greater spacing of water molecules in lower-density fluids, which favours ion association and the formation of neutral species and, thus less effective for dissolution (Eugster, 1986). Owing to the strong impact of temperature on solubility and speciation, high-temperature experimental data are necessary for a better understanding of U(IV) speciation.

Table 1-2 The chemical assignment of metals and ligands as proposed by hard-soft-acid-base theory, in which hard and soft ions have higher and lower charge/radius ratios, respectively. After Pearson (1963), Bastrakov et al. (2010) and Williams-Jones and Migdisov (2014).

Hard	**Borderline**	**Soft**
Acid H^+ $Li^+ > Na^+ > K^+ > Rb^+ > Cs^+$ $Be^{2+} > Mg^{2+} > Ca^{2+} > Sr^{2+} > Ba^{2+}$ $Al^{3+} > Ga^{3+}$ $Sc^{3+} > Y^{3+}$; $REE^{3+}(Lu^{3+} > La^{3+})$ $Ce^{4+} > Sn^{4+}$ $Ti^{4+} > Ti^{3+} > Zr^{4+} \sim Hf^{4+}$ $Cr^{6+} > Cr^{3+}$; $Mo^{6+} > Mo^{5+} > Mo^{4+}$ $W^{6+} > W^{4+}$; $Nb^{5+} > Ta^{5+} >$ $V^{6+} > V^{5+} > V^{4+}$ $Mn^{4+} > Fe^{3+} > Co^{3+} > As^{5+} \sim Sb^{5+}$ Th^{4+}; U^{6+}; U^{4+} $PGE^{5+} > PGE^{4+}$	**Acid** $Fe^{2+} > Mn^{2+} > Co^{2+} > Ni^{2+} >$ Cu^{2+}, $Zn^{2+} > Pb^{2+}$, Sn^{2+}, $As^{3+} > Sb^{3+}$, Bi^{3+}	**Acid** $Au^+ > Ag^+ > Cu^+ >$ $Hg^{2+} > Cd^{2+}$ $Pt^{2+} > Pd^{2+} >$ other $PGE^{2+} > Tl^{3+} > Tl^+$
Base $F^- > H_2O$, OH^-, O^{2-}; $NH_3 > NO_3^-$; $CO_3^{2-} > HCO_3^{2-} > SO_4^{2-} > HSO_4^-$; $PO_4^{3-} > HPO_4^{2-} > H_2PO_4^-$; Carboxylate (acetate, oxalate, etc) $MoO_4^{2-} > WO_4^{2-}$	**Base** Cl^-	**Base** $I^- > Br^-$, CN^-; CO; $S^{2-} > HS^- > H_2S$ Organic phosphine(R_3P), organic thiols (RP); polysulphide, thiosulphate, sulphite HSe^-, Se^{2-}, HTe^-, Te^{2-}; AsS_2^-; SbS_2^-

1.2.1 Uranium solubility and speciation at ambient pressure and temperature

1.2.1.1 U(IV) hydroxide species

The thermodynamic properties of the simple ion, U^{4+}, and the U(IV) hydroxides have been well described by experimental studies at ambient conditions, shown for comparison purposes in Table 1-3. The primary hydroxide species are $U(OH)^{3+}$, $U(OH)_2^{2+}$, $U(OH)_3^{+}$, $U(OH)_{4(aq)}$, and $U(OH)_5^{-}$ and, as noted above, the hydroxide ligand number increases with increasing pH of the solution (Kraus and Nelson, 1950, Betts, 1955, Kraus and Nelson, 1955, Gayer and Leider, 1957, Sullivan and Hindman, 1959, Langmuir, 1978, Parks and Pohl, 1988, Grenthe et al., 1989, Rai et al., 1990, Shock et al., 1997, Opel et al., 2007, and Grenthe et al., 2020). The dimeric species $U_2(OH)_2^{6+}$, $U_2(OH)_3^{5+}$, $U_2(OH)_4^{4+}$, and $U_2(OH)_5^{3+}$ may also occur, though they are addressed in only one study (Allard et al., 1980) and are not discussed further here. The dominant species for pH values up to 5.5 are U^{4+}, $U(OH)_2^{2+}$ and $U(OH)_3^{+}$, as illustrated in the speciation diagram from Opel et al. (2007) shown in Figure 1-4. For a pH above 5.5, the dominant species is $U(OH)_{4(aq)}$, and as pH increases further, U(IV) hydroxide species with higher ligand numbers become more important. The species presented here are those predicted for pH values from 0.2 to 10, so as to focus on data near to the pH range that will be considered in this study.

The experimentally-measured solubility products (log K_{sp}) and formation constants (log β) for the hydroxide species are given in Table 1-3, calculated for an ionic strength of zero. The majority of the species are defined as the product of the reaction of U^{4+} and water or OH^-, as follows:

$$U^{4+} + nH_2O \leftrightharpoons U(OH)_n^{4-n} + nH^+ \quad (1)$$

$$U^{4+} + nOH^- \leftrightharpoons U(OH)_n^{4-n} \quad (2)$$

Equations 1 and 2 yield a hydrolysis constant or a formation constant, as shown in Equations 3 and 4, respectively.

$$\log K_{1n} = \log aU(OH)_n^{4-n} - npH - \log aU^{4+} \quad (3)$$

$$\log K_{2n} = \log aU(OH)_n^{4-n} - \log aU^{4+} + npOH \quad (4)$$

The hydrolysis constants involving H_2O and OH^- are labeled as log K_{1n} and log K_{2n}, respectively, where n is the number of hydroxide groups in the uranous species (Equations 1 and 2). The equilibrium constants for U^{4+} are significantly lower than those of the hydroxides shown in Table 1-3, as the formation of the free ion from UO_2 dissolution requires the breaking of either amorphous or crystalline UO_2 into U^{4+} and hydroxide, whereas the uranium hydroxide species presented use free U^{4+} as shown in Equations 1 and 2 (Grenthe et al., 2020).

The equilibrium constants for U^{4+} and UOH^{3+} were initially determined by Kraus and Nelson (1950, 1955), Betts (1955), and Rai et al. (1990). Later studies, such as those by Rai et al. (2003) and Fujiwara et al. (2003), report values that agree with the former within some degree of error (Table 1-3). The U^{4+} constants determined by Rai et al. (1990) are within the range of measurement error for the use of $UO_{2(cr)}$ which, according to Neck and Kim (2001), has a solubility product (log K_{sp}) of -54.5±0.1. Amorphous and crystalline UO_2 have differing log K_{sp} values, reported by Opel et al. (2007) to be -54.6±1.0 and -59.6±1.0, respectively. In other studies, such as that of Fujiwara et al. (2003), the thermodynamic properties of U^{4+} and UOH^{3+} were calculated from the results of experiments involving solvent extraction instead of hydrolysis, in which the U(IV) hydroxide interacted with thenoyltrifluoroacetone (TTA) and the

uranium was bonded to the TTA, whereas the hydroxide formed hydrogen ions and water. This paper only presents data in the form of Equation 2 and a log K is not provided for UOH^{3+}. Nevertheless, the formation constant presented agrees with that estimated as -13.6 ± 0.2 by Neck and Kim (2001).

The simple U^{4+} ion and UOH^{3+} predominate under acidic conditions, as seen in Figure 1-4. The latter species is relatively unimportant, being present in only small concentrations at pH levels below 3.5. Opel et al. (2007) found that U^{4+} predominates under extremely acidic conditions (pH less than 1.5), a result supported by results reported by Rai et al. (2003), who measured the stability constant of U^{4+} in acidic solutions with pH values as low as 0.2. The increased stability of U^{4+} is due to the low concentrations of OH^- in acidic solutions. Under highly acidic conditions (e.g., pH 1), there is a potential for uranium colloids to form, which can increase the true solubility by orders of magnitude (Opel et al., 2007). In order to avoid this problem, Opel et al. (2007) used laser-induced breakdown detection to determine the presence of these colloids when measuring the proportions of uranium species.

The stability of the $U(OH)_2^{2+}$ and $U(OH)_3^{+}$ species were determined by Grenthe et al. (1989) and Bruno et al. (1986), respectively (Table 1-3). The equilibrium constants determined in these studies are similar to those derived in later studies by Rai et al. (1990) and Fujiwara et al. (2003). These later values are the most widely accepted and have been used in thermodynamic modeling studies such as those by Opel et al. (2007; Fig. 1-4) and Shock et al. (1997; Fig. 1-5). Opel et al. (2007) demonstrated through modeling stability constants that $U(OH)_2^{2+}$ is dominant at pH values of approximately 1.5 to 3.5 (Fig. 1-4).

The log K value for $U(OH)_{4(aq)}$ was originally determined to be -4.4 by Bruno et al. (1986), which is far lower than the value of -10.3 later reported by Rai et al. (1990), the latter of

which is supported by the log K value of -8.5 ± 1.0 calculated by Neck and Kim (2001) (Table 1-3). The difference is potentially due to Bruno et al. (1986) having an error in reporting the $UO_{2(c)}$ values (Rai et al. 2003). Fujiwara et al. (2003), as stated earlier, performed experiments using solvent extraction instead of hydrolysis, and obtained a log β value for $U(OH)_{4(aq)}$ that is different from those obtained by Bruno et al. (1986) and Rai et al. (1990), but, their value of 45.44±0.40 is in agreement with the estimate of 46.0±1.0 by Neck and Kim (2001). This is likely due to the fact that the constants determined by Fujiwara et al. (2003) and Neck and Kim (2001) were calculated for an ionic strength of zero. A limitation of the study of Fujiwara et al. (2003) is that it reports formation constants (Table 1-3) but does not report equilibrium constants. As seen in Figure 1-4, $U(OH)_{4(aq)}$ is the dominant hydroxide species at a pH of 5.5 and above (Opel et al., 2007).

Rai et al. (1990) derived a log K value for $U(OH)_5^-$ of -16.0. For an ionic strength of zero, the value for this constant was recalculated to be < -48.10 by Grenthe et al. (2020). However, $U(OH)_5^-$ is thought to be dominant only at pH values greater than 10 (Parks and Pohl, 1988) and, as such, its behaviour is beyond the scope of this study. Similarly, the stability constant for $U(OH)_6^{2-}$ has been determined (Table 1-3), but this species likely is present only at conditions more basic than those for the $U(OH)_5^-$ species.

Table 1-3 Experimentally-determined equilibrium constants for U^{4+} and U(IV) hydroxide species. The pressure is 1 bar except for the data of Parks and Pohl (1988) that are for a pressure of 500 bars. Log K_{sp} is the solubility product of UO_2, log K_{1n} is the hydrolysis constant, and log K_{2n} is the equilibrium constant for the reaction of U^{4+} with OH^- (see text for details).

U(IV) species	Ionic Strength (M)	T (°C)	Experimental method	Equilibrium constants	Reference
U^{4+}	0.1 HCl, NaOH, NaCl	300	Spectrophotometric	Log K_{sp}=-63.0[a]	Parks and Pohl, 1988
	0.05±0.01 HCl, NaOH	21±2	Spectroscopic	log K_{sp}=-52.6±0.8	Rai et al., 1990
	0.05±0.01 HCl, NaOH	22		logK_{sp}=≤ -60.20±0.24	Rai et al., 2003
	I = 0	25		log$K°_{sp(amor)}$=-54.5±1.0	Neck and Kim, 2001[b]
	0.1,0.5,1 $HClO_4$, $NaClO_4$	25	Solvent extraction	logK_{sp}=-53.93 ±0.20	Fujiwara et al., 2003
	0.2 $NaClO_4$	23±2	Laser fluorescence spectroscopy	log$K_{sp(amor)}$=-54.6±1.0 log$K_{sp(cr)}$ = -59.6±1.0	Opel et al., 2007
UOH^{3+}	0.017 to 2.0 $HClO_4$, $NaClO_4$	25	Spectrophotometric	logK_{11}=-1.63 ± 0.09 to -0.92 ± 0.09	Kraus and Nelson, 1950
	0.5 $HClO_4$, $NaClO_4$	10-43		logK_{11}=-1.00 to -1.90 ±0.09	Kraus and Nelson, 1955
	0.19 $HClO_4$	25		logK_{11}= -1.1±0.2	Bett, 1955
	0.5 $HClO_4$	25	Potentiometric	logK_{11}= -1.44	Gayer and Leider, 1957
	3 $HClO_4$, $NaClO_4$	25	Spectrophotometry	logK_{11}= -1.65±0.05	Grenthe et al., 1989
	0.05±0.01 HCl, NaOH	21±2	Spectroscopic	logK_{11}= -0.50	Rai et al., 1990
	I = 0	25		log$β°_1$= 13.6±0.2	Neck and Kim, 2001[b]
	0.1,0.5,1 $HClO_4$, $NaClO_4$	25	Solvent extraction	log$β_1$= 13.71±0.21	Fujiwara et al., 2003[c]
$U(OH)_2^{2+}$	3 $HClO_4$, $NaClO_4$	25	Spectrophotometry	logK_{12}= <-4.50	Grenthe et al., 1989
	0.05±0.01HCl, NaOH	21±2	Spectroscopic	logK_{12}= -2.6	Rai et al., 1990
	I = 0	25		log$β°_{12}$= 26.9±1.0	Neck and Kim, 2001[b]
	0.1,0.5,1 $HClO_4$, $NaClO_4$	25	Solvent extraction	log$β_2$= 26.12 ±0.21	Fujiwara et al, 2003[c]
$U(OH)_3^{+}$	0.5 $NaClO_4$	25	Spectrophotometric	logK_{13} = -0.5 ± 0.1 log$β_{13}$ = -1.1 ± 0.1	Bruno et. al, 1986
	0.05±0.01 HCl, NaOH	21±2	Spectroscopic	logK_{13}= -5.8	Rai et al., 1990
	I = 0	25		log$β°_{13}$= 37.3±1.0	Neck and Kim., 2001[b]
	0.1,0.5,1 $HClO_4$, $NaClO_4$	25	Solvent extraction	log$β_3$= 36.85±0.36	Fujiwara et al., 2003[c]
$U(OH)_4$	0.5 $NaClO_4$	25	Spectrophotometric	logK_{14} = -4.4 ± 0.2 log$β_{14}$ = -5.4 ± 0.2	Bruno et. al, 1986
	0.1 HCl, NaOH, NaCl	300	Spectrophotometric	logK_{sp4}= -9.47±0.3	Parks and Pohl, 1988
	0.05±0.01 HCl, NaOH	21±2	Spectroscopic	logK_{14}= -10.3	Rai et al., 1990
	I = 0	25		log$β°_{14}$= 46.0±1.4	Neck and Kim., 2001[b]
	0.1,0.5,1 $HClO_4$, $NaClO_4$	25	Solvent extraction	log$β_4$= 45.44±0.40	Fujiwara et al., 2003[c]
$U(OH)_5^{-}$	0.05±0.01 HCl, NaOH	21±2	Spectroscopic	logK_{15}= -16.0	Rai et al., 1990
	0.1,0.5,1 $HClO_4$, $NaClO_4$	25	Solvent extraction	log$β_5°$= <48.10	Fujiwara et al., 2005[c]
$U(OH)_6^{2-}$	0.1,0.5,1 $HClO_4$, $NaClO_4$	25		log$β_6°$= 48.95±1.01	Fujiwara et al., 2005[c]

[a] Calculated in Rai et al. (2003). [b] Calculated using data from NEA and IAEA. [c] Log K was not reported in this study.

The low-temperature data reviewed above were assessed by Shock et al. (1997), who have recalculated these data for elevated temperatures and pressures. The 200 ºC speciation model presented in this study indicates that the dominant hydroxide species at a pH of 10 is HUO_3^-, whereas $UO_{2(aq)}$ predominates at pH values between 2 and 10 and the dominant species below a pH of 2 are UO^{2+} and $U(OH)^{3+}$ (Fig. 1-7a). Shock et al. (1997) also investigated the impact of oxygen fugacity (presented as hydrogen fugacity, fH_2, in their study) on the solubility of various species. For example, if log fH_2 is -2 at 200 °C, $UO_{2(aq)}$ predominates from a pH of 2 to 10, and from a pH of 4 to 8 at a log fH_2 of -7 (Fig. 1-7).

1.2.1.2 U(IV) fluoride species

This discussion focuses on U(IV) fluoride and carbonate species, which have been investigated in numerous experimental and theoretical studies under ambient conditions and are of direct relevance to the present study. The reliability of the available experimental data were critically reviewed by Langmuir (1978), who produced a set of thermodynamic data for uranium species for groundwater conditions, and later by Grenthe et al. (1992, 2020) and Guillaumont (2003), who also determined the average formation constants of U species based on prior studies.

Langmuir (1978) modeled the speciation of uranium in both reduced and oxidized aqueous fluids at ambient temperatures with phosphate, sulphate, chloride, and fluoride. The model predicted the formation in oxidized groundwater of a mixture of U(VI) fluoride, oxide, and sulphate species at pH < 4, U(VI) phosphate species at pH 4-8, and U(VI) carbonate species at pH >8. Under reducing conditions, however, only U(IV) fluoride (pH < 3) and hydroxide (pH > 3) species were important, whereas the sulphate, phosphate and chloride concentrations were

negligible (Fig. 1-8b). The model also predicted an increase in UO_2 solubility of over two orders of magnitude in acidic fluids if fluoride was present (Fig. 1-8a). These results suggest that fluoride can be an important ligand for U(IV) transport under acidic conditions and furthermore, as suggested by the author, dissolved fluoride precipitated as fluorite can lead to precipitation of U(IV) because of the destabilization of U(IV) fluoride complexes. These findings were later used in the model of Bastrakov et al. (2010) (Fig. 1-6). The speciation of uranium hydroxides differs between models with and without fluoride (Fig. 1-4 vs Fig. 1-8b). This is potentially due to the displacement of hydroxide species by fluoride species, as discussed latter in this section.

The solubility of U(IV) and U(VI) in acidic fluids at ambient temperature was evaluated by Grenthe et al. (1969) and Norén (1969), who determined the equilibrium constants for the U(IV) fluoride species UF^{3+} and UF_2^{2+} (Table 1-4). Their results are supported by data from Kakihana and Ishiguro (1974) and Sawant et al. (1990), after correcting the data from the latter studies to the same ionic strength of zero with specific ion interaction theory and the following reaction and equation:

$$mM + qL + nH_2O \leftrightharpoons M_mL_q(OH)_n + nH^+ \quad (5)$$

$$log^*\beta^o_{q,n,m} = log^*\beta_{q,n,m} + m\ log\ \gamma_M + q\ log\ \gamma_L + n\ log\ a_{H_2O} - log\ \gamma_{q,n,m} - n\ log\ \gamma_{H^+} \quad (6)$$

In this correction, the stability constant at an ionic strength of zero ($log^*\beta°_{q,n,m}$) is obtained by taking the formation constant at a given ionic strength ($log^*\beta_{q,n,m}$) and either adding or subtracting the log activity coefficients and the log activity of water depending on whether they are the products or the reactants (Grenthe et al., 1992). At fluoride concentrations from $10^{-7.5}$ to 10^{-6} m and 10^{-6} to $10^{-4.5}$ m, the dominant U(IV) fluoride species are UF^{3+} and UF_2^{2+}, respectively

(Kakihana and Ishiguro, 1974). At these relatively low fluoride concentrations, the higher ligand number U(IV) fluoride species are less likely to form due to ligand unavailability. Many of these experiments were performed under acidic conditions, that favour the formation of fluoride species (Langmuir, 1978).

Table 1-4 Experimentally-determined equilibrium constants for U(IV) fluoride species at 20-25 °C and 1 bar.

U(IV) species	Ionic Strength (M)	T (°C)	Experimental method	Equilibrium constants	References
UF^{3+}	1 $NaClO_4$ & $HClO_4$	25	Potentiometric	$\log K_1 = 5.37 \pm 0.01$ $\log\beta_1 = 9.42 \pm 0.25$[b]	Grenthe et al., 1969
	4 $HClO_4$	20	Fluoride membrane electrode	$\log K_1 = 5.55 \pm 0.2$ $\log\beta_1 = 9.54 \pm 0.25$[b]	Norén, 1969
	1 NaCl & HCl	25	Potentiometric and spectrophotometric	$\log K_1 = 4.50 \pm 0.04$ $\log\beta_1 = 9.28 \pm 0.15$[b]	Kakihana and Ishiguro, 1974
	1 $NaClO_4$ & $HClO_4$	25	Fluoride membrane electrode	$\log K_1 = 4.82 \pm 0.16$[a] $\log\beta_1 = 9.09 \pm 0.17$[b]	Choppin and Unrein, 1976 [a]
	1 M $HClO_4$	25	Potentiometric	$\log K_1 = 8.47 \pm 0.01$ $\log\beta_1 = 9.78 \pm 0.12$[b]	Sawant et al., 1990
Average $\log\beta_1$				$\log\beta_1 = 9.42 \pm 0.51$	Grenthe et al., 2003
UF_2^{2+}	1 $NaClO_4$ & $HClO_4$	25	Potentiometric	$\log K_2 = 8.29 \pm 0.01$ $\log\beta_2 = 16.37 \pm 0.50$[b]	Grenthe et al., 1969
	4 $HClO_4$	20	Fluoride membrane electrode	$\log K_2 = 8.72 \pm 0.3$ $\log\beta_2 = 16.72 \pm 0.50$[b]	Norén, 1969
	1 NaCl & HCl	25	Potentiometric and spectrophotometric	$\log K_2 = 7.45 \pm 0.02$ $\log\beta_2 = 16.16 \pm 0.16$[b]	Kakihana and Ishiguro, 1974
	1 $HClO_4$	25	Potentiometric	$\log K_2 = 14.66 \pm 0.02$ $\log\beta_2 = 16.97 \pm 0.13$[b]	Sawant et al., 1990
Average $\log\beta_2$				$\log\beta_2 = 16.56 \pm 0.71$	Grenthe et al., 2003
UF_3^{+}	4 $HClO_4$	20	Fluoride membrane electrode	$\log K_3 = 10.71 \pm 0.5$ $\log\beta_3 = 22.06 \pm 0.50$[b]	Norén, 1969
	1 NaCl & HCl	25	Potentiometric and spectrophotometric	$\log K_3 = 8.95 \pm 0.05$ $\log\beta_3 = 21.23 \pm 0.17$[b]	Kakihana and Ishiguro, 1974
	1 $HClO_4$	25	Potentiometric	$\log K_3 = 19.50 \pm 0.04$ $\log\beta_3 = 22.38 \pm 0.14$[b]	Sawant et al., 1990
Average $\log\beta_3$				$\log\beta_3 = 21.89 \pm 0.89$	Grenthe et al., 2003
$UF_{4(aq)}$	1 NaCl & HCl	25	Potentiometric and spectrophotometric	$\log K_4 = 10.11 \pm 0.21$ $\log\beta_4 = 25.61 \pm 0.23$[b]	Kakihana and Ishiguro, 1974
	1 $HClO_4$	25	Potentiometric	$\log K_4 = 23.93 \pm 0.07$ $\log\beta_4 = 27.06 \pm 0.12$[b]	Sawant et al., 1990
Average $\log\beta_4$				$\log\beta_4 = 26.34 \pm 0.96$	Grenthe et al., 2003
UF_5^{-}	0.12 $HClO_4$	25	Radioassay	$\log K_5 = -2.39 \pm 0.025$ $\log\beta_5 = 27.01 \pm 0.31$[a]	Savage and Browne, 1960
UF_6^{2-}	0.12 $HClO_4$	25		$\log K_6 = -0.08 \pm 0.08$ $\log\beta_6 = 29.08 \pm 0.20$[a]	Savage and Browne, 1960

[a] Data listed in Grenthe et al. (1992); [b] Calculated for I=1 and 23 °C $HClO_4$, $NaF_{(aq)}$

The equilibrium constants for the formation of UF_3^{+} and $UF_{4(aq)}$ were determined by Norén (1969) and Kakihana and Ishiguro (1974) and are listed in Table 1-4. These values are in agreement with those of Sawant et al. (1990). The UF_3^{+} species is present under acidic conditions, though it is not usually the most important species in solution (Langmuir, 1978). This

species is present at a fluoride concentration of 10^{-4} m, though the peak concentration of the species is predicted to occur at $10^{-4.5}$ m F^- (Fig. 1-10). Above a fluoride concentration of $10^{-4.5}$ m, the dominant U(IV) fluoride species is $UF_{4(aq)}$ (Kakihana and Ishiguro, 1974).

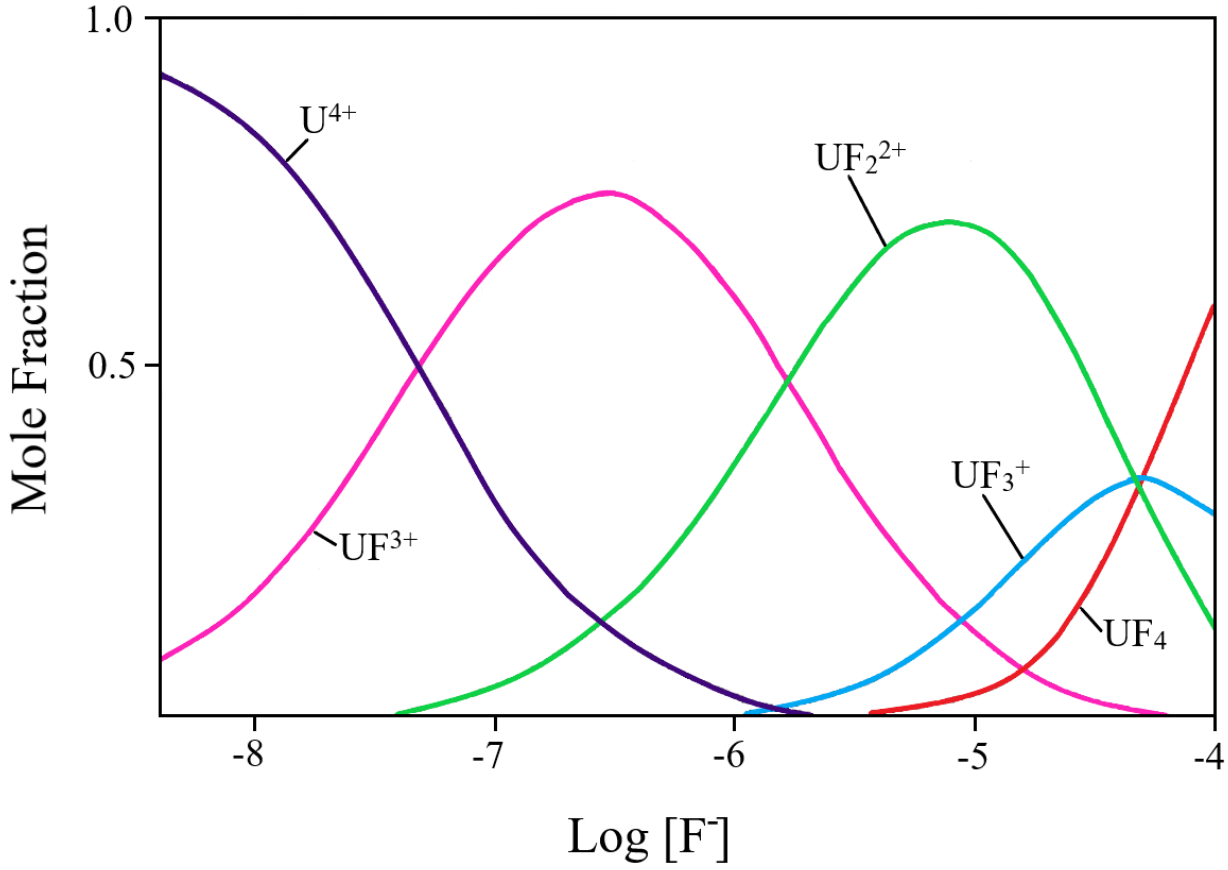

Figure 1-10 A speciation diagram displaying the dominant U(IV) fluoride species as a function of fluoride concentration at ambient and acidic conditions ($[H^+]$ >0.1 M), modified from Kakihana and Ishiguro (1974).

The higher ligand number fluorides, UF_5^- and UF_6^{2-}, have only been considered by Savage and Browne (1960). These authors determined uranium speciation constants for UF_5^- using the equilibria in the following reactions:

$$2UF_4 \cdot 5H_2O \leftrightharpoons 2UF_4^0(aq) + 5H_2O \quad (7)$$

$$UF_4^0 + F^- \leftrightharpoons UF_5^- \quad (8)$$

The formation constant for the species UF_6^{2-} may be determined using an equation similar to Equation 8 in which UF_5^- replaces UF_4 with one fluoride to form UF_6^{2-}. The use of $2UF_4 \bullet 5H_2O$ as a reagent could have impacted on the relevance of their results, as most uranium ore occurs as UO_2 or U_3O_8 (Cunningham et al., 1998, Hu et al., 2008). The data could also be less dependable as there is no reliable secondary source to verify their accuracy, and for some of the log K values such as those for UF_6^{2-}, the magnitude of the log K value is similar to that of the error (Table 1-4).

In a fluoride-bearing fluid at low pH, the more stable U(IV) fluoride species may displace the low-ligand number U(IV) hydroxide species that occur at low pH in a fluoride-free fluid (Fig. 1-4 vs. Fig. 1-8b). As seen in Tables 1-3 and 1-4, the fluorides are more stable than the hydroxides, which is reflected in their higher formation constants. The U(IV) fluoride species are also more abundant than hydroxides in acidic, high-fluoride, reduced fluids (Figs. 1-6 and 1-8b). Given the stability of these U(IV) fluoride species at ambient conditions, they are likely important at high temperature as well, and must be studied under hydrothermal conditions.

1.2.2 U(IV) species at elevated temperatures

Few experimental studies have been conducted on the solubility of UO_2 at elevated temperature, and two of these (Kovalenko et al., 2011; Timofeev et al., 2018) employed HCl-bearing solutions. Only the study of Kovalenko et al. (2012) evaluated U(IV) speciation in HF solutions. Chloride solutions are less relevant to this thesis but are nonetheless important to

understand how U(IV) might be transported in hydrothermal fluids. Another such high temperature experimental study is that of Parks and Pohl (1988) who investigated U(IV) hydroxide speciation.

Parks and Pohl (1988) determined stability constants for U(IV) hydroxide species at temperatures of 100 to 300 °C and 500 bars. They determined the log K value for $U(OH)_{4(aq)}$ at 300 °C to be -9.47, which is several times higher than predicted by ambient temperature data. Using the data of Parks and Pohl (1988), Rai et al. (2003) calculated a stability constant for U^{4+} of -63.0. An issue with the study of Parks and Pohl (1988) is a local solubility maximum at pH 3, that the authors attributed to fluoride contamination leached from the fluorocarbon plastic used in the H_2 diffuser valve and buffer capsules present in some runs. Another issue with this study is that the authors filtered their cooled experimental solutions prior to acidification, which would have removed any uranium precipitated from solution during quenching and resulted in a minimum UO_2 solubility.

Kovalenko et al. (2011) performed experiments to assess uranium hydroxy-chloride speciation at 500 °C and 1 kbar. The fO_2 of the experiments was buffered using the nickel-nickel oxide assemblage to ensure that the uranium was in the +4 state. The authors concluded that there was a progressive shift in the dominant uranium species with increasing HCl concentration, from $U(OH)_{4(aq)}$ at low chloride concentrations, to $U(OH)_3Cl_{(aq)}$ at 0.05-0.1 m Cl^-, $U(OH)_2Cl_{2(aq)}$ at 0.1-0.3 m Cl^-, $UOHCl_{3(aq)}$ at > 0.5 m Cl^-, and finally to $UCl_{4(aq)}$ at > 1 m Cl^-. However, whereas their range of chloride concentrations extends from 0.001 to 2 m HCl, only two data points were collected between 0.01 and 0.001 m, so the nature of the chloride-free species is poorly constrained. Using their experimental data, the authors calculated the solubility constants for the formation of $U(OH)_3Cl_{(aq)}$, $U(OH)_2Cl_{2(aq)}$ and $U(OH)Cl_{3(aq)}$ as -5.00, -3.56, and -3.05

respectively (Kovalenko et al., 2011). The authors then used the Bryzgalin-Ryzhenko model and existing 25 °C data for $U(OH)_{4(aq)}$ to calculate a log K of $UCl_{4(aq)}$ of -7.02. A potential shortcoming of these experiments is that chloride concentration and pH were not independently controlled, and higher HCl concentrations resulted in more acidic solutions, thus, the changes in speciation may have been affected by pH as well as ligand content, i.e., differences in pH may have affected the concentrations of a particular uranium hydroxy-chloride species (Opel et al., 2007).

Timofeev et al. (2018) investigated the solubility of UO_2 in chloride-bearing acidic solutions at temperatures ranging from 250 to 350 °C. As with the experiments of Kovalenko et al. (2011), oxygen fugacity was buffered with Ni-NiO to maintain reducing conditions. In this study, chloride concentrations (0.3 to 1.5 m) and pH (1.40 to 1.70) were assessed independently with variable concentrations of HCl and NaCl. The authors found that, with decreasing pH and increasing temperature, the concentration of uranium in solution increased. They also found that the activity of chloride and uranium increased in parallel, showing that the U(IV) was dissolved as a chloride species (Timofeev et al., 2018), $UCl_{4(aq)}$, and used their data to calculate a formation constant for this species of 19.8±0.06 at 350 °C (Table 1-5). This value is very different from that of Kovalenko et al. (2011) at 500 °C, likely because the latter authors calculated their log K by extrapolation from room temperature data. The results of Timofeev et al. (2018) showed that the transport of U(IV) in solution is important for reduced ore systems such as those discussed in Section 1.1.

Using a method similar to that of Kovalenko et al. (2011), Kovalenko et al. (2012) performed experiments at 500 °C and 1 kbar with the Ni-NiO fO_2 buffer, and investigated the solubility of UO_2 in fluoride-bearing solutions in which both the pH (4.04-5.75) and the fluoride

concentration were controlled by HF (0.0001-0.5 m). As shown in Figure 1-11, the authors observed an increase in uranium solubility with increasing concentration of HF to 0.1 m, above which the uranium concentration was relatively constant. From their experimental data, the authors determined that the dominant U(IV) species are $U(OH)_3F_{(aq)}$, $U(OH)_2F_{2(aq)}$, $U(OH)F_{3(aq)}$, and UF_4. However, based on an analogy with unpublished work on Ti- and Zr fluorides, they assumed that only neutral species were present, which means that charged species such as U^{4+} were not considered in their study. This assumption is not likely valid for the lower-temperature fluids of most hydrothermal U deposits (Eugster, 1985). The log K values for $U(OH)_3F_{(aq)}$, $U(OH)_2F_{2(aq)}$, and $U(OH)F_{3(aq)}$, were determined by them to be -1.29, -3.15 and -2.24, respectively (Kovalenko et al., 2012). They also determined that the equilibrium constant for the reaction of UO_2 and HF to produce $UF_{4(aq)}$ was log K_4 = -1.17.

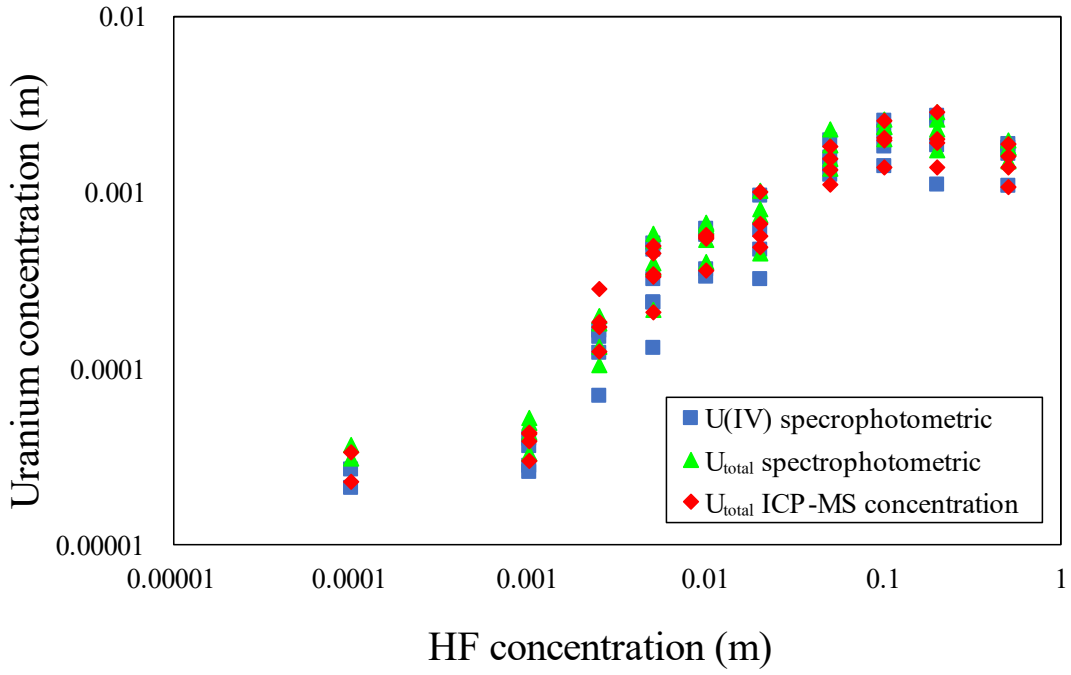

Figure 1-11 Uranium concentrations versus HF concentrations for solubility measurements at 500 °C and 1 kbar, from Kovalenko et al. (2012). The blue squares are spectrophotometric measurements of U(IV), the green triangles are spectrophotometric measurements of total uranium concentration, and the red diamonds are the total uranium concentration measured with ICP-MS.

Insights into the speciation of uranium in aqueous fluids can also be gained from fluid-melt partitioning experiments. Keppler and Wyllie (1990) conducted experiments on uranium partitioning between a HF solution and a U-doped haplogranitic melt at 750 °C and 2 kbar, using the Ni-NiO fO_2 buffer to ensure the stability of U(IV), as well as variable HF concentrations. They observed a notable increase in the fluid-melt partition coefficient ($D_{fluid/melt}$) from 0 to 0.45 with an increase in HF from 0 to 4 m, which is compelling evidence for aqueous U(IV) fluoride speciation. The authors also assessed the effect of CO_2 on uranium partitioning and found that $D_{fluid/melt}$ (0-0.033 m) increased with CO_2 molality (0-5 m). This increase, however, was much lower than that seen in the fluoride system, indicating that complexation of uranium with carbonate is likely to be less important than uranium-fluoride complexation. In similar partitioning studies performed at 770 °C and 2 kbar, Peiffert et al. (1994, 1996) concluded that the concentration of U(IV) in a NaF solution equilibrated with a haplogranitic melt was about 200x higher than the U(IV) concentration in a Na_2CO_3 solution, again suggesting that fluoride complexation with uranium is far stronger than that of carbonate.

Table 1-5 Solubility products (Log K_{sp}) for the dissolution of $UO_{2(c)}$ as chloride and fluoride complexes from Kovalenko et al. (2011,2012) and Timofeev et al. (2018), and the formation constant of UCl_4^0 from U^{4+} ($log\beta_1$) from Timofeev et al. (2018).

Speciation reaction	T (°C)	Equilibrium constants	References
$UO_{2(cr)} + 4Cl^- + 4H^+ = UCl_4 + 2H_2O$	350	logK = 7.96 ±0.14	Timofeev et al, 2018
$U^{4+} + 4Cl^- + 4H^+ = UCl_4$		$log\beta_1$ = 19.8 ± 0.06	
$UO_{2(cr)} + H_2O + HCl^- = U(OH)_3Cl$	500	logK = -5.25	Kovalenko et al, 2011
$UO_{2(cr)} + 2HCl^- = U(OH)_2Cl_2$		logK = -3.56	
$UO_{2(cr)} + 3HCl^- = U(OH)Cl_3$		logK = -3.05	
$UO_{2(cr)} + 4HCl^- = UCl_4 + 2H_2O$		logK = -7.02	
$UO_{2(cr)} + H_2O + HF^- = U(OH)_3F$		logK = -1.29	Kovalenko et al, 2012
$UO_{2(cr)} + 2HF^- = U(OH)_2F_2$		logK = -3.15	
$UO_{2(cr)} + 3HF^- = U(OH)F_3$		logK = -2.24	
$UO_{2(cr)} + 4HF^- = UF_4 + 2H_2O$		logK = -1.17	
$UO_{2(cr)} + 4HCl^- = UCl_4 + 2H_2O$ [a]		logK= 4.33	Timofeev et al, 2018

[a] Predicted by Timofeev et al. (2018) for 500 °C and 1 kbar.

1.2.3 Theoretical models of natural systems using uranium fluoride species

The models for U(IV) fluoride species discussed in this section are based on data collected at 25 °C and 1 bar (Grenthe et al., 1969, Norén, 1969, Kakihana and Ishiguro, 1974, Choppin and Unrein, 1976, Sawant et al., 1990, and Guillaumont et al., 2003), employed at both ambient conditions for an investigation of surface water chemistry (Barsukov and Borisov, 2003) and at elevated temperature using extrapolations to study ore deposit genesis (Bastrakov et al., 2010, Xing et al., 2018). Although, in principle, extrapolation of data collected at ambient conditions can be used to determine stability relationships at elevated temperatures, such extrapolations are commonly unreliable. These extrapolations used the thermodynamic modeling software HydroChemistry (HCh), which employs a Gibbs free energy minimization approach to calculate the species at equilibrium in a fluid or fluid-rock system at given P-T-X conditions (Shvarov, 1999).

A thermodynamic modeling study by Barsukov and Borisov (2003) using HCh assessed the solubility of various crystalline uranium-bearing solids and uranium speciation in groundwater and deep seawater. The primary uranium species predicted to occur at pH 4.5-9 were $U(OH)_{4(aq)}$, $UO_2(OH)_{2(aq)}$ and $UO_2(OH)_3^-$, among which $U(OH)_{4(aq)}$ occurs at equilibrium with U and UO_2 solids and at low Eh, whereas the U(VI) species occur at equilibrium with U_3O_8 and $UO_2(OH)_2$ solids and at high Eh. Minor concentrations of U(VI) oxychloride species were observed in acidic fluids, and U(VI) carbonate species were found to be dominant at alkaline conditions. In agreement with Langmuir (1978), U(IV) fluoride species were predicted to be important in acidic fluids with pH values of 0.16 to 3.8.

Bastrakov et al. (2010) carried out an HCh modeling study presenting a more complete assessment of uranium speciation in higher-temperature environments (up to 300 °C), using data extrapolated from 25 °C. The model investigates the speciation of U(IV), (V) and (VI) in a multi-ligand fluid (NaCl, KCl, H_3PO_4, H_2S) under a variety of P-T-X conditions. Similar to the 25°C studies of Langmuir (1978) and Barsukov and Borisov (2003), this study predicted that U(IV) fluoride species may be important at low pH, whereas carbonate and hydroxide complexes become important under alkaline conditions (Fig. 1-6). They incorporate the results were incorporated into models for various hydrothermal systems, including a roll-front uranium deposit, which involved the reaction of a multi-ligand fluid with a sandstone. The authors found that, in keeping with the current dogma, uranium is most soluble as U(VI), and precipitates as U(IV) when the fluid encounters more reduced rocks. However, at the time of this model, the high-temperature formation constants from Kovalenko et al. (2011, 2012) and Timofeev et al. (2018) were not available, so the U(IV) species were under-represented.

A HCh model of the Olympic Dam IOCG deposit involving uranium fluoride and chloride speciation at elevated temperature was carried out by Xing et al. (2018). The authors noted that an abundance of reliable ambient-temperature data exists for U(IV) fluoride species but, as discussed in this review, there are limited high temperature data. The authors modeled the solubility of UO_2 and U_3O_8 in reduced and oxidized fluids, respectively, all under acidic conditions (0.5 m HCl and 0.5 m HF). For their model of UO_2 solubility in reduced, fluoride- and chloride-bearing fluids, the authors found that as the temperature increased from 25 to 450 °C, the free F^- concentration decreased and the $HF_{(aq)}$ concentration increased, along with a corresponding decrease in U fluoride species and the disappearance of dissolved NaF in solution (Fig. 1-12a-b). The precipitation of uraninite begins at about 180 °C and increases with

decreasing free fluoride concentration, likely in response to fluorite precipitation (Fig. 1-12b). The most important species at temperatures up to 130 °C, from 130 to 275 °C, and above 275 °C are $UF_{4(aq)}$, UF_3^+, and UCl_2^{2+} respectively (Fig. 1-12b). The U(IV) fluoride species UF_2^{2+} and UF^{3+} are both present in low concentrations below a temperature of 275 °C but they are not the dominant species and, above a temperature of 275 °C, the concentration of all U(IV) fluoride species becomes negligible. In the model of more oxidized, acidic fluids (0.5 m HCl and 0.5 m HF) addressing U_3O_8 solubility, the dominant species for temperatures up to 90 °C, from 90 to 170 °C, and above 170 °C are $UO_2F_{2(aq)}$, UO_2F^+, and $UO_2Cl_{2(aq)}$, respectively (Fig. 1-12c). Lesser concentrations of other uranyl oxyfluoride, oxychloride and oxide species are also present at temperatures ranging from 25 to 450 °C. Overall, the model predicts the predominance of U(IV) fluorides and U(VI) oxyfluorides and oxychloride in the reduced and oxidized fluids, respectively, of the Olympic Dam ore-forming system. Though the lack of reliable high-temperature U(IV) fluoride data brings into question the accuracy of the model, it nonetheless provides a useful comparison to the high-temperature experimental data obtained during the preparation of this thesis.

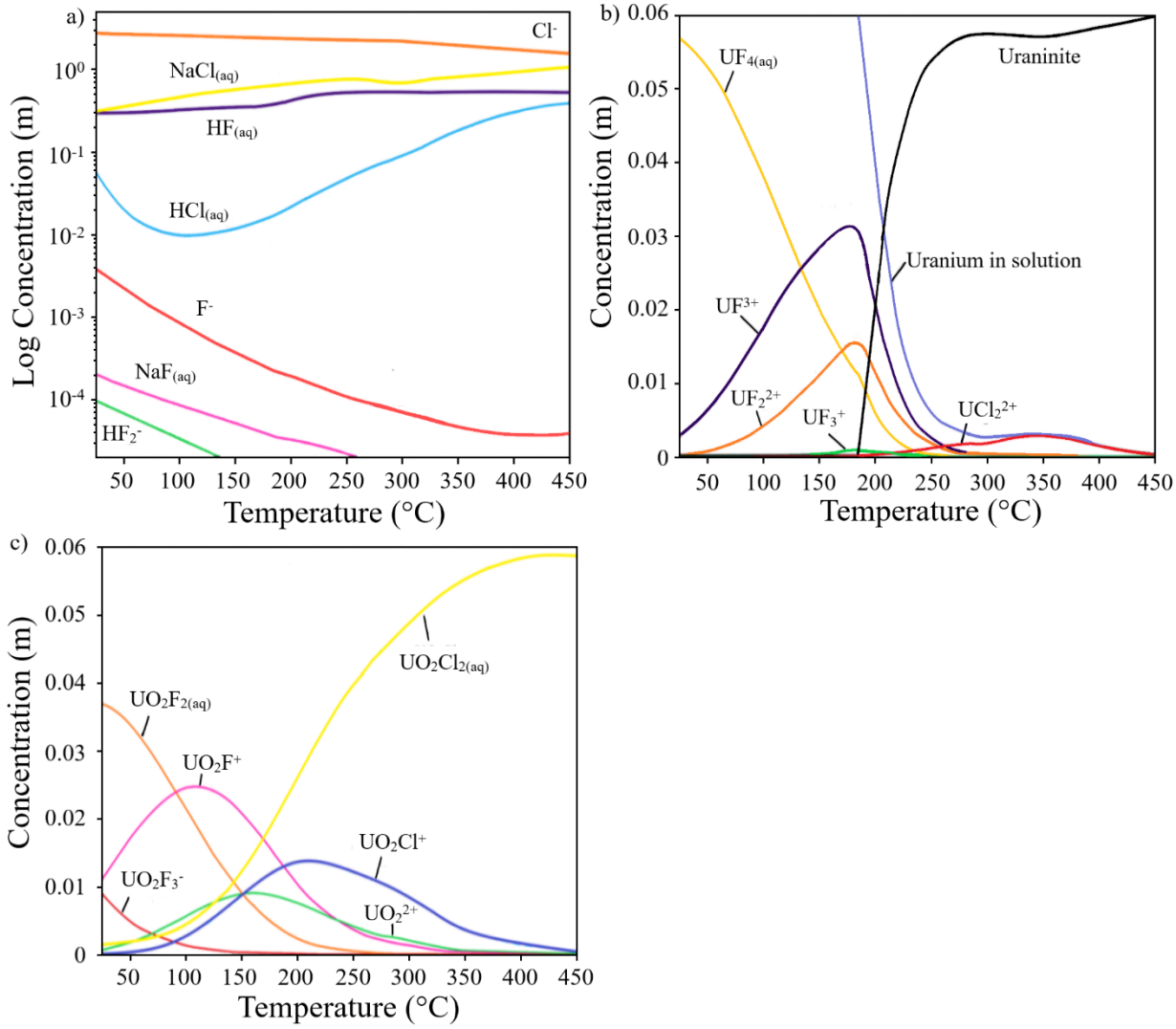

Figure 1-12 Results of the model of Xing et al. (2018) showing (a) the speciation of a fluid in the system Na-HCl-HF in equilibrium with either $UO_{2(s)}$ or $U_3O_{8(s)}$ (b) the U speciation of the fluid in equilibrium with $UO_{2(s)}$ under reduced conditions and (c) the U speciation of the fluid in equilibrium with $U_3O_{8(s)}$ under oxidized conditions. The modeled system is closed and isobaric at 3 kbar, with a uranium concentration of 60 mmolal.

1.3 Objective of this study

Although the generally-accepted model of uranium ore formation involves hydrothermal uranium transport as U(VI) and ore deposition as U(IV) (Eriksen et al., 2012), recent experimental data suggest that uranium may also be dissolved and transported in reduced fluids

as U(IV) complexes (Timofeev et al., 2018). In order to further elucidate factors that control the transport of U(IV) in fluoride-bearing hydrothermal systems, this thesis addresses the solubility and speciation of UO_2 as U(IV) fluoride complexes at 200 °C.

The objective of this study is to provide high-temperature solubility data for aqueous uranium fluoride species. These data are needed to reduce the error that arises from extrapolating ambient-temperature data to high temperatures, as seen in geochemical models by Bastrakov et al. (2010) and Xing et al. (2018). In order to gain a more complete understanding of the U(IV) fluoride speciation in ore fluids, experiments were performed over a range of fluoride concentrations and pH values. To ensure that the data obtained were for U(IV), the oxygen fugacity of the experiments was buffered to appropriately reducing conditions with the hematite-magnetite assemblage. Finally, the data obtained at the elevated experimental temperature were applied to a model of uranium transport in hydrothermal deposits.

1.4 Thesis organization

This thesis comprises three chapters. The first chapter is the introduction, which; 1) reviews the geology of deposits displaying evidence of having formed from fluoride-rich hydrothermal fluids and previous low- and high-temperature experimental studies of U(IV) hydroxide and fluoride species; and 2) explains how the data obtained from these studies have been used to model uranium transport and deposition. The second chapter is a manuscript for future submission to a peer-reviewed journal, in which the experimental data are presented and potential applications to uranium ore deposits are discussed. The final chapter is the extended conclusion of the study. The experimental methodology was based on the methodology of

(Migdisov and Williams-Jones, 2007) and was performed at a temperature of 200 °C and a pressure of 15 bars.

1.5 References

Allard B., Kipatsi H. and Liljenzin J. O. (1980) Expected species of uranium, neptunium and plutonium in neutral aqueous solutions. Journal of Inorganic and Nuclear Chemistry 42, 1015–1027.

Barnes H. Lloyd. (1979) Geochemistry of hydrothermal ore deposits. 1st ed., Wiley, New York.

Barsukov V. L. and Borisov M. V. (2003) Models of uranium dissolution in natural waters of various compositions. Geochemistry International 41, 38–63.

Bastrakov E. N., Jaireth S. and Mernagh T. P. (2010) Solubility of uranium in hydrothermal fluids at 25 to 300 C. Geoscience Australia 29, 91.

Betts R. H. (1955) Heat of hydrolysis of uranium(IV) in perchloric acid solutions. Canadian Journal of Chemistry 33, 1775–1779.

Bonnetti C., Liu X., Cuney M, Mercadier J., Riegler T., Yu Chida. (2020) Evolution of the uranium mineralisation in the Zoujiashan deposit, Xiangshan ore field: Implications for the genesis of volcanic-related hydrothermal U deposits in South China. Ore Geology Reviews 122, 103514

Bruno J., Casas I., Lagerman B. and Munoz M. (1986) The determination of the solubility of amorphous UO_2 (S) and the mononuclear hydrolysis constants of uranium(IV) at 25 °C. MRS Online Proceedings Library 84, 153–160.

Burt D. M. and Sheridan M. F. (1981) Model for formation of uranium/lithophile element deposits in fluorine-enriched volcanic rocks. AAPG Bulletin 65, 755–756.

Changkakoti A., Ghosh D. K., Krstic D., Gray J. and Morton R. D. (1986) Pb and Sr isotope compositions of hydrothermal minerals from the Great Bear Lake silver deposits, NWT, Canada. Economic Geology 81, 739–743.

Choppin G. R. and Unrein P. J. (1976) Thermodynamic study of actinide fluoride complexation. in transplutonium elements (eds. W. Muller and R. Linder). North Holland Publishing Company, Amsterdam.

Cuney M. (2014) Felsic magmatism and uranium deposits. Bulletin de la Société Géologique de France 185, 75-92.

Cunningham C. G., Rasmussen J. D., Steven T. A., Rye R. O., Rowley P. D., Romberger S. B. and Selverstone J. (1998) Hydrothermal uranium deposits containing molybdenum and fluorite in the Marysvale volcanic field, west-central Utah. Mineralium Deposita 33, 477–494.

Dahlkamp F. J. (1993) Uranium ore deposits., Springer, Berlin, Heidelberg.

Davidson G. J., Paterson H., Meffre S. and Berry R. F. (2007) Characteristics and origin of the Oak Dam East breccia-hosted, iron oxide Cu-U-(Au) deposit: Olympic Dam region, Gawler Craton, South Australia. Economic Geology 102, 1471–1498.

Day Jr R. A., Wilhite R. N. and Hamilton F. D. (1955) Stability of complexes of uranium (IV) with chloride, sulfate and thiocyanate. Journal of the American Chemical Society 77, 3180–3182.

Dmitrijeva M., Ehrig K.J., Ciobanu C.L., Cook N.J., Verdugo-Ihla M.R. and Metcalfe A.V. (2019) Defining IOCG signatures through compositional data analysis: A case study of lithogeochemical zoning from the Olympic Dam deposit, South Australia. Ore Geology Reviews 105, 86-101.

Eriksen T. E., Shoesmith D. W. and Jonsson M. (2012) Radiation induced dissolution of UO_2 based nuclear fuel – A critical review of predictive modeling approaches. Journal of Nuclear Materials 420, 409–423.

Eugster H.P. (1986) Minerals in hot water. American Mineralogist 71, 655-673.

Frimmel H.E., Schedel S. and Brätz H. (2014) Uraninite chemistry as forensic tool for provenance analysis. Applied Geochemistry 48, 104-121.

Fujiwara K., Yamana H., Fujii T., Kawamoto K., Sasaki T. and Moriyama H. (2005) Solubility of uranium(IV) hydrous oxide in high pH solution under reducing condition. Radiochimica Acta 93, 347–350.

Fujiwara K., Yamana H., Fujii T. and Moriyama H. (2003) Determination of uranium(IV) hydrolysis constants and solubility product of $UO_2 \cdot xH_2O$. Radiochimica Acta 91, 345–350.

Gayer K. H. and Leider H. (1957) The solubility of uranium(IV) hydroxide in solutions of sodium hydroxide and perchloric acid at 25 C. Canadian Journal of Chemistry 35, 5–7.

Goad R.E., Mumin A.H., Duke N.A., Neale K.L., Mulligan D.L. and Camier W.J. (2000) The NICO and Sue-Dianne Proterozoic, iron oxide-hosted, polymetallic deposits, Northwest

Territories: Application of the Olympic Dam model in exploration. Exploration and Mining Geology 9, 123-140.

Grenthe I. and Varfeldt J. (1969) A potentiometric study of fluoride complexes of uranium(IV) and uranium(VI) using the U(VI)/U(IV) redox couple. Acta Chemica Scandinavica 23, 988–998.

Grenthe I., Bidoglio G. and Omenetto N. (1989) Use of thermal lensing spectrophotometry (TLS) for the study of mononuclear hydrolysis of uranium(IV). Inorganic Chemistry 28, 71–74.

Grenthe I., Fuger J., Konings R. J., Lemire R. J., Muller A. B., Nguyen-Trung C. and Wanner H. (1992) Chemical thermodynamics of uranium., Elsevier Amsterdam.

Grenthe I., Gaona X., Rao L., Plyasunov A., Runde W., Grambow B., Konings R., Smith A., Moore E. and Ragoussi M.-E. (2020) Second update on the chemical thermodynamics of uranium, neptunium, plutonium, americium and technetium. Chemical Thermodynamics volume 14., Organisation for Economic Co-Operation and Development.

Guillaumont R., Fanghänel T., Neck V., Fuger J., Palmer D. A., Grenthe I. and Rand M. H. (2003) Update on the chemical thermodynamics of uranium, neptunium, plutonium, americium and technetium. Eds. F. J. Mompean, M. Illemanssene, C. Domenech-Orti, and K. Ben Said, Elsevier, Amsterdam.

Hitzman M. W. and Valenta R. K. (2005) Uranium in iron oxide-copper-gold (IOCG) systems. Economic Geology 100, 1657–1661.

Hu R.-Z., Bi X.-W., Zhou M.-F., Peng J.-T., Su W.-C., Liu S. and Qi H.-W. (2008) Uranium metallogenesis in South China and its relationship to crustal extension during the cretaceous to tertiary. Economic Geology 103, 583–598.

Jiang Y., Ling H., Jiang S., Shen W., Fan H. and Ni P. (2006) Trace element and Sr-Nd isotope geochemistry of fluorite from the Xiangshan uranium deposit, Southeast China. Economic Geology 101, 1613–1622.

Kakihana H. and Ishiguro S. (1974) Potentiometric and spectrophotometric studies of fluoride complexes of uranium(IV). Bulletin of the Chemical Society of Japan 47, 1665–1668.

Kelly C. J., Davis W. J., Potter E. G. and Corriveau L. (2020) Geochemistry of hydrothermal tourmaline from IOCG occurrences in the Great Bear magmatic zone: Implications for fluid source(s) and fluid composition evolution. Ore Geology Reviews 118, 103329.

Keppler H. and Wyllie P. J. (1990) Role of fluids in transport and fractionation of uranium and thorium in magmatic processes. Nature 348, 531–533.

Kerr P. F., Brophy G. P., Dahl H. M., Green J. and Woolard L. E. (1957) Marysvale, Utah, uranium area: geology, volcanic relations, and hydrothermal alteration., Geological Society of America, New York.

Kovalenko N. I., Ryzhenko B. N., Prisyagina N. I. and Bychkova Ya. V. (2011) Experimental study of uraninite solubility in aqueous HCl solutions at 500°C and 1 kbar. Geochem. Int. 49, 262–273.

Kovalenko N. I., Ryzhenko B. N., Prisyagina N. I. and Bychkova Y. V. (2012) Experimental determination of uranium (IV) speciation in HF solutions at 500 °C and 1000 bar. Geochemistry International 50, 18–25.

Kraus K. A. and Nelson F. (1950) Hydrolytic behavior of metal ions. I. The acid constants of uranium(IV) and plutonium(IV). Journal of the American Chemical Society 72, 3901–3906.

Kraus K. A. and Nelson F. (1955) Hydrolytic behavior of metal ions. IV. The acid constant of uranium(IV) as a function of temperature. Journal of the American Chemical Society 77, 3721–3722.

Langmuir D. (1978) Uranium solution-mineral equilibria at low temperatures with applications to sedimentary ore deposits. Geochimica et Cosmochimica Acta 42, 547–569.

McPhie J., Kamenetsky V., Allen S., Ehrig K., Agangi A. and Bath A. (2011) The fluorine link between a supergiant ore deposit and a silicic large igneous province. Geology 39, 1003–1006.

Montreuil J.-F., Corriveau L. and Potter E. G. (2015) Formation of albitite-hosted uranium within IOCG systems: the southern breccia, Great Bear magmatic zone, Northwest Territories, Canada. Miner Deposita 50, 293–325.

Montreuil J.-F., Corriveau L., Potter E. G. and De Toni A. F. (2016) On the Relationship Between Alteration Facies and Metal Endowment of Iron Oxide-Alkali-Altered Systems, Southern Great Bear Magmatic Zone (Canada). Economic Geology 111, 2139–2168.

Murphy W. M. and Shock E. L. (1999) Environmental aqueous geochemistry of actinides. Reviews in Mineralogy and Geochemistry 38, 221–253.

Neck V. and Kim J. I. (2001) Solubility and hydrolysis of tetravalent actinides. Radiochimica Acta 89, 1–16.

Norén B. (1969) A solvent extraction and potentiometric study of fluoride complexes of thorium(IV) and uranium(IV). Acta Chemica Scandinavia 23.

Opel K., Weiss S., Hübener S., Zänker H. and Bernhard G. (2007) Study of the solubility of amorphous and crystalline uranium dioxide by combined spectroscopic methods. Radiochimica Acta 95, 143–149.

Oreskes N. and Einaudi M. T. (1992) Origin of hydrothermal fluids at Olympic Dam; preliminary results from fluid inclusions and stable isotopes. Economic Geology 87, 64–90.

Parks G. A. and Pohl D. C. (1988) Hydrothermal solubility of uraninite. Geochimica et Cosmochimica Acta 52, 863–875.

Pearson R. G. (1963) Hard and soft acids and bases. J. Am. Chem. Soc. 85, 3533–3539.

Peiffert C., Cuney M. and Nguyen-Trung C. (1994) Uranium in granitic magmas: Part 1. Experimental determination of uranium solubility and fluid-melt partition coefficients in the uranium oxide-haplogranite-H_2O-Na_2CO_3 system at 720–770 °C, 2 kbar. Geochimica et Cosmochimica Acta 58, 2495–2507.

Peiffert C., Nguyen-Trung C. and Cuney M. (1996) Uranium in granitic magmas: Part 2. Experimental determination of uranium solubility and fluid-melt partition coefficients in

the uranium oxide-haplogranite-H_2O-NaX (X = Cl, F) system at 770 °C, 2 kbar. Geochimica et Cosmochimica Acta 60, 1515–1529.

Potter E.G., Montreuil J.-F., Corriveau L. and Davis W.J. (2019). The Southern Breccia metasomatic uranium system of the Great Bear Magmatic Zone, Canada: Iron oxide-copper-gold (IOCG) and albitite-hosted uranium linkages. In: Decrée, S., Robb, L. (Eds.), In Ore Deposits: Origin, Exploration, and Exploitation. American Geophysical Union, Geophysical Monograph 242, pp. 109–130.

Rai D., Felmy A. R. and Ryan J. L. (1990) Uranium(IV) hydrolysis constants and solubility product of $UO_2 \cdot xH_2O$(am). Inorganic Chem. 29, 260–264.

Rai D., Yui M. and Moore D. A. (2003) Solubility and solubility product at 22 C of UO_2 (c) precipitated from aqueous U(IV) solutions. Journal of Solution Chemistry 32, 1–17.

Richardson C. K. and Holland H. D. (1979) The solubility of fluorite in hydrothermal solutions, an experimental study. Geochimica et Cosmochimica Acta 43, 1313–1325.

Roberts D. E. and Hudson G. R. T. (1983) The Olympic Dam copper-uranium-gold deposit, Roxby Downs, South Australia. Economic Geology 78, 799–822.

Robinson B. W. and Ohmoto H. (1973) Mineralogy, fluid inclusions, and stable isotopes of the Echo Bay U-Ni-Ag-Cu deposits, Northwest Territories, Canada. Economic Geology 68, 635–656.

Roedder E. (1984) Fluid inclusions: an introduction to studies of all types of fluid inclusions, gas, liquid, or melt, trapped in materials from earth and space, and their application to the

understanding of geologic processes., Mineralogical Society of America;, Washington, D.C.

Rogers J. J., Ragland P. C., Nishimori R. K., Greenberg J. K. and Hauck S. A. (1978) Varieties of granitic uranium deposits and favorable exploration areas in the eastern United States. Economic Geology 73, 1539–1555.

Savage A. W. and Browne J. C. (1960) The solubility of uranium (IV) fluoride in aqueous fluoride solutions. Journal of the American Chemical Society 82, 4817–4821.

Sawant R. M., Chaudhuri N. K. and Patil S. K. (1990) Potentiometric studies on aqueous fluoride complexes of actinides: stability constants of Th(IV)-, U(IV)-, Np(IV)-and Pu(IV)-fluorides. Journal of Radioanalytical and Nuclear Chemistry 143, 295–306.

Shvarov Y. V. (1999) Algorithmization of the numeric equilibrium modeling of dynamic geochemical processes. Geochemistry International 37, 571–576.

Shvarov Y. V. and Bastrakov E. N. (1999) HCh: A software package for geochemical equilibrium modeling, user's guide. Australian Geological Survey Organisation Record 25, 60.

Shock E. L., Sassani D. C. and Betz H. (1997) Uranium in geologic fluids: estimates of standard partial molal properties, oxidation potentials, and hydrolysis constants at high temperatures and pressures. Geochimica et Cosmochimica Acta 61, 4245–4266.

Skirrow R. G., Jaireth S., Huston D., Bastrakov E., Schofield A. and Wielen S. (2009) Uranium mineral systems; processes, exploration criteria and a new deposit framework. Geoscience Australia Record 2009/20

Sobkowski J. (1961) The oxidation-reduction potential of UO_2^{2+}-U^{4+} system—II: The influence of $HClO_4$, HCl, H_2SO_4 and of temperature on the oxidation potential of UO_2^{2+}-U^{4+} Journal of Inorganic and Nuclear Chemistry 23, 81–90.

Sullivan J. C. and Hindman J. C. (1959) The hydrolysis of neptunium (IV). The Journal of Physical Chemistry 63, 1332–1333.

Timofeev A., Migdisov A. A., Williams-Jones A. E., Roback R., Nelson A. T. and Xu H. (2018) Uranium transport in acidic brines under reducing conditions. Nature Communications 9, 1469.

Wei W.-F., Chen X., Yu Z.-Q., Chen W.-F., Fang Q.-C., Tang X.-S. and Ling H.-F. (2021) Different hydrothermal fluids inducing alteration and uranium mineralisation in the Baquan deposit of the Xiangshan uranium ore field: Constraints from geochemistry of altered rocks and ores. Ore Geology Reviews 139, 104475.

Williams-Jones A. E. and Migdisov A. A. (2014) Experimental Constraints on the Transport and Deposition of Metals in Ore-Forming Hydrothermal Systems. In Building Exploration Capability for the 21st Century (eds. K. D. Kelley and H. C. Golden). Society of Economic Geologists. pp. 77–96.

Wood S. A. and Samson I. M. (1998) Solubility of ore minerals and complexation of ore metals in hydrothermal solutions. In: Techniques in Hydrothermal Ore Deposits Geology (Eds. J. P. Richards and P. B. Larson). Society of Economic Geologists, pp. 33–80.

Xing Y., Mei Y., Etschmann B., Liu W. and Brugger J. (2018) Uranium transport in F-Cl-bearing fluids and hydrothermal upgrading of U-Cu ores in IOCG deposits. Geofluids.

Chapter 2 An experimental study on the solubility and speciation of uranium(IV) in reduced fluoride-bearing solutions

K. Fuller, A. E. Williams-Jones, K. Rempel

2.1 Abstract

The solubility and speciation of U(IV) in fluoride-bearing aqueous fluids were determined experimentally at a temperature of 200 °C and saturated vapour pressure (15.5 bars). The experiments were performed at fluoride activities ranging from $1.6x10^{-7}$ to 0.17 and pH values ranging from 2.1 to 7.5. The uranium molality in these solutions range from about $1.28x10^{-5}$ to $2.32x10^{-3}$ m, increasing with decreasing pH and increasing fluoride activity. The U(IV) speciation at the experimental conditions was found to comprise a mixture of $UO_{2\,(aq)}$, HUO_2^+, UO_2F^- and $HUO_2F_{(aq)}$. The $\Delta_fG^{T,P,0}$ values for these species at the experimental conditions are -1006.5 ± 1.1, -1039.6 ± 2.8, -1299.7 ± 0.4 and -1360.8 ± 0.7 kJ/mol and the log K values for their formation reactions, based on uraninite dissolution at the experimental conditions, are -4.7 ± 0.1, -1.0 ± 0.3, -2.64 ± 0.04 and 4.10 ± 0.07, respectively. The species $UO_{2\,(aq)}$ predominates in solutions with low aF^- and low aH^+, and HUO_2^+ is also important at low aF^- and low aH^+; the stability of these species is relatively low. The UO_2F^- species predominates in solutions at high aF^- and low aH^+, whereas $HUO_2F_{(aq)}$ predominates in solutions with moderate to high aF^- and high aH^+. The high solubility of U(IV) measured under experimental conditions is much more mobile in solution than is commonly thought and may have an important role to play in the transport of uranium in hydrothermal U deposits.

2.2 Introduction

In modeling the genesis of hydrothermal uranium ore-forming systems, it has been assumed that uranium is transported as U(VI) species in solution. They are believed to be reduced to low-solubility U(IV) species at the site of deposition and precipitate as U(IV) ore minerals (Romberger 1984, Dahlkamp, 1993, Cunningham et al., 1998, and Bastrakov et al., 2010). However, a recent study by Timofeev et al. (2018) found that in reduced HCl solutions, U(IV) is also carried in solution as the chloride complex UCl_4 in concentrations of 4.9 ppb to 780 ppb at 250-350 ºC and saturated vapour pressure. The solubility of U(IV) was also assessed in HCl and HF solutions at 500 ºC and 1 kbar by Kovalenko et al. (2011, 2012), who measured concentrations of 0.19 to 180 ppm U and 5.4 to 680 ppm U in chloride- and fluoride-bearing solutions, respectively. The results of these studies show that the transport of U(IV) in ore fluids is far more important than previously thought, and the solubility and speciation of U(IV) at hydrothermal conditions merits further experimental investigation.

Hydrothermal uranium deposits vary widely in type and setting, including associations with basinal sediments, intrusions or caldera activity, and breccia complexes (reviews by Dahlkamp, 1993, Plant et al., 1999, Cuney, 2009, Skirrow et al., 2009). Models for sediment-hosted uranium deposits favour U deposition due to reduction, owing to a common association of the ore with organic matter or other reductants (Nakashima et al., 1984, Meunier et al., 1990, Komninou and Sverjensky, 1996, Bastrakov et al., 2010), but vein- or breccia-hosted U deposits sociated to felsic granites or rhyolites generally lack these reducing components. Instead, genetic models for this latter group of deposits involve destabilization of aqueous species due to pH change from boiling or fluid-rock interaction (Cunningham et al., 1998, Plant et al., 1999, Skirrow et al., 2009). As these models do not involve the reduction of U(VI), reduced U(IV) may

well play a role in uranium transport. Furthermore, uranium ore in volcanic-hosted deposits is commonly associated with fluorite, due to the high abundance of both U and F in the felsic source rocks (Rogers et al., 1978, Burt and Sheridan, 1981, Chabiron et al., 2001, Cuney, 2014), raising the possibility that U(IV) fluoride complexes are important in the genesis of these hydrothermal U deposits.

Uranium fluoride complexation in ore fluids is predicted by the hard-soft-acid-base model of Pearson (1963), and the formation of U(IV) fluorides UF^{3+}, UF_2^{2+}, UF_3^{+}, $UF_{4\,(aq)}$, UF_5^{-} and UF_6^{2-} are well described at ambient conditions (Kakihana and Ishiguro, 1974, Sawant et al., 1990, Guillaumont et al., 2003, Bastrakov et al., 2010, Grenthe et al., 2020). The stability constants for these species were extrapolated to elevated temperatures and pressures for use in thermodynamic models of uranium ore-forming systems (~150-400 °C, up to 600 bars; Shock et al., 1997, Cunningham et al., 1998, Hu et al., 2008, Xing et al., 2019). However, such extrapolations are highly prone to error, and experiments on U(IV) solubility in fluoride-bearing hydrothermal fluids are required for accurate modeling of uranium transport in ore fluids.

Should U(IV) species be significant at hydrothermal temperatures, then U(IV) fluoride complexation may indeed lead to enhanced uranium endowments in fluoride-rich U deposits. In this study experiments were carried out to determine the relationship between pH, fluoride content, and U(IV) solubility in hydrothermal fluids. The objective is to quantitatively evaluate U(IV) fluoride speciation at 200 ºC and a range of pH and fluoride concentrations as well as determine the stoichiometry and formation constants of the U(IV) species present under these conditions. The results will be used to assess the significance of U(IV) fluoride species for hydrothermal uranium ore-forming systems.

2.3 Experimental methodology

The experiments conducted in this study were designed to assess the solubility of UO_2 and speciation of dissolved U(IV) in fluoride-bearing hydrothermal solutions following a procedure similar to that used by Migdisov and Williams-Jones (2007), Migdisov et al. (2009), and Nisbet et al. (2018). They were run at 200 °C and saturated vapour pressure (15.5 bars) in titanium autoclaves with graphite O-ring seals and removable, gas-tight lidded PTFE liners (Fig. 2-1). The PTFE liners have a 20 cm^3 volume. The autoclaves were loaded with one PTFE tube

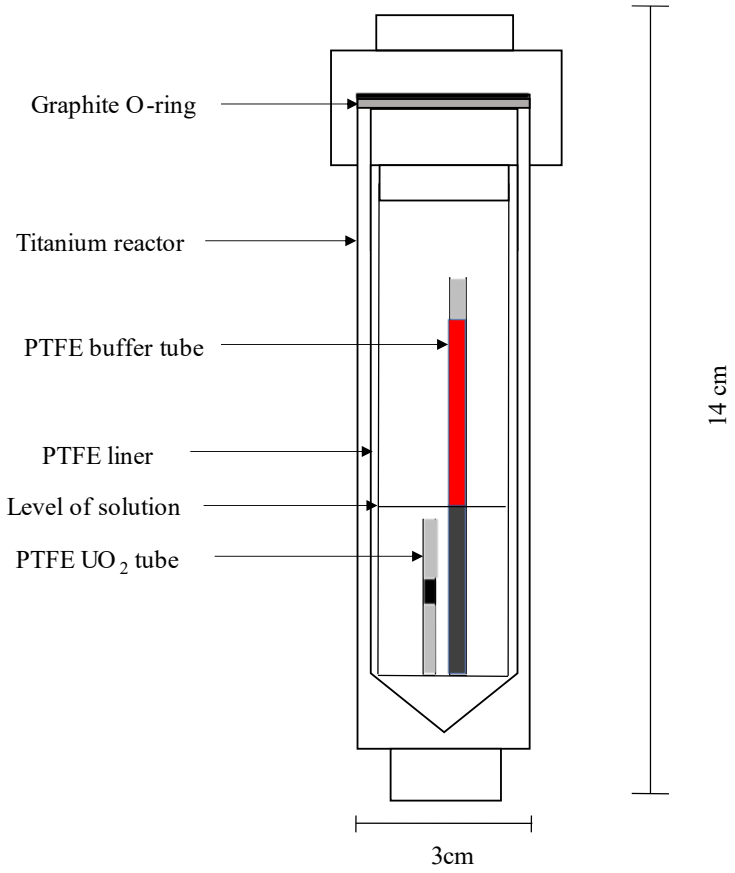

Figure 2-1 A schematic diagram showing the titanium autoclave with a PTFE liner used in the experiments, and the PTFE holders for the fO_2 buffer and UO_2.

containing an oxygen fugacity (fO_2) buffer and a second tube containing pieces of depleted uranium dioxide, as well as an aliquot of experimental solution. These PTFE tubes were sealed at the bottom, and topped with 0.127 mm PTFE mesh. The mesh allowed the UO_2 to interact with the experimental solutions but prevented the reagent from escaping and contaminating the

samples. The UO_2 pieces were washed in an ultrasonic bath in Nanopure water for 4 minutes to remove any fine particulates before use. A total mass of 0.1 g of the UO_2 pieces, which ranged in size from 1 to 4 mm, were contained in 3.5 cm-high holders.

The fO_2 buffer was contained in 8.5-cm high holders, which were long enough for the open top to remain above the level of the solution and allowed the buffer to react only with the vapour. The UO_2 holders, on the other hand were short enough to be submerged in the solution and allowed reaction between the reagent and the liquid (Fig. 2-1). The hematite-magnetite buffer, which has a substantially lower fO_2 than the UO_2-U_3O_8 phase boundary at the experimental temperature (Fig. 2-2), was employed to prevent the oxidation of U(IV) to U(VI). This would

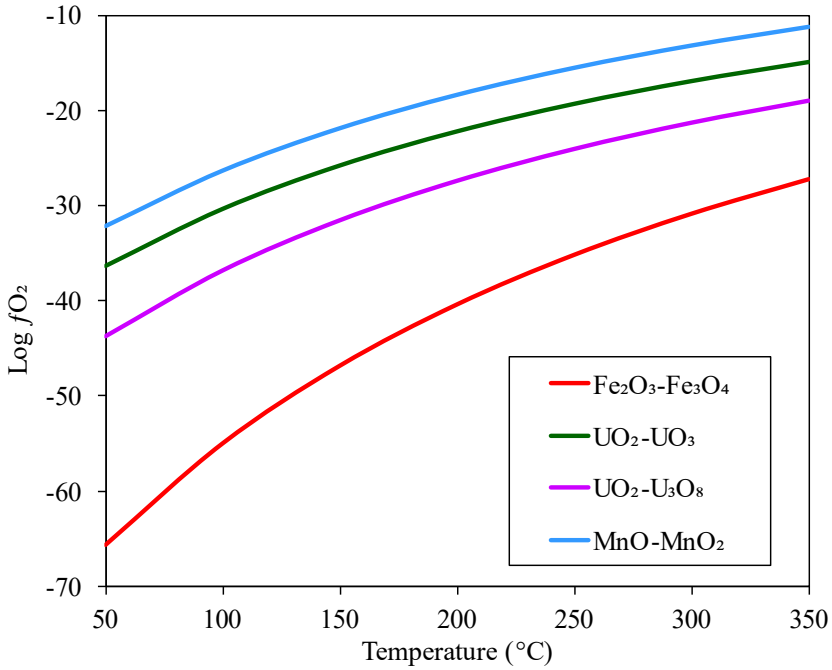

Figure 2-2 The oxygen fugacity versus temperature of selected oxide buffers, which were used to choose an appropriate fO_2 buffer for each set of experiments; calculated using HCh (Shvarov and Bastrakov, 1999).

have produced a spuriously high solubility, as U(VI) is far more soluble than U(IV) (Gayer and Leider, 1955, Gayer and Leider, 1957, Langmuir, 1978, Shock et al., 1997, and Eriksen et al.,

2012). The chosen fO_2 buffer was composed of a mixture of powdered Fe_2O_3 and Fe_3O_4. Owing to the marked colour difference between the red hematite and the black magnetite, a visual inspection was sufficient to determine whether both phases were still present at the end of the experiments. To remove excess oxygen from the system and increase the effectiveness of the fO_2 buffer, the autoclaves were sealed inside a closed chamber and flushed with argon gas for at least 30 minutes prior to closing.

The autoclaves were loaded with 8 ml of experimental solution of variable pH and fluoride activity. The pH of the acidic solutions was set at either 2, 3, or 5 using trace-metal grade $HClO_4$, which, in combination with $NaClO_4$, provided a background electrolyte for the calculation of activity coefficients. Neutral-pH solutions were made by excluding $HClO_4$ and $NaClO_4$, and alkaline solutions were prepared with NaOH and $NaClO_4$. Sodium perchlorate was used as the background electrolyte because perchlorate is a non-complexing ion and does not interfere with the assessment of metal complexation (Schilt et al., 1979; Migdisov and Williams-Jones, 2007). The fluoride concentrations of the starting solutions (0.001, 0.01, 0.1, 0.2, and 0.3 m) were set using NaF.

An initial kinetic series was conducted to assess the time required for the UO_2 dissolution reaction to reach equilibrium. The sealed autoclaves were placed in a fan-forced air oven at 200 °C, then successively removed at 1-day intervals. After removal from the oven, the autoclaves

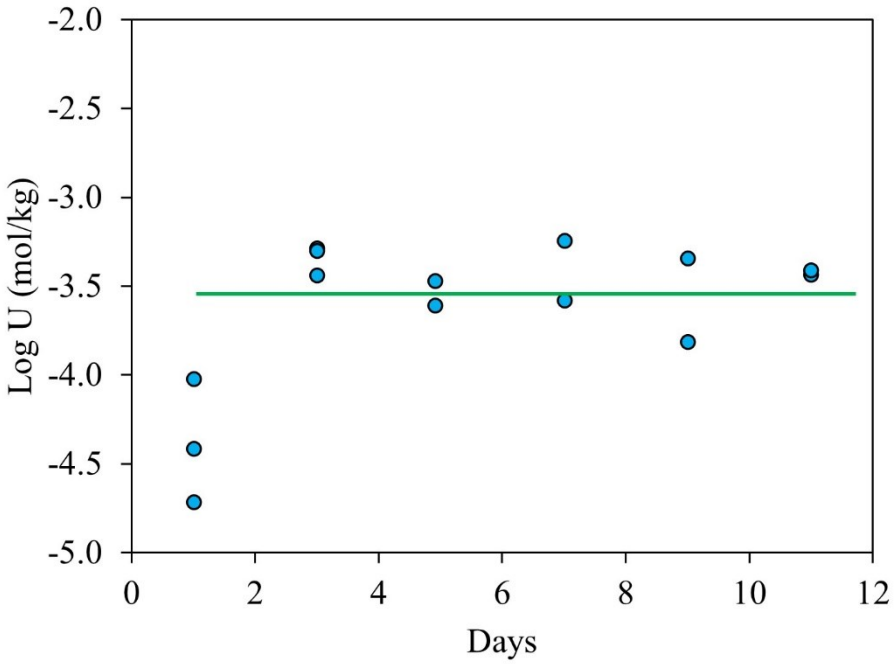

Figure 2-3 Time series data showing log U concentrations vs days for a solution of pH 5 containing 0.1 m NaF. The system reached equilibrium after about 3 days, as shown by the green line at the equilibrium log U concentration of -3.5 m.

were quenched in cold water until room temperature was attained, then analyzed for uranium concentration. As is evident from the results of this kinetic experiment, equilibrium was reached after approximately 3 days (Fig. 2-3).

Following quenching and removal of the uranium and buffer tubes, 0.1- and 1-ml aliquot solutions were extracted to measure the pH and total fluoride concentrations, respectively. Prior to analysis with a pH electrode, the 0.1-ml aliquots were diluted 10x with Nanopure water to bring the F^- concentrations to below 0.01 m, to avoid corrosion of the glass electrode by F^-. The

1-ml aliquots for analysis with a fluoride ion-selective electrode were diluted with 3 ml of a TISAB II solution to maintain a constant ionic strength and pH.

A 1-ml aliquot of aqua regia was added to the remaining solution in the autoclaves in order to wash the sides of the PTFE liner and dissolve any uranium solids that may have precipitated during cooling. The aqua regia also served to stabilize the solutions for storage. The solution was then removed and placed in labelled tubes for later analysis, as discussed below. The PTFE liners were cleaned to remove contamination by submersion in a 50% aqua regia bath for one day, then triple-rinsed with de-ionized and Nanopure water. All other PTFE components were cleaned sequentially in 10% nitric acid, de-ionized water and Nanopure water.

Blank experiments with $HClO_4$-$NaClO_4$-NaF solutions in which no UO_2 was added were run in tandem with the time series and solubility experiments in initial runs to ensure that any contaminants were completely removed from the autoclaves during the cleaning process. The measured uranium concentrations of the blanks range from 0 to 3.5 ppb, with the majority of the blanks having concentrations below 1 ppb, indicating that contamination of the experimental solutions by external sources of uranium was insignificant. Experiments run with zero-fluoride solutions had measured fluoride concentrations of up to ~10 ppm after quenching, most likely derived from the PTFE autoclave liners. As this concentration was less than 1% of the F^- in most of the starting solutions, it likely had an insignificant effect on the results of those experiments, but sufficient F^- was present in some zero-fluoride series to modify the F^- speciation, so these post-experiment F^- concentrations were included in the data interpretation.

The solutions were analyzed using inductively coupled plasma mass spectrometry (ICP-MS) at the Université du Québec à Montréal and the Department of Earth and Planetary Sciences at McGill University, Montreal. The initial UO_2 solutions were diluted 500x with a 3% $HClO_4$

solution in order to bring the U concentration into the ppb- level range of the instruments, which have a detection limit of ~1 ppb and an upper limit of 1 ppm. The reliability of the uranium analysis was confirmed using the uranium standard 1000ppm supplied by Alfa Aesar which was diluted 2000x, 6667x, 20000x, 40000x, 100000x, 200000x, and 1000000x. A 1-ppb rhenium internal standard was included in all samples to account for ICP-MS signal drifts.

2.4 Results and data treatment

In order to evaluate the data and derive the stoichiometry of the U(IV) species present in the experimental solutions, the measured uranium concentrations were plotted versus the activity of F^- and H^+, as F^-, OH^- and H^+ are potential ligands for the uranium species (Fig. 2-4a-b). Because HF is a weak acid and does not completely dissociate, the activities of F^- and H^+ in solution are interrelated by the $HF_{(aq)}$ association reaction:

$$H^+ + F^- = HF_{(aq)} \quad (1)$$

Thus, $HF_{(aq)}$ association is favoured at low pH, resulting in a decrease in the fluoride concentrations of the starting solutions, whereas the reverse is true at higher pH. Additionally, the pH values of the starting solutions decreased during heating (neutral pH at 200 °C is 5.64). Because of these two factors, the compositions of the solutions at the experimental conditions differed widely from those of the starting solutions at room temperature.

The concentrations of F^- and H^+, ionic strength and the activity coefficients at 200 °C and 15.5 bar were calculated for each starting solution using the HCh (HydroChemistry) thermodynamic modeling software package (Shvarov and Bastrakov, 1999), which employs a Gibbs free energy-minimizing algorithm to determine the stable ions or complexes and their

concentrations. For activity coefficient calculations, HCh uses the extended Debye-Hückel equation obtained from Helgeson et al., 1981,

$$\log \gamma_j = -\frac{Az_j^2\sqrt{I}}{1+Bå\sqrt{I}} + b_\gamma I \qquad (2)$$

where A and B are Debye-Hückel parameters, z_j is the ionic charge, I is the ionic strength, b_y is the extended Debye-Hückel parameter for $NaClO_4$ as the background electrolyte ($b_\gamma = 0.19$; Migdisov and Williams-Jones, 2007), and å is the distance of closest approach (Helgeson et al. 1981). The values of å are 9.0 Å for H^+, 3.5 Å for OH^- and F^-, 4.0 for Na^+, and 4.5 Å for ClO_4^- (Garrels and Christ, 1965, Truesdell and Jones, 1974). Neutral-pH starting solutions were made without the perchlorate background electrolyte, so the activity coefficients for the components of these solutions were calculated without the b_γ term.

As shown in Figure 2-4, the concentrations of uranium in the experimental solutions range from $1.3x10^{-5}$ to $2.3x10^{-3}$ m (3.1 to 552 ppm), and for the most part increase linearly with increasing aF^- and aH^+ (Fig. 4-2a-b, Table 2-1). For the solutions with the highest pH and aF^- (pH 7.4-7.6 and aF^- from 0.06 to 0.2), however, the trend differs: uranium concentration is higher than in the pH 6.9-7 solutions (Fig. 4-2a) and appears to be independent of pH (Fig. 4-2b).

The trendlines plotted in Figure 2-4 are the linear least squares lines of best fit to groups of data collected at near-constant aF^- and aH^+. Because of the changes to solution composition at the experimental conditions, the compositions vary somewhat within each group (Table 2-1). Nonetheless, as indicated by the high R^2 values of the trendlines, the data groupings provide a good first approximation for data evaluation.

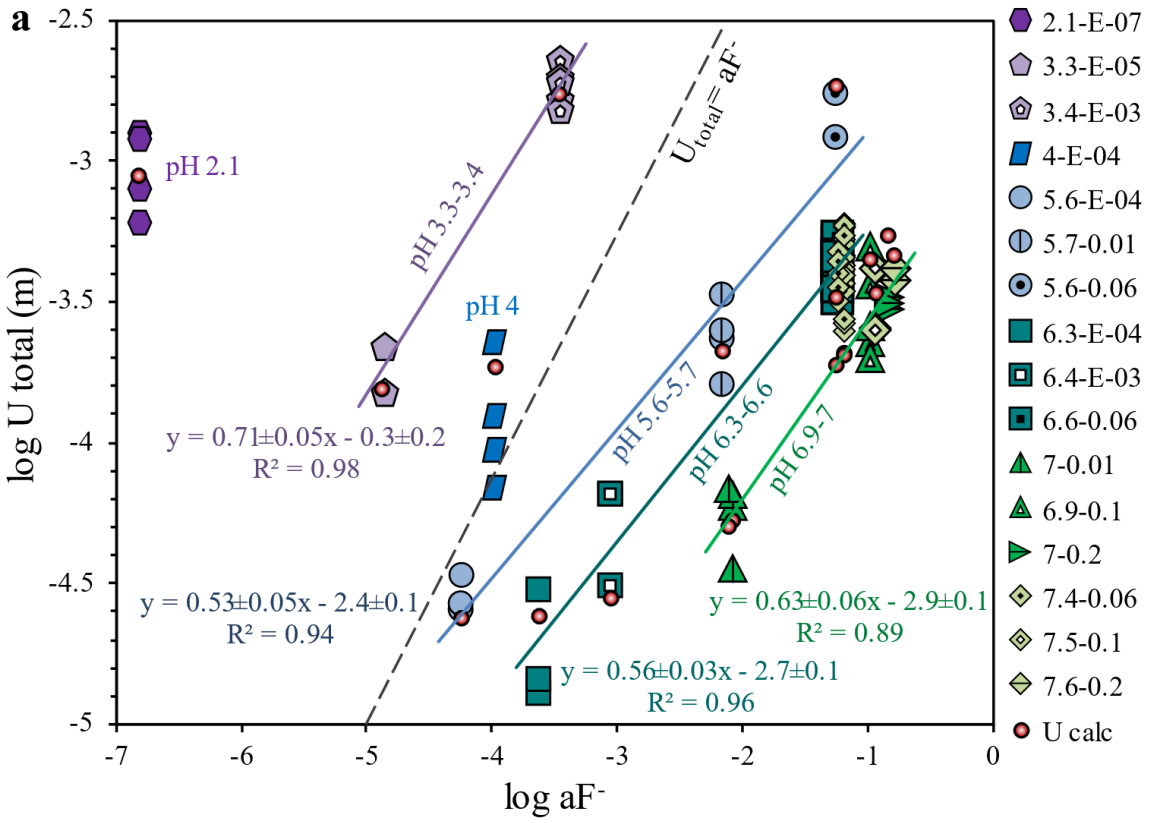
a
log U total (m)
log aF⁻
pH 2.1
pH 3.3-3.4
pH 4
pH 5.6-5.7
pH 6.3-6.6
pH 6.9-7
U_total = aF⁻
y = 0.71±0.05x - 0.3±0.2
R² = 0.98
y = 0.53±0.05x - 2.4±0.1
R² = 0.94
y = 0.56±0.03x - 2.7±0.1
R² = 0.96
y = 0.63±0.06x - 2.9±0.1
R² = 0.89
2.1-E-07
3.3-E-05
3.4-E-03
4-E-04
5.6-E-04
5.7-0.01
5.6-0.06
6.3-E-04
6.4-E-03
6.6-0.06
7-0.01
6.9-0.1
7-0.2
7.4-0.06
7.5-0.1
7.6-0.2
U calc

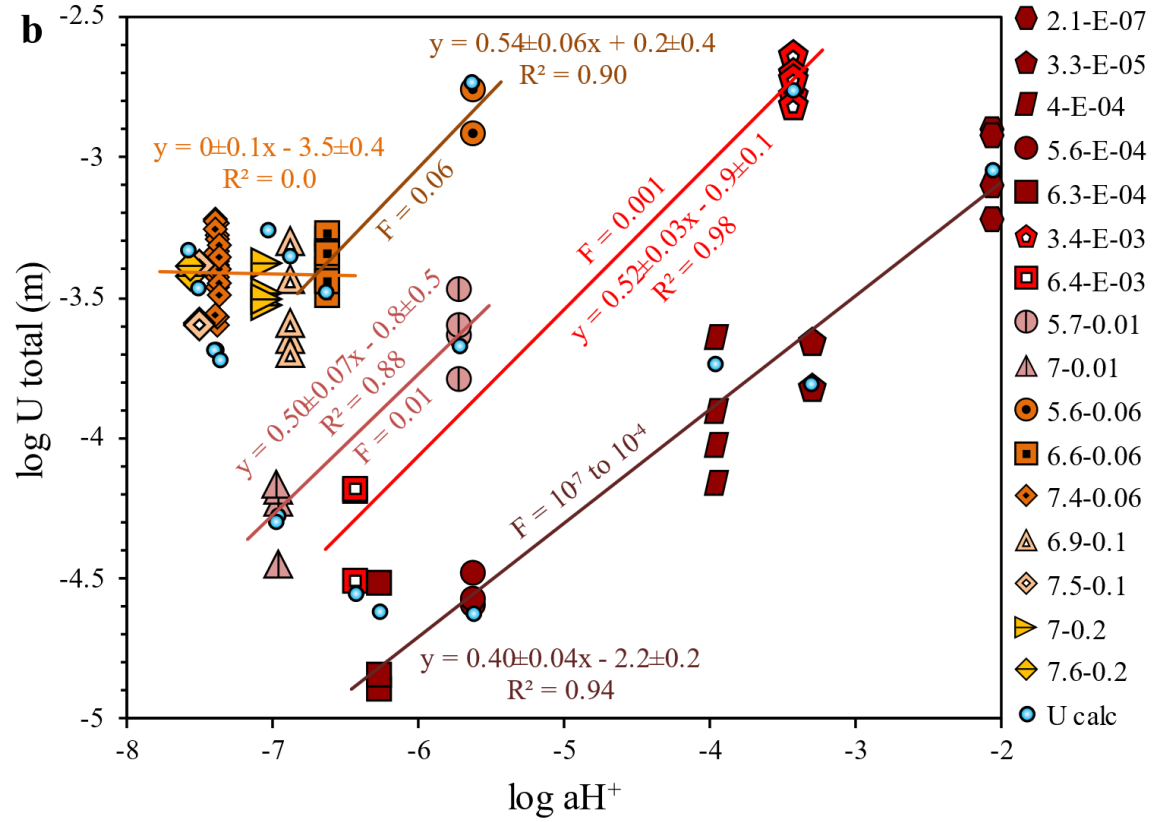
b
log U total (m)
log aH⁺
y = 0.54±0.06x + 0.2±0.4
R² = 0.90
y = 0±0.1x - 3.5±0.4
R² = 0.0
F = 0.06
F = 0.001
y = 0.52±0.03x - 0.9±0.1
R² = 0.98
y = 0.50±0.07x - 0.8±0.5
R² = 0.88
F = 0.01
F = 10⁻⁷ to 10⁻⁴
y = 0.40±0.04x - 2.2±0.2
R² = 0.94
2.1-E-07
3.3-E-05
4-E-04
5.6-E-04
6.3-E-04
3.4-E-03
6.4-E-03
5.7-0.01
7-0.01
5.6-0.06
6.6-0.06
7.4-0.06
6.9-0.1
7.5-0.1
7-0.2
7.6-0.2
U calc

Figure 2-4 Plots of the measured molal uranium concentrations versus the calculated ligand activity at the experimental conditions. (a) log U_{total} vs log aF^-, showing groups of data at near-constant pH, and (b) log U_{total} vs. log aH^+ showing groups of data at near-constant aF^-. The same symbols are used for each series in both (a) and (b), and colours are used to highlight data groups, trendlines, and trendline equations. The trendlines are linear least squares lines of best fit to each group. Also shown are the calculated UO_2 solubility based on optimized log K values for mixtures of $UO_{2\,(aq)}$, HUO_2^+, UO_2F^- and $HUO_2F_{(aq)}$.

The slopes of the trendlines on the log U_{total} vs log aF^- plot are 0.71 ± 0.05 at pH 3.3-3.4, 0.53 ± 0.03 at pH 5.6-5.7, 0.56 ± 0.03 at pH 6.3-6.6, and 0.63 ± 0.06 at pH 6.9-7 (Fig. 2-4a). The range of aF^- for the pH 7.4-7.6, given the scatter in the points, is too narrow for a meaningful trendline, though the relatively constant U_{total} suggests a horizontal trend. If log U_{total} is plotted versus log aH^+, the trendline slopes are 0.34 ± 0.04 for data with aF^- values in the $1.6x10^{-7}$ to $2.5x10^{-4}$ range, 0.52 ± 0.03 for the $aF^- = 0.001$ group, 0.5 ± 0.07 for the $aF^- = 0.01$ group, and 0.54 ± 0.05 for the $aF^- = 0.06$, pH 5.6-6.6 group. The zero slope of the trendline fit to the high-pH, high-aF^- data is accompanied by an R^2 value of zero, which shows that, for these data, none of the variation in the U solubility results from a pH variation.

2.5 Identification of species

The trendline slopes reported above were used to estimate the stoichiometry of the uranium species in solution. Firstly, the horizontal distribution of the high pH, high aF^- data (Figs. 2-4 a and b) indicates that the speciation under these conditions is independent of both aH^+ and aF^-. Hence the dominant species under these conditions is most likely $UO_{2\,(aq)}$, species that is postulated at ambient conditions (e.g., review by Grenthe et al., 2020) and forms by the following reaction:

$$UO_{2\,(s)} = UO_{2\,(aq)} \quad (3)$$

Table 2-1 Chemical parameters of the starting solutions, calculated aF^- and aH^+ at the experimental conditions, and measured U concentrations in molal and ppm.

	Starting solution compositions, m				Compositions at 200 °C, 15.5 bar			
Sample[a]	**NaF**	**$HClO_4$**	**$NaClO_4$**	**NaOH**	**log aF^-**	**log aH^+**	**log U, m**	**U, ppm**[b]
2.1-E-07-2	-	0.0100	-	-	-6.80	-2.06	-2.90	298 ± 65
2.1-E-07-3	-	0.0100	-	-	-6.80	-2.06	-3.10	189 ± 65
2.1-E-07-4	-	0.0100	-	-	-6.80	-2.06	-3.22	143 ± 65
2.1-E-07-5	-	0.0100	-	-	-6.80	-2.06	-2.92	283 ± 65
3.3-E-05-4	-	0.0010	-	-	-4.86	-3.31	-3.81	36.7 ± 8
3.3-E-05-5	-	0.0010	-	-	-4.86	-3.31	-3.65	53.1 ± 8
4-E-04-1	0.00100	0.0010	0.0010	-	-3.96	-3.96	-3.64	54 ± 14
4-E-04-2	0.00100	0.0010	0.0010	-	-3.96	-3.96	-3.91	30 ± 14
4-E-04-4	0.00100	0.0010	0.0010	-	-3.96	-3.96	-4.03	22 ± 14
4-E-04-5	0.00100	0.0010	0.0010	-	-3.96	-3.96	-4.16	16 ± 14
5.6-E-04-3	-	$1.0x10^{-5}$	0.010	-	-4.23	-5.62	-4.48	7.8 ± 1
5.6-E-04-4	-	$1.0x10^{-5}$	0.010	-	-4.23	-5.62	-4.60	6.0 ± 1
5.6-E-04-5	-	$1.0x10^{-5}$	0.010	-	-4.23	-5.62	-4.57	6.4 ± 1
6.3-E-04-2	-	-	0.010	$1.0x10^{-6}$	-3.61	-6.26	-4.89	3.1 ± 2
6.3-E-04-3	-	-	0.010	$1.0x10^{-6}$	-3.61	-6.26	-4.52	7.2 ± 2
6.3-E-04-5	-	-	0.010	$1.0x10^{-6}$	-3.61	-6.26	-4.84	3.4 ± 2
3.4-E-03-1	0.100	0.0100	0.034	-	-3.45	-3.43	-2.63	552 ± 64
3.4-E-03-2	0.100	0.0100	0.034	-	-3.45	-3.43	-2.77	400 ± 64
3.4-E-03-3	0.100	0.0100	0.034	-	-3.45	-3.43	-2.69	481 ± 64
3.4-E-03-4	0.100	0.0100	0.034	-	-3.45	-3.43	-2.71	459 ± 64
3.4-E-03-5	0.100	0.0100	0.034	-	-3.45	-3.43	-2.81	369 ± 64
6.4-E-03-1	0.00100	$1.0x10^{-5}$	0.010	-	-3.04	-6.43	-4.19	15.5 ± 4
6.4-E-03-2	0.00100	$1.0x10^{-5}$	0.010	-	-3.04	-6.43	-4.51	7.4 ± 4
6.4-E-03-4	0.00100	$1.0x10^{-5}$	0.010	-	-3.04	-6.43	-4.18	15.7 ± 4
5.7-0.01-1	0.0100	0.0010	0.010	-	-2.14	-5.72	-3.63	55 ± 15
5.7-0.01-2	0.0100	0.0010	0.010	-	-2.14	-5.72	-3.60	60 ± 15
5.7-0.01-3	0.0100	0.0010	0.010	-	-2.14	-5.72	-3.79	38 ± 15
5.7-0.01-5	0.0100	0.0010	0.010	-	-2.14	-5.72	-3.47	80 ± 15
5.7-0.01-1	0.0100	0.0010	0.010	-	-2.14	-5.72	-3.63	55 ± 15
5.7-0.01-2	0.0100	0.0010	0.010	-	-2.14	-5.72	-3.60	60 ± 15
5.7-0.01-3	0.0100	0.0010	0.010	-	-2.14	-5.72	-3.79	38 ± 15
5.7-0.01-5	0.0100	0.0010	0.010	-	-2.14	-5.72	-3.47	80 ± 15
7-0.01a-1	0.0100	$1.0x10^{-5}$	0.010	-	-2.07	-6.96	-4.22	14.2 ± 3
7-0.01a-4	0.0100	$1.0x10^{-5}$	0.010	-	-2.07	-6.96	-4.18	15.6 ± 3
7-0.01a-5	0.0100	$1.0x10^{-5}$	0.010	-	-2.07	-6.96	-4.45	8.5 ± 3
7-0.01b-1	0.0100	-	0.010	$1.0x10^{-6}$	-2.10	-6.98	-4.16	16.4 ± 3
5.6-0.06-1	0.0100	0.0100	0.0034	-	-1.24	-5.63	-2.76	412 ± 61
5.6-0.06-2	0.0100	0.0100	0.0034	-	-1.24	-5.63	-2.91	290 ± 61

[a] *Sample names include the pH and aF^- at experimental conditions.*

[b] *The uncertainty in U concentrations is 1 standard deviation; an extra significant figure is added to avoid rounding errors.*

Table 2-1, continued.

	Starting solution compositions, m				Compositions at 200 °C, 15.5 bar			
Sample[a]	**NaF**	**$HClO_4$**	**$NaClO_4$**	**NaOH**	**log aF^-**	**log aH^+**	**log U, m**	**U, ppm**[b]
6.6-0.06a-1	0.100	0.0010	0.10	-	-1.23	-6.63	-3.49	77 ± 16
6.6-0.06a-2	0.100	0.0010	0.10	-	-1.23	-6.63	-3.29	121 ± 16
6.6-0.06a-3	0.100	0.0010	0.10	-	-1.23	-6.63	-3.40	95 ± 16
6.6-0.06a-5	0.100	0.0010	0.10	-	-1.23	-6.63	-3.44	85 ± 16
6.6-0.06b-1	0.100	0.0010	0.10	-	-1.23	-6.63	-3.42	90 ± 16
6.6-0.06b-2	0.100	0.0010	0.10	-	-1.23	-6.63	-3.27	127 ± 16
6.6-0.06b-4	0.100	0.0010	0.10	-	-1.23	-6.63	-3.44	86 ± 16
6.6-0.06b-5	0.100	0.0010	0.10	-	-1.23	-6.63	-3.33	110 ± 16
6.6-0.06b-6	0.100	0.0010	0.10	-	-1.23	-6.63	-3.36	105 ± 16
6.6-0.06b-7	0.100	0.0010	0.10	-	-1.23	-6.63	-3.34	108 ± 16
7.4-0.06a-3	0.100	$1.0x10^{-5}$	0.10	-	-1.18	-7.39	-3.37	101 ± 24
7.4-0.06b-4[c]	0.100	$1.0x10^{-5}$	0.10	-	-1.18	-7.39	-3.28	125 ± 24
7.4-0.06b-5[c]	0.100	$1.0x10^{-5}$	0.10	-	-1.18	-7.39	-3.29	121 ± 24
7.4-0.06b-6[c]	0.100	$1.0x10^{-5}$	0.10	-	-1.18	-7.39	-3.43	88 ± 24
7.4-0.06b-7[c]	0.100	$1.0x10^{-5}$	0.10	-	-1.18	-7.39	-3.46	82 ± 24
7.4-0.06b-8[c]	0.100	$1.0x10^{-5}$	0.10	-	-1.18	-7.39	-3.60	60 ± 24
7.4-0.06b-9[c]	0.100	$1.0x10^{-5}$	0.10	-	-1.18	-7.39	-3.24	138 ± 24
7.4-0.06b-10[c]	0.100	$1.0x10^{-5}$	0.10	-	-1.18	-7.39	-3.57	64 ± 24
7.4-0.06b-11[c]	0.100	$1.0x10^{-5}$	0.10	-	-1.18	-7.39	-3.33	110 ± 24
7.4-0.06b-13[c]	0.100	$1.0x10^{-5}$	0.10	-	-1.18	-7.39	-3.38	98 ± 24
7.4-0.06b-14[c]	0.100	$1.0x10^{-5}$	0.10	-	-1.18	-7.39	-3.40	94 ± 24
7.4-0.06c-2	0.100	-	0.10	-	-1.18	-7.40	-3.22	143 ± 16
7.4-0.06c-3	0.100	-	0.10	-	-1.18	-7.40	-3.23	141 ± 16
7.4-0.06c-4	0.100	-	0.10	-	-1.18	-7.40	-3.34	109 ± 16
7.4-0.06d-1	0.100	-	-	-	-1.18	-7.40	-3.56	65 ± 33
7.4-0.06d-2	0.100	-	-	-	-1.18	-7.40	-3.26	130 ± 33
7.4-0.06e-1	0.100	-	0.10	$1.0x10^{-5}$	-1.23	-7.36	-3.32	114 ± 33
7.4-0.06e-2	0.100	-	0.10	$1.0x10^{-5}$	-1.23	-7.36	-3.40	95 ± 33
7.4-0.06e-3	0.100	-	0.10	$1.0x10^{-5}$	-1.23	-7.36	-3.45	85 ± 33
7.4-0.06e-4	0.100	-	0.10	$1.0x10^{-5}$	-1.23	-7.36	-3.36	105 ± 33
7.4-0.06e-5	0.100	-	0.10	$1.0x10^{-5}$	-1.23	-7.36	-3.50	76 ± 33
6.9-0.1-1	0.200	0.0010	0.20	-	-0.971	-6.88	-3.64	55 ± 33
6.9-0.1-2	0.200	0.0010	0.20	-	-0.971	-6.88	-3.69	48 ± 33
6.9-0.1-3	0.200	0.0010	0.20	-	-0.971	-6.88	-3.43	88 ± 33
6.9-0.1-4	0.200	0.0010	0.20	-	-0.971	-6.88	-3.30	120 ± 33
6.9-0.1-5	0.200	0.0010	0.20	-	-0.971	-6.88	-3.59	62 ± 33
7.5-0.1-3	0.200	-	-	-	-0.922	-7.51	-3.59	61 ± 18
7.5-0.1-4	0.200	-	-	-	-0.922	-7.51	-3.38	98 ± 18
7.5-0.1-5	0.200	-	-	-	-0.922	-7.51	-3.60	60 ± 18
7-0.2-1	0.300	0.0010	0.30	-	-0.820	-7.03	-3.48	78 ± 11
7-0.2-2	0.300	0.0010	0.30	-	-0.820	-7.03	-3.38	99 ± 11
7-0.2-4	0.300	0.0010	0.30	-	-0.820	-7.03	-3.53	71 ± 11
7-0.2-5	0.300	0.0010	0.30	-	-0.820	-7.03	-3.51	74 ± 11
7.6-0.2-2	0.300	-	-	-	-0.771	-7.58	-3.42	89.5 ± 4
7.6-0.2-5	0.300	-	-	-	-0.771	-7.58	-3.39	97.8 ± 4

[c] *Time series data.*

The relationships between the measured log [U] and ligand activities at lower pH and aF^- are more difficult to interpret. The trendline slopes are all positive, indicating the formation of a uranium complex with both H^+ and F^-, such as the oxyfluoride HUO_2F. This species forms from the dissolution reaction:

$$UO_{2\,(s)} + H^+ + F^- = HUO_2\,F_{(aq)} \tag{4}$$

and the expression for the equilibrium constant is given by

$$\log K = \log aHUO_2\,F_{(aq)} - \log aH^+ - \log aF^- \tag{5}$$

Partial differentiation of this expression with respect to log aF^- at constant aH^+ gives

$$\frac{\partial}{\partial log\ aF^-}(log\ aHUO_2F_{(aq)}) = 1 \tag{6}$$

Thus, if HUO_2F was the dominant species in solution, a log-log plot of measured U_{total} vs aF^- should fit a trendline with a slope of 1. Similarly, partial differentiation of Equation 4 with respect to log aH^+ at constant aF^- indicates that a log-log plot of U_{total} vs aH^+ would also fit a trendline with a slope of 1. However, the observed slopes are all less than unity, so the speciation cannot be explained by a single complex with a log U_{total}: log aF^-: log aH^+ ratio of 1:1:1. In Figure 2-4a, excluding the higher slope of the pH 3.3-3.4 trend (0.71 ± 0.05), the trendline slopes average 0.57 ± 0.05. Similarly, apart from the lower slope of the low-fluoride trendline (0.40 ± 0.04), the average of the slopes in Figure 2-4b is 0.52 ± 0.05.

The trendlines with slopes near 0.5 suggest a log U_{total}: log aF^-: log aH^+ ratio of ~2:1:1, indicating the presence of two U^{4+} ions for every F^- and H^+ in solution at the experimental conditions. This ratio could result from the formation of a dimer containing both F^- and H^+, such as $(UO_2)_2(OH)F^{2-}$. Polynuclear complexes, however, are typically less stable at higher

temperature, and as U(IV) dimers have not been detected at ambient conditions, the presence of a dimer is unlikely (Plyasunov and Grenthe, 1994, Grenthe et al., 2020). A combination of two uranium species in a roughly 1:1 mixture could also explain the observed 2:1:1 ratio. For example, a mixture of $UO_{2\,(aq)}$ and $HUO_2F_{\,(aq)}$ is consistent with the observations, and $UO_{2\,(aq)}$ is most likely already present in the high pH, high aF^- solutions. Furthermore, a variation in the proportions of the two species could explain the variations in the trendline slopes.

An additional level of complexity in the species mixture is introduced by the 2.1-E-07 and 3.3-E-05 series of experiments. The fluoride activity of these solutions is too low for the presence of a predominant uranium fluoride complex (Fig. 4-2a), but the positive trend of the low-fluoride (aF- $\approx 10^{-7}$ to 10^{-4}) data in Figure 4-2b indicates the formation of an H^+-bearing species. Explanation of these observations requires the presence of a fluoride-free, hydrogen-bearing complex, and the 0.4 ± 0.04 slope of the trend indicates the presence of ~60% $UO_{2\,(aq)}$.

Thus, to explain the observed variation in slopes, a species mixture that would allow for independent variation of the F^- and H^+ is needed and could be provided by a combination of one F^- species and one H^+ species, in addition to a third species that is independent of both aF^- and aH^+. An appropriate compositional ratio is given by a mixture of UF^{3+} and UOH^{3+}, which are both well-described at ambient conditions (Grenthe et al., 2020). However, the solubility reactions for the formation of these species would require four and three H^+ ions for charge balance respectively, i.e.,

$$UO_{2(s)} + 4H^+ + F^- = UF^{3+} + 2H_2O \quad (7)$$

and

$$UO_{2(s)} + 3H^+ = UOH^{3+} + H_2O \quad (8)$$

Using the same partial differentiation method as for Reaction (3), the formation of these two species would result in an H^+ dependence of either 3 or 4 for each species, or a log U_{total}: log aF^-: log aH^+ ratio of 2:1:7. Thus, a mixture of these species does not explain the data distribution. To fit the observed 2:1:1 ratio, avoiding additional pH dependence, and allowing independent variation in aF^- and aH^+, a mixture of two singly-charged species is required. An appropriate species with an H^+ ligand is HUO_2^+, which has been postulated to exist at ambient conditions. This species is known as $U(OH)_3^+$ in conventional notation (i.e., $HUO_2^+ + H_2O = U(OH)_3^+$), but this study will use the simplified notation of Shock et al. (1997) for ease of calculation, i.e., no more than one H^+ in the stoichiometry of each species. For fluoride complexation, the species UO_2F^-, though not described in the literature, fits the charge and stoichiometry requirements. The solubility reactions for the formation of these species do not require additional H^+ for charge balance:

$$UO_{2(s)} + F^- = UO_2F^- \quad (9)$$

and

$$UO_{2(s)} + H^+ = HUO_2{}^+ \quad (10)$$

Given the above deductions, a species mixture of $UO_{2\,(aq)}$, HUO_2^+, UO_2F^- and perhaps $HUO_2F_{(aq)}$ may adequately describe the experimental data.

2.6 Thermodynamic constants

The distribution of species in the experimental mixture was further resolved with calculations done in OptimA, a module of the HCh thermodynamic modeling software package (Shvarov, 2015). OptimA determines the Gibbs free energies of user-specified species by minimizing the sum of squares for the experimental data via multiple iterations of equilibrium calculations, but initial estimates of the free energies must be provided. These estimates were derived from the log K values of dissolution reactions 3, 4, 9 and 10. The log K of the reactions were calculated by distributing the measured U concentration among the possible species mixtures discussed above.

Optimizations involving multiple combinations of species were attempted, but only the Gibbs free energies of a mixture of $UO_{2\,(aq)}$, HUO_2^+, UO_2F^- and $HUO_2F_{\,(aq)}$ provided a good fit to the experimental data. The mixture of species also explains the scatter in the data, as a slight fluctuation in fluid composition may favour the formation of a stronger or weaker species. The optimized $\Delta_f G^{T,P,0}$ values were used to calculate the $\Delta_r G^{T,P}$ values for each dissolution reaction, which were, in turn, used to calculate the log K values for these reactions (Table 2-2). The reported uncertainties for each constant were propagated from the 95% confidence intervals calculated by OptimA for the optimized $\Delta_f G^{T,P,0}$ values.

Table 2-2 Thermodynamic constants calculated for each U species from the results of this study. The initial $\Delta_f G^{T,P,0}$ is the initial estimate of the Gibbs free energy of formation used as OptimA input, the final $\Delta_f G^{T,P,0}$ is the final optimized value, and $\Delta_r G^{T,P}$ and log $K^{T,P}$ are the Gibbs free energy of reaction and the equilibrium constant for the listed dissolution reaction, respectively. Uncertainties in $\Delta_r G^{T,P}$ and log $K^{T,P}$ were propagated from the 95% confidence interval for the final $\Delta_f G^{T,P,0}$ calculated by OptimA. Free energies are in kJ/mol.

Solubility reaction	**Initial $\Delta_f G^{T,P,0}$**	**Final $\Delta_f G^{T,P,0}$**	**$\Delta_r G^{T,P}$**	**log $K^{T,P}$**
$UO_{2\,(s)} = UO_{2\,(aq)}$	-1017.6	-1006.5 ± 1.1	42.26 ± 1.1	-4.7 ± 0.1

$UO_{2\,(s)} + H^+ = HUO_2^+$	-1065.2	-1039.6 ± 2.8	9.15 ± 2.8	-1.0 ± 0.3
$UO_{2\,(s)} + F^- = UO_2F^-$	-1326.4	-1299.7 ± 0.4	23.95 ± 0.4	-2.64 ± 0.04
$UO_{2\,(s)} + F^- + H+ = HUO_2F_{(aq)}$	-1364.8	-1360.8 ± 0.7	-37.14 ± 0.7	4.10 ± 0.07

The U(IV) solubility for each experimental series calculated using these optimized log K values are a good fit to the experimental measurements, as shown by the "U calc" points for each series in Figure 2-4a-b. The proportions of the four species for each experimental point, given in Table 2-3, are also consistent with the observations. For example, the uranium speciation for the 2.1-E-07 series, which had very low aF^- and high aH^+, is 96% HUO_2^+. Solutions with low aF^- and low aH^+, on the other hand, have high proportions of $UO_{2\,(aq)}$. Overall, only a few solutions had major proportions of $UO_{2\,(aq)}$ or HUO_2^+, resulting in higher uncertainty in the constants for those species. The most abundant species is $HUO_2F_{(aq)}$, closely followed by UO_2F^-. The former is prevalent in solutions with low to moderate pH and moderate to high aF^-, whereas the latter predominates at high pH and high aF^-. The distribution of these species at different pH and aF^- are shown in Bjerrum-type diagrams in Figure 2-5.

Table 2-3 The proportions of the four U species in each experimental solution calculated from the optimized log K values of their dissolution reactions.

Series	**$aUO_{2\,(aq)}$**	**$aHUO_2^+$**	**aUO_2F^-**	**$aHUO_2F_{(aq)}$**
2.1-E-07	2%	96%	0%	2%
3.3-E-05	14%	31%	0%	55%
4-E-04	12%	6%	0%	82%
5.6-E-04	91%	1%	1%	7%
6.3-E-04	90%	0%	2%	7%
3.4-E-03	1%	2%	0%	97%
6.4-E-03	77%	0%	7%	15%
5.7-0.01	10%	0%	8%	82%
7-0.01a	41%	0%	37%	22%

7-0.01b	43%	0%	36%	21%
5.6-0.06	1%	0%	7%	92%
6.6-0.06	7%	0%	41%	53%
7.4-0.06ab	11%	0%	73%	16%
7.4-0.06cd	11%	0%	73%	16%
7.4-0.06e	12%	0%	71%	17%
6.9-0.1	5%	0%	55%	40%
7.5-0.1	6%	0%	80%	14%
7-0.2	4%	0%	63%	33%
7.6-0.2	5%	0%	83%	12%

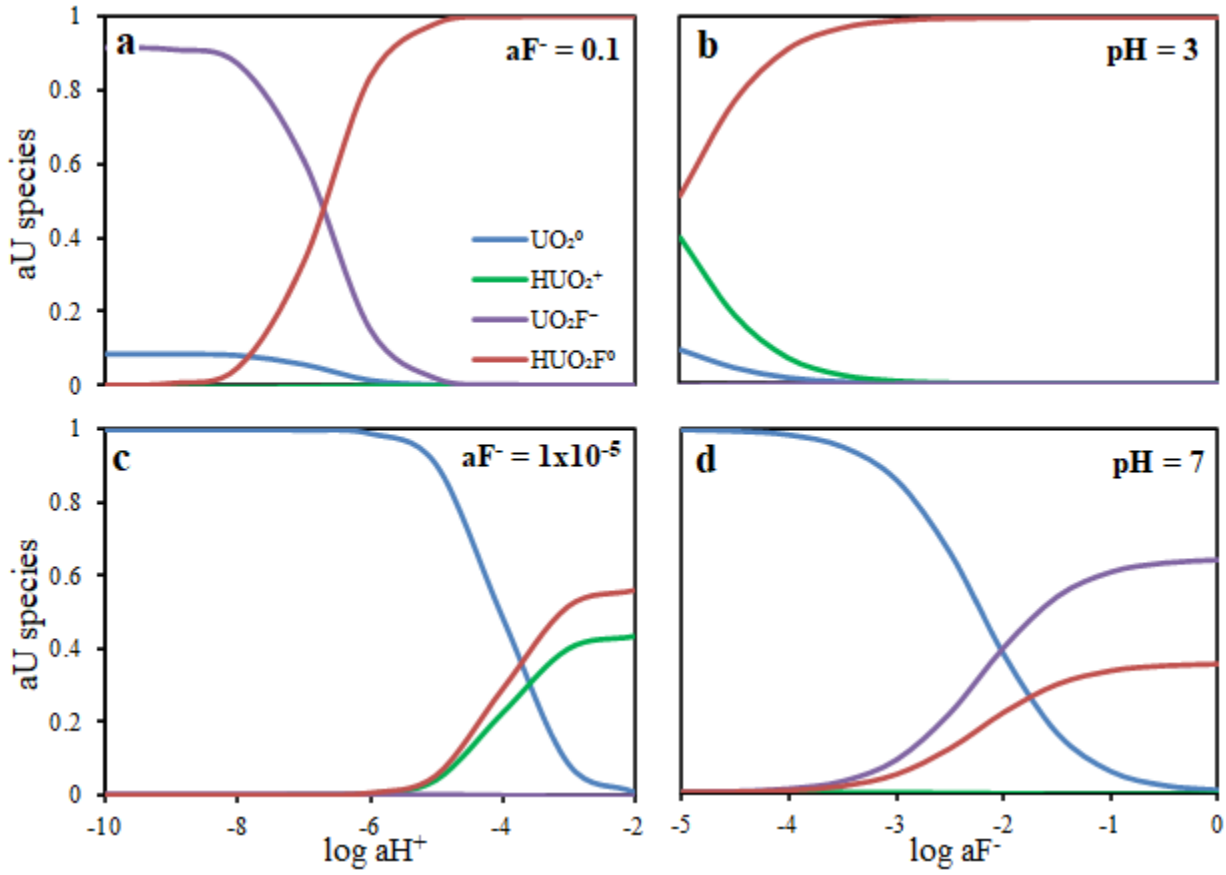

Figure 2-5 Bjerrum speciation diagrams showing the calculated solubility of $UO_{2\,(aq)}$, HUO_2^+, UO_2F^- and $HUO_2F_{\,(aq)}$ at 200 °C and 15.5 bar versus log aH^+ in (a) at $aF^- = 0.1$ m and (c) at $aF^- = 1x10^{-5}$ m, and vs log aF^- in (b) at pH 3 and (d) at pH 7.

Using the optimized log K values, it was possible to correct for the disparate aF^- and aH^+ within each data group in Figure 2-4. The calculated solubility for each adjusted experimental solution and the total solubility of each species are shown in Figure 2-6; the adjusted aF^-, aH^+ and species proportions are given in Table 2-4. These adjustments were mostly minor but comparing the uranium solubilities in solutions with identical aF^- or aH^+ allows for a more accurate interpretation of the trendline slopes. The slopes are mostly in keeping with those of the raw data (Fig. 2-4), but changes in the slopes of the trendlines occur at each data point, and are also indicated by the "U calc" points in Figure 2-4. For example, the slope of the pH 5.6 trendline changes from 0.58 to 0.97 at the midpoint, and that of the pH 6.4 trend changes from 0.11 to 0.67 (Fig. 2-6a). Similarly, the slopes of the $aF^- = 0.06$ and $aF^- = 10^{-4}$ trends change from 0.36 to 0.81 and 0.07 to 0.50, respectively (Fig. 2-6b).

The above changes in slope correspond to changes in speciation, as seen by the species proportions for each series shown in Table 2-4. For example, the change in slope of the pH 5.6 trend is caused by a shift from $UO_{2\,(aq)}$- to HUO_2F-dominated solutions, or a fluoride-independent species to a fluoride-dependent one, and the same shift occurs in the pH 6.4 trend. Interestingly, the plotted slopes of the shorter trendlines are identical in terms of the average aF^- or aH^+ dependence of the species mixture at each trendline endpoint, and those of the longer trendlines are generally within ± 0.03 of the calculated dependencies (Table 2-5). This observation indicates that, even for a four-species mixture, the slope method of determination for species stoichiometry is applicable, which is of importance for future solubility studies of this type.

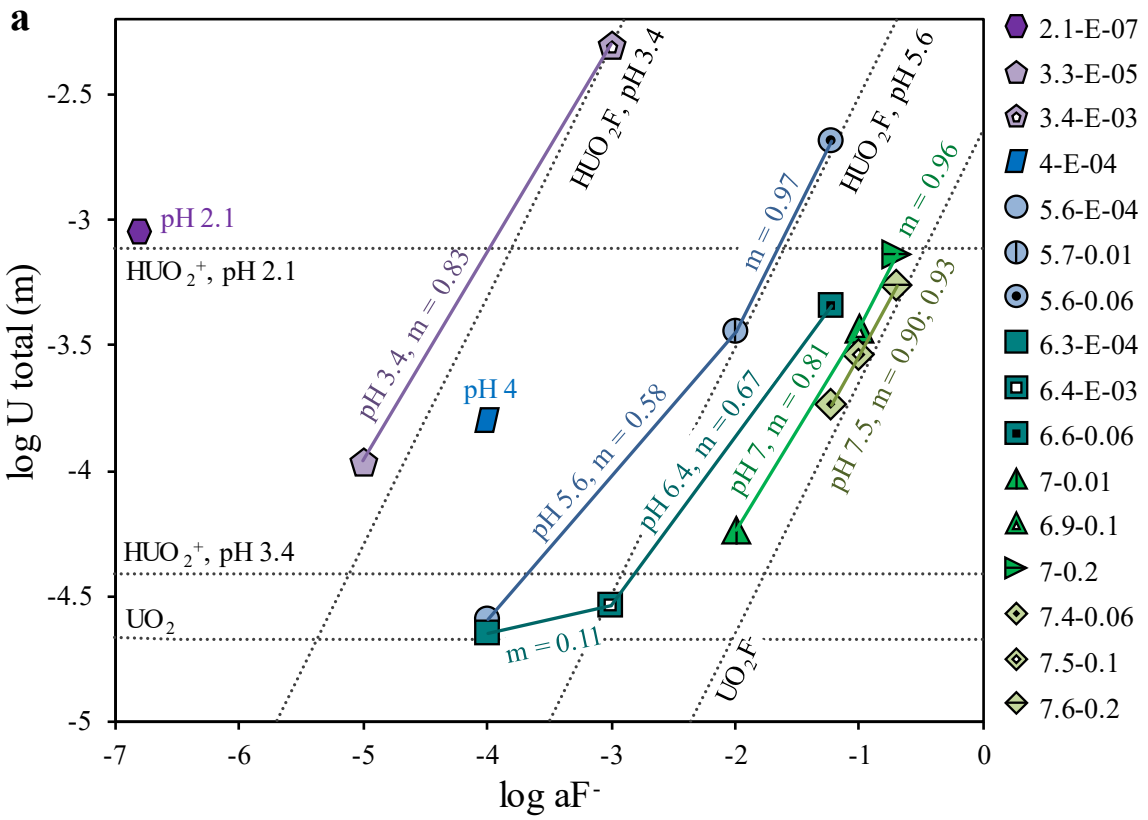
a
log U total (m)
log aF⁻
pH 2.1
HUO2+, pH 2.1
HUO2+, pH 3.4
UO2
pH 4
pH 3.4, m = 0.83
HUO2F, pH 3.4
pH 5.6, m = 0.58
m = 0.97
HUO2F, pH 5.6
pH 6.4, m = 0.67
pH 7, m = 0.81
m = 0.96
pH 7.5, m = 0.90; 0.93
m = 0.11
UO2F
2.1-E-07
3.3-E-05
3.4-E-03
4-E-04
5.6-E-04
5.7-0.01
5.6-0.06
6.3-E-04
6.4-E-03
6.6-0.06
7-0.01
6.9-0.1
7-0.2
7.4-0.06
7.5-0.1
7.6-0.2

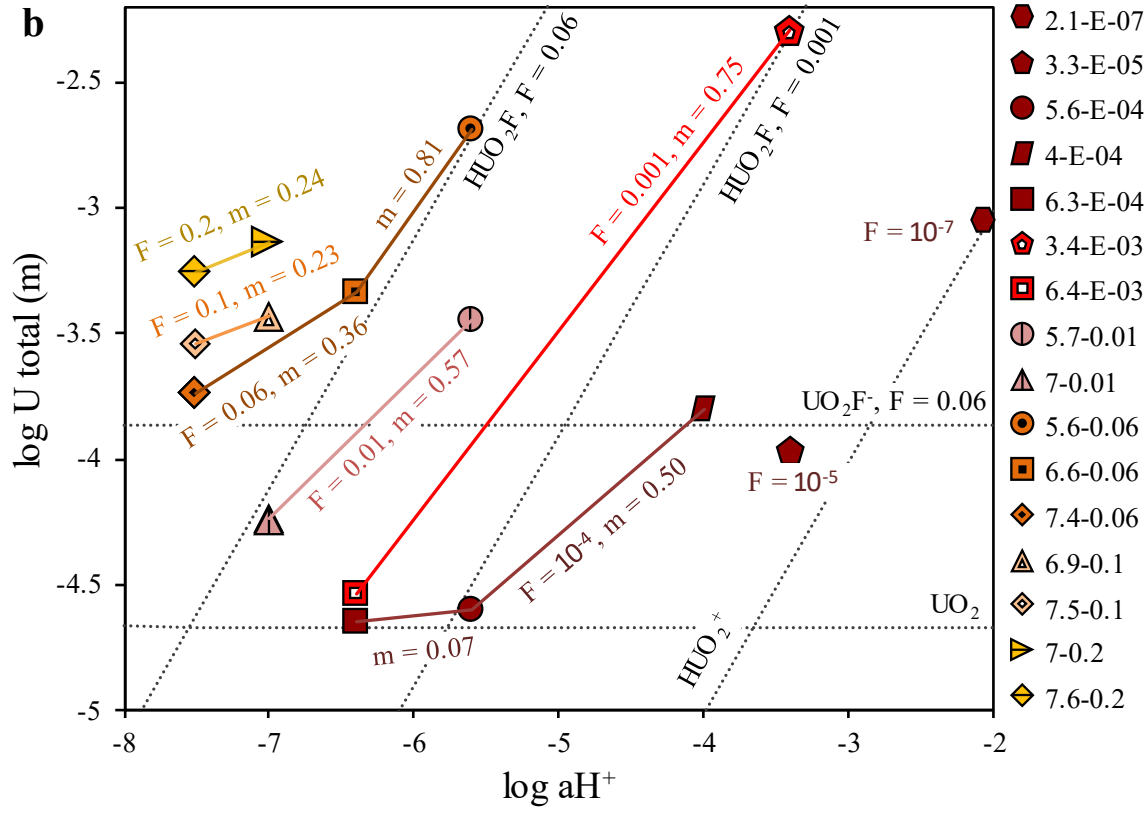
b
log U total (m)
log aH⁺
F = 0.2, m = 0.24
F = 0.1, m = 0.23
F = 0.06, m = 0.36
m = 0.81
HUO2F, F = 0.06
F = 0.01, m = 0.57
F = 0.001, m = 0.75
HUO2F, F = 0.001
F = 10⁻⁷
UO2F⁻, F = 0.06
F = 10⁻⁵
F = 10⁻⁴, m = 0.50
m = 0.07
UO2
HUO2+
2.1-E-07
3.3-E-05
5.6-E-04
4-E-04
6.3-E-04
3.4-E-03
6.4-E-03
5.7-0.01
7-0.01
5.6-0.06
6.6-0.06
7.4-0.06
6.9-0.1
7.5-0.1
7-0.2
7.6-0.2

Figure 2-6 Plots of the calculated UO_2 solubility based on optimized log K values for mixtures of $UO_{2\,(aq)}$, HUO_2^+, UO_2F^- and $HUO_2F_{(aq)}$ versus adjusted ligand activities. (a) log U_{total} vs log aF^-, comparing points at constant pH, and (b) log U_{total} vs log aH^+, comparing points at constant aF^-. The symbols and colours are as in Figure 2-4. The trendlines are plotted between each point within a given group, and are labelled with the slope, m. The dotted lines represent the calculated solubility of the four species. In (a), solubility contours of the pH-dependent species are shown at pH 2.1 and 3.4 for HUO_2^+, and at pH 3.4 and 5.6 for $HUO_2F_{(aq)}$ in order to illustrate the proportion of these species in the solubility data at those pH values. Similarly, in (b), solubility contours of the fluoride-dependent species are shown at $aF^- = 0.06$ m for UO_2F^- and $HUO_2F_{(aq)}$.

Table 2-4 The proportions of each U species for each solution calculated using adjusted aF^- and aH^+ values to allow for the comparison of data with identical aF^- or aH^+, and the total dependence of each species mixture on the two ligands, i.e., the number of H^+ and F^- ions for each U^{4+} ion.

	Adjusted activities		**Species mixture**				**Dependence**	
Series	**log aF^-**	**log aH^+**	**$aUO_{2\,(aq)}$**	**$aHUO_2^+$**	**aUO_2F^-**	**$aHUO_2F_{(aq)}$**	**H^+**	**F^-**
3.3-E-05	-5	-3.4	20%	35%	0%	45%	0.45	0.80
4-E-04	-4	-4	14%	6%	0%	80%	0.80	0.86
5.6-E-04	-4	-5.6	86%	1%	1%	13%	0.13	0.13
6.3-E-04	-4	-6.4	97%	0%	1%	2%	0.03	0.02
3.4-E-03	-3	-3.4	0%	1%	0%	99%	0.99	1.00
6.4-E-03	-3	-6.4	75%	0%	8%	17%	0.25	0.17
5.7-0.01	-2	-5.6	6%	0%	6%	88%	0.94	0.88
7-0.01	-2	-7	38%	0%	40%	22%	0.62	0.22
5.6-0.06	-1.22	-5.6	1%	0%	7%	92%	0.99	0.92
6.6-0.06	-1.22	-6.4	5%	0%	30%	66%	0.95	0.66
7.4-0.06	-1.22	-7.5	12%	0%	75%	13%	0.88	0.13
6.9-0.1	-1	-7	6%	0%	61%	34%	0.94	0.34
7.5-0.1	-1	-7.5	7%	0%	79%	14%	0.93	0.14
7-0.2	-0.70	-7	3%	0%	62%	35%	0.97	0.35
7.6-0.2	-0.70	-7.5	4%	0%	82%	14%	0.96	0.14

Table 2-5 Series numbers for the endpoints of each trendline plotted in Figure 2-6, the average ligand dependence of the two endpoints calculated from the species mixtures, and the plotted slopes of each trendline. Trendline labels are as in Figure 2-6; "low" and "high" refer to the U concentrations of individual line segments. The ligand dependence refers to F^- for the U_{total} vs aF^- data, and to H^+ for the U_{total} vs H^+ data.

			Ligand dependence	
Trendline	**Endpoint A**	**Endpoint B**	**Calculated**	**Plotted**
U_{total} vs aF^-				
pH 3.4	3.3-E-05	3.4-E-03	0.72	0.83
pH 5.6 low	5.6-E-04	5.7-0.01	0.54	0.58
pH 5.6 high	5.7-0.01	5.6-0.06	0.96	0.97
pH 6.4 low	6.3-E-04	6.4-E-03	0.14	0.11
pH 6.4 high	6.4-E-03	6.6-0.06	0.60	0.67
pH 7 low	7-0.01	6.9-0.1	0.78	0.81
pH 7 high	6.9-0.1	7-0.2	0.96	0.96
pH 7.5 low	7.4-0.06	7.5-0.1	0.90	0.90
pH 7.5 high	7.5-0.1	7.6-0.2	0.94	0.93
U_{total} vs H^+				
F = E-04 low	6.3-E-04	5.6-E-04	0.08	0.07
F = E-04 high	5.6-E-04	4-E-04	0.50	0.50
F = 0.001	6.4-E-03	3.4-E-03	0.58	0.75
F = 0.01	5.7-0.01	7-0.01	0.55	0.55
F = 0.06 low	7.4-0.06	6.6-0.06	0.39	0.39
F = 0.06 high	6.6-0.06	5.6-0.06	0.79	0.81
F = 0.1	6.9-0.1	7.5-0.1	0.24	0.23
F = 0.2	7-0.2	7.6-0.2	0.24	0.24

2.7 Discussion

Few experimental studies of U(IV) solubility in aqueous solution have been conducted at elevated temperatures and pressures, and of those, only one has evaluated fluoride complexation. Nevertheless, since two of the uranium species evaluated here do not contain fluoride, the results of prior experimental studies of fluoride-free fluids may still be of relevance to this study. These experiments are discussed below.

Tremaine et al. (1981) investigated UO_2 solubility in highly alkaline fluids at 25-300 °C, and found that $U(OH)_5^-$ (or HUO_3^- in nonconventional notation) was the dominant species in solution due to a dependence of uranium concentrations on OH^- activity, though most of their data were not reported. The equilibrium constant for the species was given as -5.86 + 32/T, which at 200 °C and the highest pH of this study (7.6), yields a log a $U(OH)_5^-$ of -3.83. This result is within the range of U concentrations reported here, but lower than the measured solubility at pH 7.6 and an aF^- of 0.2 (-3.41). Thus, the dominant species under those conditions (UO_2F^-) is most likely more stable than $U(OH)_5^-$ in fluoride-bearing solutions, but their work confirms the importance of U(IV) in uranium transport.

Two studies have investigated the solubility of uraninite under reducing conditions in solutions that likely favour the formation of $UO_{2\,(aq)}$. Parks and Pohl (1988) conducted experiments at 100 to 300°C in HCl, NaOH, and LiOH solutions and found a general increase in U(IV) solubility with decreasing pH from ~9 to 1, which they attributed to the formation of UOH_3^+ at pH < 4 and $UO_{2\,(aq)}$ at pH > 4. However, all the measured U concentrations were below that of the $UO_{2\,(aq)}$ stability determined in this study (log U from -10 to -6 vs. -4.67) and, based on scatter in the data of up to an order of magnitude, the authors concluded that equilibrium had not been reached. The second study was conducted by Red'kin et al. (1989), who reported log U molal concentrations of -8.5 to -3.5 in pure water at 500 °C and 1 kbar, which are within the same range as those of Parks and Pohl (1988) at a lower temperature and pH. Red'kin et al. (1989) also stated that UO_2 solubility increases in the presence of chloride and fluoride, but did not report the data needed to support the statement.

Timofeev et al. (2018) carried out UO_2 solubility experiments at 250-350 °C in solutions with acidic pH (1.4-1.7 at 25 °C) and variable NaCl concentrations, and found that U

concentration increased with increasing temperature and aCl^-. At 350 °C, log U molal concentrations increased from -7.08 to -5.69 with increasing log aCl^- in a 4:1 ratio, and the authors attributed this result to the formation of $UCl_{4\,(aq)}$. This solubility, while higher than that in the chloride-free fluids of Red'kin et al. (1989), is still relatively low compared to those of this study. As demonstrated in a review of available thermodynamic data for uranium by Guillaumont et al. (2003), U-fluoride species are much stronger than U chlorides; for example, the log K values of UF_3^+ and UCl_3^+ at ambient conditions are 9.42 and 1.72, respectively. Thus, the higher solubility observed in the fluoride-bearing solutions of the current study are unsurprising.

The solubility of uraninite at 500 °C and 1 kbar was investigated by Kovalenko et al. (2011) in highly acidic chloride-bearing solutions (pH -0.3-3 at 25 °C) and yielded log U molal concentrations of -2.06 to 0.84 that increased sharply with increasing aCl^-. The authors found that the solubility at a pH of 1.3 to 3 was controlled by $UO_{2\,(aq)}$, and at lower pH by $UO_2Cl_{2\,(aq)}$ and $HUOCl_3$, with possible contributions of $UCl_{4\,(aq)}$ at the lowest pH conditions. The log K value for $UO_{2\,(aq)}$ was reported to be -6.64, i.e., lower than that of this study (-4.67), but no information was provided on how the constant was determined.

Finally, Kovalenko et al. (2012) assessed UO_2 solubility in fluoride-bearing solutions at 500 °C, 1 kbar and near-neutral pH. They reported log U molal concentrations of -4.64 to -2.54, i.e., very similar to those of this study (-4.89 to -2.63) and showed that the species were a mixture of $UO_{2\,(aq)}$, $HUO_2F_{\,(aq)}$ with a minor contribution from $UOF_{2\,(aq)}$, and the possible presence of $U(OH)F_{3\,(aq)}$ and/or $UF_{4\,(aq)}$. Their log K value for $UO_{2\,(aq)}$ is the same as that given in Kovalenko et al. (2011), and that for $HUO_2F_{\,(aq)}$ is 6.34 (vs 4.10 for this study). Given the different temperature and fluid density involved, our results are in reasonable agreement. The

charged species HUO_2^+ and UO_2F^- described in this study are unlikely to be stable in the low-density fluids of their work, which favour ion association (Plyasunov and Grenthe, 1994). The high solubility measured in their experiments confirm the greater strength of fluoride complexes over chlorides, as well as the importance of U(IV) species in the hydrothermal transport of uranium.

2.7.1 Implications for hydrothermal uranium deposits

The results of this study show that U(IV) is highly mobile as fluoride complexes in acidic to alkaline hydrothermal fluids at 200 °C and a fO_2 near that of the hematite-magnetite buffer. These parameters coincide or overlap with those of many known hydrothermal uranium deposits, particularly breccia- or vein-hosted deposits associated with fluoride-rich magmas (e.g., Cuney, 2009, Skirrow et al., 2009), indicating that U(IV) fluoride species may play an important role in the transport and deposition of uranium. As an example, an ore-forming model for the giant IOCG-type Olympic Dam deposit, South Australia, is outlined below.

At Olympic Dam, uranium ore is hosted in extensive hematite breccias and is associated with Cu-Fe sulphide minerals as well as abundant fluorite (Oreskes and Einaudi, 1992). The deposit history is thought to consist of an early magnetite-pyrite stage followed by a hematite-uraninite-fluorite stage and a later Cu-Fe sulphide stage. Models by Bastrakov et al. (2007) and Verdugo-Ihl et al. (2020) provide fO_2 estimates for the deposit within several log units below the hematite-magnetite buffer. The ore fluids have a wide range of salinity, from 7.3 to 23.7 wt% NaCl, together with other solutes, including CaF^+, and a pH within about one log unit below neutral (5.6 at 200 °C; Oreskes and Einaudi, 1992 Bastrakov et al., 2007, Verdugo-Ihl et al., 2020). Homogenization temperatures of two-phase fluid inclusions in fluorite range from about

130 to 280 °C, and some inclusions host probable fluorite crystals that suggest supersaturation of the fluid with respect to CaF_2 (Oreskes and Einaudi, 1992).

Based on the above characteristics, the uranium-bearing ore fluids of this deposit were very likely to have provided the necessary conditions for the formation of aqueous U(IV) fluoride species. The most critical parameter, the oxygen fugacity, was below the U_3O_8-UO_2 reaction boundary (Fig. 2-2), which promoted the stability of U(IV) over U(VI) species in solution. The ore fluid was enriched in chloride, but also in fluoride, and as noted above, U fluoride species are more stable than U chloride species. Furthermore, the pH of the fluid was at the appropriate level to favour $HF_{(aq)}$ dissociation and the formation of UO_2F^- and $HUO_2F_{(aq)}$, rather than the less soluble and fluoride-independent $UO_{2\,(aq)}$ and HUO_2^+. Finally, we note that the uranium concentrations measured in our experiments, which were on the order of 100s of ppm, are more than sufficient for the formation of this giant orebody.

2.8 Conclusion

The data obtained from this study demonstrate that U(IV) is highly soluble in fluoride-bearing aqueous solutions under reduced conditions, due to the formation of the species UO_2F^- and $HUO_2F_{(aq)}$, which promoted a measured U solubility of up to 552 ± 64 ppm. In solutions with very low aF^-, the species $UO_{2\,(aq)}$ and HUO_2^+ yielded a solubility of up to 298 ± 65 ppm. Contrary to common perception, therefore, U(IV) may be as important as U(VI) in the transport of U in ore fluids, and must be considered in models of hydrothermal uranium ore deposit genesis.

2.9 References

Bastrakov, E.N., Skirrow, R.G. and Davidson, G.J., 2007. Fluid evolution and origins of iron oxide Cu-Au prospects in the Olympic Dam District, Gawler Craton, South Australia. Economic Geology 102, 1415-1440.

Bastrakov E. N., Jaireth S. and Mernagh T. P. (2010) Solubility of uranium in hydrothermal fluids at 25 to 300 C. Geoscience Australia 29, 91.

Burt D. M. and Sheridan M.F. (1981) Model for the formation of uranium/lithophile element deposits in fluorine-rich volcanic rocks. In: AAPG Studies in Geology V 13, Uranium in Volcanic and Volcaniclastic Rocks (eds. P.C. Goodell and A.C. Waters).

Chabiron A., Alyoshin A. P., Cuney M., Deloule E., Golubev V. N., Velitchkin V. I. and Poty B. (2001) Geochemistry of the rhyolitic magmas from the Streltsovka caldera (Transbaikalia, Russia): a melt inclusion study. Chemical Geology 175, 273–290.

Choppin G. R. and Unrein P. J. (1976) Thermodynamic study of actinide fluoride complexation. In Transplutonium Elements (eds. W. Muller and R. Linder). North Holland Publishing Company, Amsterdam.

Cuney M. (2009) The extreme diversity of uranium deposits. Mineralium Deposita 44, 3-9.

Cuney M. (2014) Felsic magmatism and uranium deposits. Bulletin de la Société Géologique de France 185, 75-92.

Cunningham C. G., Rasmussen J. D., Steven T. A., Rye R. O., Rowley P. D., Romberger S. B. and Selverstone J. (1998) Hydrothermal uranium deposits containing molybdenum and

fluorite in the Marysvale volcanic field, west-central Utah. Mineralium Deposita 33, 477–494.

Dahlkamp F. J. (1993) Uranium Ore Deposits., Springer Berlin Heidelberg, Berlin, Heidelberg.

Fujiwara K., Yamana H., Fujii T. and Moriyama H. (2003) Determination of uranium (IV) hydrolysis constants and solubility product of $UO_2 \cdot xH_2O$. Radiochimica Acta 91, 345–350.

Garrels, R.M. and Christ, C.L. 1965, Solutions, Minerals, and Equilibria: New York, Harper & Row, Harper's Geoscience Series.

Grenthe I. and Varfeldt J. (1969) A potentiometric study of fluoride complexes of uranium (IV) and uranium (VI) using the U (VI)/U (IV) redox couple. Acta Chemica Scandinavica 23, 988–998.

Gayer K. H. and Leider H. (1955) The solubility of uranium trioxide, $UO_3 \cdot H_2O$, in solutions of sodium hydroxide and perchloric acid at 25°. Journal of the American Chemical Society 77, 1448–1450.

Gayer K. H. and Leider H. (1957) The solubility of uranium(IV) hydroxide in solutions of sodium hydroxide and perchloric acid at 25 C. Canadian Journal of Chemistry 35, 5–7.

Grenthe I., Gaona X., Rao L., Plyasunov A., Runde W., Grambow B., Konings R., Smith A. and Moore E. (2020) Second update on the chemical thermodynamics of uranium, neptunium, plutonium, americium and technetium. Chemical thermodynamics Volume 14. ed. M.-E. Ragoussi, Organisation for Economic Co-Operation and Development, Paris, France.

Guillaumont R., Fanghänel T., Neck V., Fuger J., Palmer D. A., Grenthe I. and Rand M. H. (2003) Update on the chemical thermodynamics of uranium, neptunium, plutonium, americium and technetium. eds. F. J. Mompean, M. Illemanssene, C. Domenech-Orti, and K. Ben Said, Elsevier, Amsterdam.

Helgeson, H.C., Kirkham, D.H., and Flowers, G.C., 1981, Theoretical prediction of the thermodynamic behavior of aqueous electrolytes by high pressures and temperatures; IV, Calculation of activity coefficients, osmotic coefficients, and apparent molal and standard and relative partial molal properties to 600 degrees C and 5kb: American journal of science, v. 281, p. 1249–1516.

Hu R.-Z., Bi X.-W., Zhou M.-F., Peng J.-T., Su W.-C., Liu S. and Qi H.-W. (2008) Uranium metallogenesis in South China and its relationship to crustal extension during the Cretaceous to Tertiary. Economic Geology 103, 583–598.

Kakihana H. and Ishiguro S. (1974) Potentiometric and spectrophotometric studies of fluoride complexes of uranium (IV). Bulletin of the Chemical Society of Japan 47, 1665–1668.

Kerr P. F., Brophy G. P., Dahl H. M., Green J. and Woolard L. E. (1957) Marysvale, Utah, uranium area: geology, volcanic relations, and hydrothermal alteration., Geological Society of America, New York.

Kovalenko N. I., Ryzhenko B. N., Prisyagina N. I. and Bychkova Ya. V. (2011) Experimental study of uraninite solubility in aqueous HCl solutions at 500°C and 1 kbar. Geochem. Int. 49, 262–273.

Kovalenko N. I., Ryzhenko B. N., Prisyagina N. I. and Bychkova Ya. V. (2012) Experimental determination of uranium (IV) speciation in HF solutions at 500°C and 1000 bar. Geochem. Int. 50, 18–25.

Langmuir D. (1978) Uranium solution-mineral equilibria at low temperatures with applications to sedimentary ore deposits. Geochimica et Cosmochimica Acta 42, 547–569.

Meunier J. D., Landais P. and Pagel M. (1990) Experimental evidence of uraninite formation from diagenesis of uranium-rich organic matter. Geochimica et Cosmochimica Acta 54, 809–817.

Migdisov A. A. and Williams-Jones A. E. (2007) An experimental study of the solubility and speciation of neodymium(III) fluoride in F-bearing aqueous solutions. Geochimica et Cosmochimica Acta 71, 3056–3069.

Migdisov Art. A., Williams-Jones A. E. and Wagner T. (2009) An experimental study of the solubility and speciation of the rare earth elements(III) in fluoride- and chloride-bearing aqueous solutions at temperatures up to 300 °C. Geochimica et Cosmochimica Acta 73, 7087–7109.

Nakashima S., Disnar J. R., Perruchot A. and Trichet J. (1984) Experimental study of mechanisms of fixation and reduction of uranium by sedimentary organic matter under diagenetic or hydrothermal conditions. Geochimica et Cosmochimica Acta 48, 2321–2329.

Neck V. and Kim J. I. (2001) Solubility and hydrolysis of tetravalent actinides. Radiochimica Acta 89, 1–16.

Nisbet H., Migdisov A., Xu H., Guo X., van Hinsberg V., Williams-Jones A. E., Boukhalfa H. and Roback R. (2018) An experimental study of the solubility and speciation of thorium in chloride-bearing aqueous solutions at temperatures up to 250 °C. Geochimica et Cosmochimica Acta 239, 363–373.

Norén B. (1969) A solvent extraction and potentiometric study of fluoride complexes of thorium (IV) and uranium (IV). Acta Chem. Scand 23.

Oreskes N. and Einaudi M. T. (1992) Origin of hydrothermal fluids at Olympic Dam; preliminary results from fluid inclusions and stable isotopes. Economic Geology 87, 64–90.

Parks G. A. and Pohl D. C. (1988) Hydrothermal solubility of uraninite. Geochimica et Cosmochimica Acta 52, 863–875.

Pearson R. G. (1963) Hard and soft acids and bases. J. Am. Chem. Soc. 85, 3533–3539.

Plant J.A, Simpson P.R., Smith B. and Windley B. (1999) Uranium ore deposits – Product of the radioactive Earth. In Reviews in Mineralogy V. 38, Uranium: Mineralogy, Geochemistry and the Environment, 696 pp.

Plyasunov, A.V. and Grenthe, I., 1994. The temperature dependence of stability constants for the formation of polynuclear cationic complexes. Geochimica et Cosmochimica Acta 58, 3561-3582.

Red'kin, A.F., Savelyeva N.I., Sergeyeva E.I., Omelyanenko, B.I. and Khodakovsky, I.L., 1989. Investigation of uraninite (UO_2) solubility under hydrothermal conditions. Sciences Géologiques, bulletins et mémoires 42, 329-334.

Robinson B. W. and Ohmoto H. (1973) Mineralogy, fluid inclusions, and stable isotopes of the Echo Bay U-Ni-Ag-Cu deposits, Northwest Territories, Canada. Economic Geology 68, 635–656.

Rogers J. J., Ragland P. C., Nishimori R. K., Greenberg J. K. and Hauck S. A. (1978) Varieties of granitic uranium deposits and favorable exploration areas in the eastern United States. Economic Geology 73, 1539–1555.

Romberger S. B. (1984) Transport and deposition of uranium in hydrothermal systems at temperatures up to 300 °C: geological implications. In uranium geochemistry, mineralogy, geology, exploration and resources (eds. B. De Vivo, F. Ippolito, G. Capaldi, and P. R. Simpson). Springer Netherlands, Dordrecht. pp. 12–17.

Sawant R. M., Chaudhuri N. K. and Patil S. K. (1990) Potentiometric studies on aqueous fluoride complexes of actinides: Stability constants of Th(IV)-, U(IV)-, Np(IV)-and Pu(IV)-fluorides. Journal of Radioanalytical and Nuclear Chemistry 143, 295–306.

Schilt A. A., McBride L. and Long J. R. (1979) Perchloric acid and perchlorates., GF Smith Chemical Company, Columbus, OH.

Shock E. L., Sassani D. C. and Betz H. (1997) Uranium in geologic fluids: estimates of standard partial molal properties, oxidation potentials, and hydrolysis constants at high temperatures and pressures. Geochimica et Cosmochimica Acta 61, 4245–4266.

Shvarov Y. V. and Bastrakov E. N. (1999) HCh: A software package for geochemical equilibrium modeling. User's guide. Australian Geological Survey Organisation Record 25, 67 pp.

Shvarov Y. V. (2015) A suite of programs, OptimA, OptimB, OptimC, and OptimS compatible with the Unitherm database, for deriving the thermodynamic properties of aqueous species from solubility, potentiometry and spectroscopy measurements. Applied Geochemistry 55, 17-27.

Skirrow R. G., Jaireth S., Huston D., Bastrakov E., Schofield A. and Wielen S. (2009) Uranium mineral systems; processes, exploration criteria and a new deposit framework. Rec. Geosci. Aus.

Timofeev A., Migdisov A. A., Williams-Jones A. E., Roback R., Nelson A. T. and Xu H. (2018) Uranium transport in acidic brines under reducing conditions. Nature Communications 9, 1469.

Tremaine, P.R., Chen, J.D., Wallace, G.J. and Bovin, W.A., 1981. Solubility of uranium (IV) oxide in alkaline aqueous solutions to 300°C. Journal of Solution Chemistry 10, 221-230.

Truesdell, A.H., and Jones, B.F., 1974, WATEQ, a computer program for calculating chemical equilibria of natural waters: J. Res. US Geol. Surv, v. 2, p. 233–248.

Verdugo-Ihl, M.R., Ciobanu, C.L., Cook, N.J., Ehrig, K.J. and Courtney-Davies, L., 2020. Defining early stages of IOCG systems: evidence from iron oxides in the outer shell of the Olympic Dam deposit, South Australia. Mineralium Deposita 55, 429-452.

Wei W.-F., Chen X., Yu Z.-Q., Chen W.-F., Fang Q.-C., Tang X.-S. and Ling H.-F. (2021) Different hydrothermal fluids inducing alteration and uranium mineralisation in the Baquan deposit of the Xiangshan uranium ore field: Constraints from geochemistry of altered rocks and ores. Ore Geology Reviews 139, 104475.

Xing Y., Mei Y., Etschmann B., Liu W. and Brugger J. (2018) Uranium transport in F-Cl-bearing fluids and hydrothermal upgrading of U-Cu ores in IOCG deposits. Geofluids 2018, 22 pages.

Xing Y., Etschmann B., Liu W., Mei Y., Shvarov Y., Testemale D., Tomkins A. and Brugger J. (2019) The role of fluorine in hydrothermal mobilization and transportation of Fe, U and REE and the formation of IOCG deposits. Chemical Geology 504, 158–176.

Chapter 3 Extended Conclusion

The solubility of U(IV) in fluoride-bearing solutions at 200 °C, saturated vapour pressure (15.5 bars), and an oxygen fugacity corresponding to that of the hematite-magnetite buffer was determined experimentally. The findings of this thesis were as follows:

(1) U(IV) is highly soluble as fluoride complexes under moderate temperature, acidic to alkaline and reduced conditions.

(2) The species in solution were postulated to be $UO_{2\,(aq)}$, HUO_2^+, UO_2F^- and HUO_2F, which have Gibbs free energies of formation of -1006.5 ± 1.1, -1039.6 ± 2.8, -1299.7 ± 0.4 and -1360.8 ± 0.7 kJ/mol, respectively, at the conditions of the experiments.

(3) The equilibrium constants for the reactions governing the dissolution of the reactant (uraninite) to $UO_{2\,(aq)}$, HUO_2^+, UO_2F^- and HUO_2F are -4.7 ± 0.1, -1.0 ± 0.3, -2.64 ± 0.04 and 4.10 ± 0.07 at the experimental conditions.

(4) The species $UO_{2\,(aq)}$ is dominant in solutions with low aF^- and low aH^+, whereas the species HUO_2^+ dominates in those with low aF^- and high aH^+. Nevertheless, the stability of these species is relatively low. The more stable UO_2F^- is favoured in solutions at high aF^- and low aH^+, whereas the most stable species, $HUO_2F_{(aq)}$, is predominates in solutions with moderate to high aF^- and aH^+.

(5) The slopes of the measured uranium concentrations plotted versus aF^- and aH^+ activity are less than one, indicating a mixture of uranium species. The solubility of uranium calculated using the log K values reported above, plotted versus adjusted aF^- and aH^+, produced trendlines with slopes equal to the average F^- or H^+ dependence of the species mixtures at each endpoint.

(6) Under hydrothermal conditions in acidic to alkaline fluids, uranium oxide, oxyacid, fluoride, or hydroxyfluoride species may be the agents of uranium (IV) transport in ore-forming systems. In fluoride-poor or fluoride-free fluids, formation of the less soluble but fluoride-independent species will dissolve considerable amounts of uranium, and high U concentrations (hundreds of ppm) can be reached in fluoride-bearing fluids through the formation of UO_2F^- and HUO_2F.

(7) The concentrations of uranium (hundreds of ppm) obtained in our experiments at elevated fluoride activity, and temperature/fO_2 conditions similar to those that formed the giant Olympic Dam Cu-U deposit in Australia, would be sufficient to make an economic uranium deposit.

3.1 Contribution to body of work

This study contributes much-needed data on the solubility and speciation of U(IV) in fluoride-bearing fluids at the temperatures common to the formation of many hydrothermal uranium deposits. The high solubility of uranium measured in this study demonstrates that, contrary to common belief, uranium is highly mobile in aqueous solutions in the 4+ valence state. The thermodynamic constants provided in Chapter 2 will find direct application in the development of genetic models of fluoride-rich uranium deposits, for which the potential role of fluoride in uranium transport has previously been ignored. This study also emphasises the importance of understanding the solubility and hydrothermal speciation of U(IV) and contributes significantly to the building of a body of experimental data, showing that U(IV) can be transported at ore-forming concentrations by species involving ligands like Cl^- and F^- that

commonly have high concentrations in hydrothermal fluids (e.g., Kovalenko et al., 2012, Timofeev et al., 2018).

3.2 Future work

The next logical step in the investigation of U(IV) fluoride speciation would be to extend the work to temperatures other that 200 ^{o}C in order to obtain temperature-dependent Ryzhenko-Bryzgalin parameters that will allow the extrapolation or interpolation of the experimental data to other temperatures of interest. Additional experiments on uranium fluoride speciation over a range of temperatures will not only serve as a secondary check on the reliability of the data presented in this study, but will allow for ever more accurate models of this speciation. Analogous solubility and speciation experiments on oxidized U(VI) fluoride speciation at high temperatures would also be an important contribution to uranium ore deposit modeling, as this system has been investigated in only one study at temperatures up to 150 °C (Kirishima et al., 2004). An experiment that could be performed would be with a flow-through apparatus in which a fluid rich in fluoride is transported through uraninite ore under conditions varying from reduced to oxidizing in order to simulate the evolving fluid compositions common to ore systems, e.g., the shift in the source of the fluid from magmatic to meteoric. Finally, it would be important to re-examine a fluoride-rich uranium deposit in detail, such as the Xiangshan ore field, China, to determine whether the application of the data acquired in this thesis could lead to an improved model of ore genesis.

3.3 References

Kirishima A., Kimura T., Tochiyama O. and Yoshida Z. (2004) Speciation study on complex formation of uranium(VI) with phosphate and fluoride at high temperatures and pressures by time-resolved laser-induced fluorescence spectroscopy. Radiochimica Acta 92, 889–896.

Kovalenko N. I., Ryzhenko B. N., Prisyagina N. I. and Bychkova Ya. V. (2012) Experimental determination of uranium (IV) speciation in HF solutions at 500°C and 1000 bar. Geochem. Int. 50, 18–25.

Timofeev A., Migdisov A. A., Williams-Jones A. E., Roback R., Nelson A. T. and Xu H. (2018) Uranium transport in acidic brines under reducing conditions. Nature Communications 9, 1469.

Chapter 4 Appendix

Certain experimental results from this study were excluded from the data analysis, and are shown in grey below. Samples showing evidence of contamination from the uraninite reagent were omitted, as were samples in which the experimental solution was prevented from circulating around the reagent due to flaws in the hydrophobic PTFE sample holders. The data from a pH 8 starting solution, in which the pH was controlled by carbonate, were also excluded, due to the potential interference of carbonate in uranium speciation, as discussed in Chapter 1 (Langmuir, 1978, De Pablo et al., 1999). A blank experiment with a fluoride-bearing solution was included in the sample set (sample UO2200/15/0.1/PH5/TS11/blank/13072021/sol).

Table 4-1 Supplementary data for both used and unused samples.

Sample	Short names	NaF (m)	$HClO_4$	$NaClO_4$	NaOH	I	log aF^-	Log aH^+	Log mU	U (ppm)
UO2200/1/0/PH2/24082021/sol	2.1-E-07-1	0	0.0100	0		0.010	-6.80	-2.06	-4.32	11.3
UO2200/2/0/PH2/24082021/sol	2.1-E-07-2	0	0.0100	0		0.010	-6.80	-2.06	-2.90	298
UO2200/3/0/PH2/24082021/sol	2.1-E-07-3	0	0.0100	0		0.010	-6.80	-2.06	-3.10	189
UO2200/4/0/PH2/24082021/sol	2.1-E-07-4	0	0.0100	0		0.010	-6.80	-2.06	-3.22	143
UO2200/5/0/PH2/24082021/sol	2.1-E-07-5	0	0.0100	0		0.010	-6.80	-2.06	-2.92	283
UO2200/1/0/PH3/25042021/sol	3.3-E-05-1	0	0.0010	0		0.001	-4.86	-3.31	-3.25	135
UO2200/2/0/PH3/25042021/sol	3.3-E-05-2	0	0.0010	0		0.001	-4.86	-3.31	-3.14	171
UO2200/3/0/PH3/25042021/sol	3.3-E-05-3	0	0.0010	0		0.001	-4.86	-3.31	-2.66	515
UO2200/4/0/PH3/25042021/sol	3.3-E-05-4	0	0.0010	0		0.001	-4.86	-3.31	-3.81	36.7
UO2200/5/0/PH3/25042021/sol	3.3-E-0.5-5	0	0.0010	0		0.001	-4.86	-3.31	-3.65	53.1
UO2200/1/0/PH5/10052021/sol	5.6-E-04-1	0	1.00E-05	0.01		0.100	-4.23	-5.62	-4.27	12.7
UO2200/2/0/PH5/10052021/sol	5.6-E-04-2	0	1.00E-05	0.01		0.100	-4.23	-5.62	-5.11	1.85
UO2200/3/0/PH5/10052021/sol	5.6-E-04-3	0	1.00E-05	0.01		0.100	-4.23	-5.62	-4.48	7.88
UO2200/4/0/PH5/10052021/sol	5.6-E-04-4	0	1.00E-05	0.01		0.100	-4.23	-5.62	-4.60	6.02
UO2200/5/0/PH5/10052021/sol	5.6-E-04-5	0	1.00E-05	0.01		0.100	-4.23	-5.62	-4.57	6.38
UO2200/1/0/PH8/12082021/sol	6.3-E-04-1	0	0	0.01	1.00E-06	0.010	-3.61	-6.26	4.29	12.2
UO2200/2/0/PH8/12082021/sol	6.3-E-04-2	0	0	0.01	1.00E-06	0.010	-3.61	-6.26	-4.89	3.05
UO2200/3/0/PH8/12082021/sol	6.3-E-04-3	0	0	0.01	1.00E-06	0.010	-3.61	-6.26	-4.52	7.19
UO2200/4/0/PH8/12082021/sol	6.3-E-04-4	0	0	0.01	1.00E-06	0.010	-3.61	-6.26	-5.17	1.62
UO2200/5/0/PH8/12082021/sol	6.3-E-04-5	0	0	0.01	1.00E-06	0.010	-3.61	-6.26	-5.84	3.40
UO2200/6/0.001/PH3/25042021/sol	4-E-04-1	0.001	0.0010	0.001		0.002	-3.96	-3.96	-3.64	54
UO2200/7/0.001/PH3/25042021/sol	4-E-04-2	0.001	0.0010	0.001		0.002	-3.96	-3.96	-3.91	29.5
UO2200/8/0.001/PH3/25042021/sol	4-E-04-3	0.001	0.0010	0.001		0.002	-3.96	-3.96	-3.12	182
UO2200/9/0.001/PH3/25042021/sol	4-E-04-4	0.001	0.0010	0.001		0.002	-3.96	-3.96	-4.03	22.4
UO2200/10/0.001/PH3/25042021/sol	4-E-04-5	0.001	0.0010	0.001		0.002	-3.96	-3.96	-4.16	16.3
UO2200/6/0.001/PH5/10052021/sol	6.4-E-03-1	0.001	1.00E-05	0.01		0.001	-3.04	-6.43	-4.19	15.5
UO2200/7/0.001/PH5/10052021/sol	6.4-E-03-2	0.001	1.00E-05	0.01		0.001	-3.04	-6.43	-4.51	7.38
UO2200/8/0.001/PH5/10052021/sol	6.4-E-03-3	0.001	1.00E-05	0.01		0.001	-3.04	-6.43	-5.06	2.08
UO2200/9/0.001/PH5/10052021/sol	6.4-E-03-4	0.001	1.00E-05	0.01		0.001	-3.04	-6.43	-4.18	15.7
UO2200/10/0.001/PH5/10052021/sol	6.4-E-03-5	0.001	1.00E-05	0.01		0.001	-3.04	-6.43	-4.82	3.62
UO2200/6/0.01/PH2/24082021/sol	5.6-0.06-1	0.01	0.0100	0.003		0.125	-1.24	-5.63	-2.76	412
UO2200/7/0.01/PH2/24082021/sol	5.6-0.06-2	0.01	0.0100	0.003		0.125	-1.24	-5.63	-2.91	290
UO2200/8/0.01/PH2/24082021/sol	5.6-0.06-3	0.01	0.0100	0.003		0.125	-1.24	-5.63	-3.29	123
UO2200/9/0.01/PH2/24082021/sol	5.6-0.06-4	0.01	0.0100	0.003		0.125	-1.24	-5.63	-4.33	11.1
UO2200/10/0.01/PH2/24082021/sol	5.6-0.06-5	0.01	0.0100	0.003		0.125	-1.24	-5.63	-3.44	123
UO2200/11/0.01/PH3/25042021/sol	5.7-0.01-1	0.01	0.0010	0.01		0.020	-2.14	-5.72	-3.63	55.2
UO2200/12/0.01/PH3/25042021/sol	5.7-0.01-2	0.01	0.0010	0.01		0.020	-2.14	-5.72	-3.60	59.7
UO2200/13/0.01/PH3/25042021/sol	5.7-0.01-3	0.01	0.0010	0.01		0.020	-2.14	-5.72	-3.79	38.3
UO2200/14/0.01/PH3/25042021/sol	5.7-0.01-4	0.01	0.0010	0.01		0.020	-2.14	-5.72	-4.07	20.4
UO2200/15/0.01/PH3/25042021/sol	5.7-0.01-5	0.01	0.0010	0.01		0.020	-2.14	-5.72	-3.47	80.2
UO2200/11/0.01/PH5/10052021/sol	7-0.01a-1	0.01	1.00E-05	0.01		0.010	-2.07	-6.96	-4.22	14.2
UO2200/12/0.01/PH5/10052021/sol	7-0.01a-2	0.01	1.00E-05	0.01		0.010	-2.07	-6.96	-5.66	0.52
UO2200/13/0.01/PH5/10052021/sol	7-0.01a-3	0.01	1.00E-05	0.01		0.010	-2.07	-6.96	-3.44	31.2
UO2200/14/0.01/PH5/10052021/sol	7-0.01a-4	0.01	1.00E-05	0.01		0.010	-2.07	-6.96	-4.18	15.6
UO2200/15/0.01/PH5/10052021/sol	7-0.01a-5	0.01	1.00E-05	0.01		0.010	-2.07	-6.96	-4.45	8.47

Sample	Short names	NaF (m)	$HClO_4$	$NaClO_4$	NaOH	I	log aF^-	Log aH^+	Log mU	U (ppm)
UO2200/6/0.01/PH8/12082021/sol	7-0.01b-1	0.01	0	0.01	1.00E-06	0.020	-2.10	-6.98	-4.16	16.4
UO2200/7/0.01/PH8/12082021/sol	7-0.01b-2	0.01	0	0.01	1.00E-06	0.020	-2.10	-6.98	-5.84	0.345
UO2200/8/0.01/PH8/12082021/sol	7-0.01b-3	0.01	0	0.01	1.00E-06	0.020	-2.10	-6.98	-5.69	0.481
UO2200/9/0.01/PH8/12082021/sol	7-0.01b-4	0.01	0	0.01	1.00E-06	0.020	-2.10	-6.98	-8.43	0.001
UO2200/10/0.01/PH8/12082021/sol	7-0.01b-5	0.01	0	0.01	1.00E-06	0.020	-2.10	-6.98	-5.91	0.290
UO2200/11/0.1/PH2/24082021/sol	3.4-E-03-1	0.1	0.0100	0.03		0.013	-3.45	-3.43	-2.63	552
UO2200/12/0.1/PH2/24082021/sol	3.4-E-03-2	0.1	0.0100	0.03		0.013	-3.45	-3.43	-2.77	400
UO2200/13/0.1/PH2/24082021/sol	3.4-E-03-3	0.1	0.0100	0.03		0.013	-3.45	-3.43	-2.69	481
UO2200/14/0.1/PH2/24082021/sol	3.4-E-03-4	0.1	0.0100	0.03		0.013	-3.45	-3.43	-2.71	459
UO2200/15/0.1/PH2/24082021/sol	3.4-E-03-5	0.1	0.0100	0.03		0.013	-3.45	-3.43	-2.81	369
UO2200/1/0.1/PH3/08042021/sol	6.6-0.06a-1	0.1	0.0010	0.10		0.193	-1.23	-6.63	-3.49	76.6
UO2200/2/0.1/PH3/08042021/sol	6.6-0.06a-2	0.1	0.0010	0.10		0.193	-1.23	-6.63	-3.29	121
UO2200/3/0.1/PH3/08042021/sol	6.6-0.06a-3	0.1	0.0010	0.10		0.193	-1.23	-6.63	-3.40	95.0
UO2200/4/0.1/PH3/08042021/sol	6.6-0.06a-4	0.1	0.0010	0.10		0.193	-1.23	-6.63	4.76	4.15
UO2200/5/0.1/PH3/08042021/sol	6.6-0.06a-5	0.1	0.0010	0.10		0.193	-1.23	-6.63	-3.44	85.7
UO2200/1/0.1/PH3/T/sol	6.6-0.06b-1	0.1	0.0010	0.10		0.193	-1.23	-6.63	-3.42	90.7
UO2200/2/0.1/PH3/T/sol	6.6-0.06b-2	0.1	0.0010	0.10		0.193	-1.23	-6.63	-3.27	127
UO2200/3/0.1/PH3/T/sol	6.6-0.06b-3	0.1	0.0010	0.10		0.193	-1.23	-6.63	-3.09	192
UO2200/4/0.1/PH3/T/sol	6.6-0.06b-4	0.1	0.0010	0.10		0.193	-1.23	-6.63	-3.44	85.5
UO2200/5/0.1/PH3/T/sol	6.6-0.06b-5	0.1	0.0010	0.10		0.193	-1.23	-6.63	-3.33	110
UO2200/6/0.1/PH3/T/sol	6.6-0.06b-6	0.1	0.0010	0.10		0.193	-1.23	-6.63	-3.36	105
UO2200/7/0.1/PH3/T/sol	6.6-0.06b-7	0.1	0.0010	0.10		0.193	-1.23	-6.63	-3.34	108
UO2200/8/0.1/PH3/T/sol	6.6-0.06b-8	0.1	0.0010	0.10		0.193	-1.23	-6.63	-4.25	13.3
UO2200/1/0.1/PH5/03062021/sol	7.4-0.06a-1	0.1	1.00E-5	0.10		0.096	-1.18	-7.39	-3.08	199
UO2200/2/0.1/PH5/03062021/sol	7.4-0.06a-2	0.1	1.00E-5	0.10		0.096	-1.18	-7.39	-3.14	172
UO2200/3/0.1/PH5/03062021/sol	7.4-0.06a-3	0.1	1.00E-5	0.10		0.096	-1.18	-7.39	-3.37	101
UO2200/4/0.1/PH5/03062021/sol	7.4-0.06a-4	0.1	1.00E-5	0.10		0.096	-1.18	-7.39	-3.03	224
UO2200/5/0.1/PH5/03062021/sol	7.4-0.06a-5	0.1	1.00E-5	0.10		0.096	-1.18	-7.39	-2.86	331
UO2200/1/0.1/PH5/TS1/13072021/sol	7.4-0.06b-1	0.1	1.00E-5	0.10		0.096	-1.18	-7.40	-4.01	23.0
UO2200/2/0.1/PH5/TS1/13072021/sol	7.4-0.06b-2	0.1	1.00E-5	0.10		0.096	-1.18	-7.40	-4.41	9.35
UO2200/3/0.1/PH5/TS1/13072021/sol	7.4-0.06b-3	0.1	1.00E-5	0.10		0.096	-1.18	-7.40	-4.71	4.69
UO2200/4/0.1/PH5/TS3/13072021/sol	7.4-0.06b-4	0.1	1.00E-5	0.10		0.096	-1.18	-7.40	-3.28	125
UO2200/5/0.1/PH5/TS3/13072021/sol	7.4-0.06b-5	0.1	1.00E-5	0.10		0.096	-1.18	-7.40	-3.29	121
UO2200/6/0.1/PH5/TS3/13072021/sol	7.4-0.06b-6	0.1	1.00E-5	0.10		0.096	-1.18	-7.40	-3.43	88.1
UO2200/7/0.1/PH5/TS5/13072021/sol	7.4-0.06b-7	0.1	1.00E-5	0.10		0.096	-1.18	-7.40	-3.46	82.1
UO2200/8/0.1/PH5/TS5/13072021/sol	7.4-0.06b-8	0.1	1.00E-5	0.10		0.096	-1.18	-7.40	-3.60	59.5
UO2200/9/0.1/PH5/TS7/13072021/sol	7.4-0.06b-9	0.1	1.00E-5	0.10		0.096	-1.18	-7.40	-3.24	138
UO2200/10/0.1/PH5/TS7/13072021/sol	7.4-0.06b-10	0.1	1.00E-5	0.10		0.096	-1.18	-7.40	-3.57	63.8
UO2200/11/0.1/PH5/TS9/13072021/sol	7.4-0.06b-11	0.1	1.00E-5	0.10		0.096	-1.18	-7.40	-3.33	110
UO2200/12/0.1/PH5/TS9/13072021/sol	7.4-0.06b-12	0.1	1.00E-5	0.10		0.096	-1.18	-7.40	-3.80	37.4
UO2200/13/0.1/PH5/TS11/13072021/sol	7.4-0.06b-13	0.1	1.00E-5	0.10		0.096	-1.18	-7.40	-3.38	98.3
UO2200/14/0.1/PH5/TS11/13072021/sol	7.4-0.06b-14	0.1	1.00E-5	0.10		0.096	-1.18	-7.40	-3.40	93.8
UO2200/15/0.1/PH5/TS11/blank/13072021/sol	7.4-0.06b-15	0.1	1.00E-5	0.10		0.096	-1.18	-7.40	-5.69	0.483
UO2200/6/0.1/PH7/03062021/sol	7.4-0.06c-1	0.1	0	0.10		0.096	-1.18	-7.40	-2.76	414
UO2200/7/0.1/PH7/03062021/sol	7.4-0.06c-2	0.1	0	0.10		0.096	-1.18	-7.40	-3.22	143
UO2200/8/0.1/PH7/03062021/sol	7.4-0.06c-3	0.1	0	0.10		0.096	-1.18	-7.40	-3.23	141
UO2200/9/0.1/PH7/03062021/sol	7.4-0.06c-4	0.1	0	0.10		0.096	-1.18	-7.40	-3.34	109
UO2200/10/0.1/PH7/03062021/sol	7.4-0.06c-5	0.1	0	0.10		0.096	-1.18	-7.40	-4.56	6.55

Sample	Short names	NaF (m)	$HClO_4$	$NaClO_4$	NaOH	I	log aF^-	Log aH^+	Log mU	U (ppm)
UO2200/1/0.1/PH7/14102021/sol	7.4-0.06d-1	0.1	0	0		0.096	-1.18	-7.40	-3.56	65.2
UO2200/2/0.1/PH7/14102021/sol	7.4-0.06d-2	0.1	0	0		0.096	-1.18	-7.40	-3.26	130
UO2200/3/0.1/PH7/14102021/sol	7.4-0.06d-3	0.1	0	0		0.096	-1.18	-7.40	-2.82	362
UO2200/4/0.1/PH7/14102021/sol	7.4-0.06d-4	0.1	0	0		0.096	-1.18	-7.40	-2.51	740
UO2200/5/0.1/PH7/14102021/sol	7.4-0.06d-5	0.1	0	0		0.096	-1.18	-7.40	-2.51	743
UO2200/11/0.1/PH9/03062021/sol	7.4-0.06e-1	0.1	0	0.10	1.00E-05	0.193	-1.23	-7.36	-3.32	114
UO2200/12/0.1/PH9/03062021/sol	7.4-0.06e-2	0.1	0	0.10	1.00E-05	0.193	-1.23	-7.36	-3.40	95.0
UO2200/13/0.1/PH9/03062021/sol	7.4-0.06e-3	0.1	0	0.10	1.00E-05	0.193	-1.23	-7.36	-3.45	85.0
UO2200/14/0.1/PH9/03062021/sol	7.4-0.06e-4	0.1	0	0.10	1.00E-05	0.193	-1.23	-7.36	-3.36	105
UO2200/15/0.1/PH9/03062021/sol	7.4-0.06e-5	0.1	0	0.10	1.00E-05	0.193	-1.23	-7.36	-3.50	75.9
UO2200/11/0.1/PH8/12082021/sol	7.4-0.06-1	0.1	0	0.10	1.00E-06	0.193	-1.23	-7.35	-3.97	25.7
UO2200/12/0.1/PH8/12082021/sol	7.4-0.06-2	0.1	0	0.10	1.00E-06	0.193	-1.23	-7.35	-4.74	4.28
UO2200/13/0.1/PH8/12082021/sol	7.4-0.06-3	0.1	0	0.10	1.00E-06	0.193	-1.23	-7.35	-4.07	20.3
UO2200/14/0.1/PH8/12082021/sol	7.4-0.06-4	0.1	0	0.10	1.00E-06	0.193	-1.23	-7.35	-3.97	25.5
UO2200/15/0.1/PH8/12082021/sol	7.4-0.06-5	0.1	0	0.10	1.00E-06	0.193	-1.23	-7.35	-4.21	14.6
UO2200/6/0.2/PH3/08042021/sol	6.9-0.1-1	0.2	0.0010	0.20		0.375	-0.971	-6.88	-3.64	54.5
UO2200/7/0.2/PH3/08042021/sol	6.9-0.1-2	0.2	0.0010	0.20		0.375	-0.971	-6.88	-3.69	48.1
UO2200/8/0.2/PH3/08042021/sol	6.9-0.1-3	0.2	0.0010	0.20		0.375	-0.971	-6.88	-3.43	88.1
UO2200/9/0.2/PH3/08042021/sol	6.9-0.1-4	0.2	0.0010	0.20		0.375	-0.971	-6.88	-3.30	120
UO2200/10/0.2/PH3/08042021/sol	6.9-0.1-5	0.2	0.0010	0.20		0.375	-0.971	-6.88	-3.59	61.9
UO2200/6/0.2/PH7/14102021/sol	7.5-0.1-1	0.2	0	0		0.186	-0.922	-7.51	-2.62	576
UO2200/7/0.2/PH7/14102021/sol	7.5-0.1-2	0.2	0	0		0.186	-0.922	-7.51	-2.62	574
UO2200/8/0.2/PH7/14102021/sol	7.5-0.1-3	0.2	0	0		0.186	-0.922	-7.51	-3.59	60.7
UO2200/9/0.2/PH7/14102021/sol	7.5-0.1-4	0.2	0	0		0.186	-0.922	-7.51	-3.38	98.3
UO2200/10/0.2/PH7/14102021/sol	7.5-0.1-5	0.2	0	0		0.186	-0.922	-7.51	-3.60	59.5
UO2200/11/0.3/PH3/08042021/sol	7-0.2-1	0.3	0.0010	0.30		0.547	-0.820	-7.03	-3.48	78.3
UO2200/12/0.3/PH3/08042021/sol	7-0.2-2	0.3	0.0010	0.30		0.547	-0.820	-7.03	-3.38	98.8
UO2200/13/0.3/PH3/08042021/sol	7-0.2-3	0.3	0.0010	0.30		0.547	-0.820	-7.03	-3.80	37.6
UO2200/14/0.3/PH3/08042021/sol	7-0.2-4	0.3	0.0010	0.30		0.547	-0.820	-7.03	-3.53	70.9
UO2200/15/0.3/PH3/08042021/sol	7-0.2-5	0.3	0.0010	0.30		0.547	-0.820	-7.03	-3.51	-74.3
UO2200/11/0.3/PH7/14102021/sol		473.15		0		0.3088	-0.7167			
UO2200/12/0.3/PH7/14102021/sol		473.15		0		0.3285	-0.6908			
UO2200/13/0.3/PH7/14102021/sol		473.15		0		0.2984	-0.7310			
UO2200/14/0.3/PH7/14102021/sol		473.15		0		0.2984	-0.7310			
UO2200/15/0.3/PH7/14102021/sol		473.15		0		0.2723	-0.7687			

4.1 References

De Pablo J., Casas I., Giménez J., Molera M., Rovira M., Duro L. and Bruno J. (1999) The oxidative dissolution mechanism of uranium dioxide. I. The effect of temperature in hydrogen carbonate medium. Geochimica et Cosmochimica Acta 63, 3097–3103.

Langmuir D. (1978) Uranium solution-mineral equilibria at low temperatures with applications to sedimentary ore deposits. Geochimica et Cosmochimica Acta 42, 547–569.